Investigation on Triple Helical Cylinders' Effects on Human Osteosarcoma U2OS Cells

by

Melika Hadjebi

A thesis submitted to the University of Birmingham for the degree of Master of Science by Research

The University of Birmingham, School of Chemistry
May 2017

Abstract

The aim of this study is to investigate the activity of supermolecular iron and ruthenium cylinders and their interactions with the DNA replication fork, as the possible target of action for cylinders.

The impacts of two homologues, triple helical iron(II) and ruthenium(II) homologous, as metallodrug agents on U2OS cells are studied using different techniques. Both complexes demonstrate toxicity with significant IC50 values against U2OS cells, although they improve the nongenotoxicity effect in this cell line. These outcomes contrast with the results of cisplatin, both in comet and MTT assays. In this study, cisplatin slightly damages the DNA helix and does not show significant cytotoxicity against the studied cells. The cellular uptake results prove that cells can absorb the ruthenium cylinder, but just one fifth of the total ruthenium concentration is detected inside the nucleus, and most is trapped in the membrane.

Confocal microscopy is applied using two different methods (live- and fixed-cell microscopy), to survey the cellular uptake of cylinders in addition to their binding affinity to the DNA major groove. Hoechst is used for this purpose, as it is a well-known minor groove binder probe. Hoechst decrease in fluorescence as a result of cylinder replacement is not observed by these imaging techniques, and the results do not show cylinder interaction with the DNA major groove in U2OS cells, despite previous results in other cell lines. Meanwhile, the protein immunoblot analysis does not produce desirable results regarding the DNA replication fork interaction with the ruthenium cylinder. The P-ChK1 detection results for the iron cylinder could not be repeated, despite the fact that in some cases they do demonstrate stress on the replication fork.

Acknowledgement

I would like to express my heartfelt gratitude to the following people who have helped make this thesis possible:

First and foremost, I would like to thank my Alireza who never left my side and kept guiding and blessing me so much. In particular, I want to thank my mum and dad for their unwavering support and encouragement throughout my studies and my sister for her sweet being. And the true friends of mine who pushed me to succeed and were always there to lift my spirits.

I would like to thank my supervisor Professor Mike Hannon for giving me the opportunity to carry out this research in his group and for providing me with an appealing research project.

I am grateful to the wonderful teacher Dr. Nik Hodges for all his time spent in training and guiding me through the project. A special thank you to Lucia Cardo and Abiola Dosumu for all their guidance and helps during the course and of course for their friendship. There is a special thank you to Alessandro Di Maio for his unique way of teaching microscopy imaging and all his kind patience to answer my never-ending questions!

I am grateful to Professor Grant Stewart for allowing me to use his laboratories and Dr. Martin Higgs to train me and devoting his time to me to achieve accurate results in western blot tests.

Finally, I would like to thank Peter Cail, Callum Campbell, Richard Young, Lois Bright and Ashleigh Freer for their support and friendship and for all the best times and memories, they made for me, I am truly grateful to you all.

Contents

List of figures

List of Tables

General Abbreviations

Å	Angstrom
aq.	aqueous
bpy	2,2’-bipyridine
CH_3CN	acetonitrile
$CHCl_3$	chloroform
DCM	dichloromethane
DSC	Differential Scanning Calorimetry
DMSO	dimethyl sulphoxide
DNA	2’-deoxyribonucleic acid
EA	Elemental Analysis
EtOH	ethanol
ICP-MS	Inductively Coupled Plasma Mass Spectrometry
ITC	Isothermal Titration Calorimetry
M	molar
Me	methyl
MeOH	methanol
MTT	3-(4,5-dimethylthiazol-2-yl)-2,5-diphenyltetrazolium bromide
NH_4PF_6	ammonium hexafluorophosphate
t-Bu_4NCl	tetrabutylammonium chloride
µM	micromolar
µmol	micromole
mmol	millimole
mp.	melting point
m/z	mass/charge

nm	nanometer
P	partition coefficient
Ph	phenyl
phen	1,10-phenanthroline
RNA	ribonucleic acid
T_m	melting temperature (ct-DNA)
terpy	2,2':6',2'-terpyridine

Spectroscopic terms

CD	Circular Dichroism
LD	Linear Dichroism
ICD	Induced Circular Dichroism
IR	Infra-Red
NMR	Nuclear Magnetic Resonance
UV-Vis	Ultra-Violet - Visible
ES	Electrospray
MS	Mass Spectrometry

NMR terms

$CDCl_3$	deuterated chloroform
CD_3CN	deuterated acetonitrile
COSY	Correlated Spectroscopy
D_2O	deuterium oxide
δ	chemical shift
s	singlet
t	triplet
δ	chemical shift

d	doublet
dd	doublet of doublets
MHz	megahertz
ppm	parts per million
q	quartet
s	singlet
t	triplet

UV-Vis terms

MLCT	Metal to Ligand Charge Transfer
ε	extinction coefficient
hν	light energy
λ	Wavelength

Fluorescence terms

λ_{ex}	Wavelength of excitation
λ_{em}	Wavelength of emission

Thermodynamic terms

ΔC_p	heat capacity change
ΔG	free energy change
ΔH	enthalpy change
ΔS	entropy change
ΔT	temperature change
K	equilibrium binding constant
R	gas constant (8.314 J K^{-1} mol^{-1})

DNA terms

ct-DNA	calf-thymus DNA
ds-DNA	double-stranded DNA
ss-DNA	single-stranded DNA
A	adenine
C	cytosine
G	guanine
T	thymine
3WJ	DNA three-way junction

Gel electrophoresis terms

ϕ	unwinding angle
σ	superhelicity
rb	coalescence point

Introduction

The *magic bullet* approach seems to be the appropriate nickname for the cancer therapy technique founded by Paul Ehrlich [1] before the dawn of the twentieth century, through detection of the specificity of antigen-antibody. He formulated this concept based on the affinity of a particular molecule for a certain organ, in order to bring therapeutically active groups to the organ to be treated.

Cancer is the second most common disease, after cardiovascular disorders, responsible for human deaths around the globe. [2] Today, battling cancers is considered to be a great hurdle and a critical milestone to overcome that directly affects the quality of life in modern societies.

There is a growing list of proposed causes when dealing with the occurrence of cancerous malignancies: air pollution, chemical pollution, radiation exposure, and a problematic genetic algorithm, to name a few. Different genes that control cell proliferation change during mutation, and this disorder can drive cells to divide. Deactivation of tumour-suppressing genes and DNA-repairing genes during the mutation is considered to be a cause of abnormal cell growth.

There are various ways to tackle the challenge of cancer treatment, by techniques that can be used individually or in combination with one another. Surgery combined with chemotherapy and/or radiation therapy are some of the most commonly used methods to cure cancers. Moreover, immunotherapy and hormone therapy (classified as targeted therapy methods) can be considered as alternative or optional treatment methods. [3,4]

In chemotherapy, cancer cells are killed by damage to their DNA through the application of anticancer drugs. It is important to point out that the type of anticancer drugs used has a significant impact on the possible side effects resulting from chemotherapy treatments. For example, some of the most common anticancer agents have severe side effects, such as anaemia; therefore, much research has been carried out with the purpose of applying the targeted drugs in chemotherapy.

Targeted cancer therapy can be regarded as a brand new and ambitious field of research which addresses the design, synthesis and application of particular drugs that target specific genes and proteins in each therapy. These drugs can inhibit or block the definite molecules that play key roles in the growth, division, progression and spreading processes in cancer cells.

Targeted therapies are generally cytostatic, in contrast to standard chemotherapies, because they target the specific molecules associated with cancer. [5, 6]

In recent years, many anticancer drugs have been studied for use in smart therapy. Metal complexes with remarkable properties and special abilities to connect with critical biomolecules are known to be effective drugs in these new cancer therapy methods. Inorganic medicinal chemistry has flourished after the discovery of cis-dichlorodiammine-platinum(II) (cisplatin). The pioneering discovery of this anticancer drug with outstanding anticancer properties has pushed the frontiers of conventional cancer therapy. Cisplatin, as one of the most famous anticancers, has been used in treating a vast range of cancer cell lines. However, this small metallodrug also exhibits some dramatic side effects. In addition, some cancers are resistant to cisplatin. These major disadvantages of this platinum-based anticancer have led to the investigation in this thesis of the design and synthesis of new and effective non platinum-based metallodrugs, in order to achieve the targeted therapy without the harmful side effects. [7]

A large number of biomolecules, such as peptides, proteins, DNA, RNA and small molecules, can be targeted by metallodrugs in biological systems. As a carrier of all human genetic information in all cell types, DNA is undoubtedly known as the best target for metallodrugs in cancer therapy. It is evident that targeting the DNA of cancerous cells can activate the system of cell apoptosis in tumours without damaging the normal cells, and these kinds of smart therapies have recently been successfully studied with metal complexes.

This study examines the synthesis methods of two iron and ruthenium cylinders as special metallodrugs, and surveys their modes of DNA binding (specifically on the DNA replication fork) and cytotoxicity in human bone osteosarcoma epithelial cells (U2OS).

Chapter one summarises the theoretical background of this investigation, and includes reviews of the DNA molecular structure, its modes of interaction with various metallodrugs, and the reasons behind their anticancer characteristics being affected by DNA binding modes. The diversity of metal complexes is then explored, particularly iron and ruthenium complexes, with a survey of their biological and antitumour properties. The study specifically focuses on iron and ruthenium cylinders, and explores their interaction modes with biological molecules and their processes of action as anticancers towards targeted cells.

Chapter two describes the experimental procedure, including the synthesis and purification of iron and ruthenium cylinders and U2OS cells cultured. It also surveys the toxicity of both cylinders against U2OS cells by MTT assay. The damage to DNA by cylinders is investigated and explained by comet assay. Moreover, cell uptakes are checked with ICP-MS, and the modes of cylinders' interactions with DNA are studied by imaging microscopy using both live- and fixed-cell techniques, followed by the western blot method.

Chapter three comprises results and discussion pertaining to each experiment. For each test, the results section explains the hypothesis behind the test, the expected data and the exact results. This is followed by a logically supported discussion of the results in relation to the initial hypothesis.

Chapter 1

THEORETICAL FUNDAMENTALS

1.1 Introduction

The anticancer metallodrugs are known to be effective tools that target intracellular biomolecules such as DNA, RNA and proteins. As a vital part of the cellular genome, DNA and its possible modes of interaction with metallodrugs has been widely studied. Various types of metal complex drugs, their effects on cancerous cells and their modes of binding with DNA or other cellular molecules are discussed extensively in this chapter.

1.2 2′-Deoxyribonucleic acid (DNA)

Deoxyribonucleic acid (DNA) is the fundamental biomolecular structure that carries the genetic codes of organisms. This long polymeric biomolecule was discovered by Friedrich Miesche at the University of Tübingen in 1869. [8] Nucleotides are the subunits of DNA. The Nucleotides are composed of a nitrogenous base (Fig. 1.2), a five-carbon sugar which has bonded with the heterocyclic base such as cytosine (C), guanine (G), adenine (A) or thymine (T) (Fig. 1.1). A phosphodiester can link the 5'-end of one sugar to the 3'-end of the other, and nucleic acid sequences are written in the 5' to 3' direction. Adenine and guanine are purines, while cytosine and thymine have a pyrimidine structure. [9]

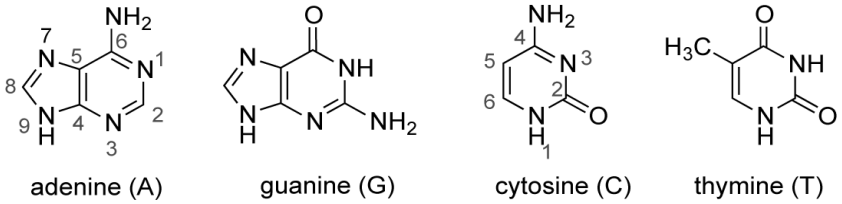

Fig. 1.1. The chemical structure of nitrogenous base amino acids found in nucleotides. Taken from ref 200.

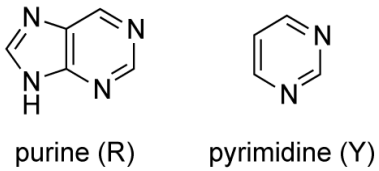

Fig. 1.2. The structure of purine and pyridine heterocyclic ring systems. Taken from ref 200.

The building blocks of DNA consist of a phosphate base on the 5′-carbon position, with the heterocyclic base linked to the 1′-position of the sugar base (Fig. 1.3). [9]

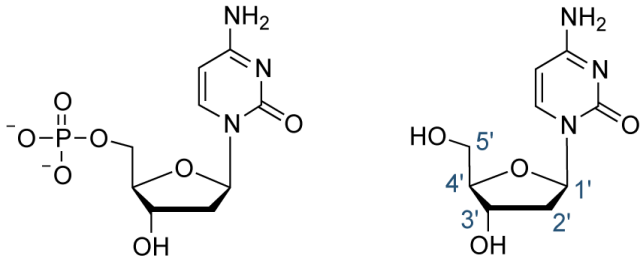

Fig. 1.3. The structure of deoxynucleotides. Taken from ref 200.

The molar amount of adenine in DNA has been found to always be equal to that of thymine; the same is also true for guanine and cytosine. [10,11] Consequently, the rule of nucleotide junctions between two different strands demonstrates that the linkage of adenine (A)–thymine (T) and guanine (G)–cytosine (C) is possible. These complementary DNA bases are connected to each other through hydrogen binding (Fig. 1.5). [9]

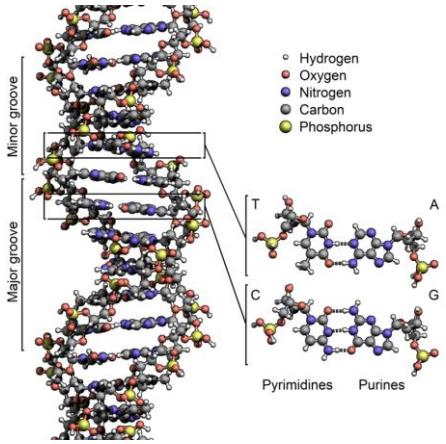

Fig. 1.4. The DNA double helical structure with structural elements indicated. Both major and minor grooves and DNA base pairs are noted separately. Taken from ref 201.

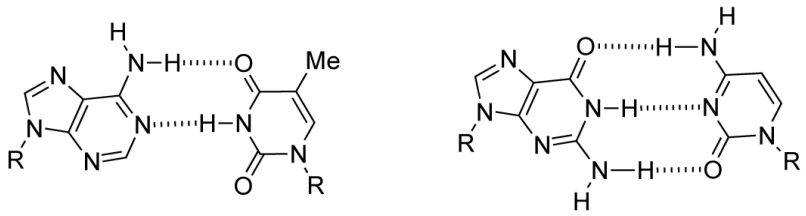

Fig. 1.5. Schematic representation of hydrogen bonding between two Watson-Crick DNA base pairs. Taken from ref 200.

In a eukaryotic cell, the DNA molecule is a double-strand biopolymer consisting of nucleotides coiled around each other to form a double helix; this form was discovered by Watson and Crick in 1953. [9] Since each nucleotide is able to form a hydrogen bond with a specific nucleotide (see Fig. 1.4), the sequence of a single strand of DNA also defines the parallel sequence. As a result, each strand has the reverse structure of its parallel strand, with the 5′-end of one strand placed adjacently to the 3′-end of the other. It is noteworthy that π-π interactions are present in DNA's double helix among the stacked aromatic rings of longitudinal bases on the polynucleotide chains, thus providing the stability of the DNA helix. The DNA backbone strands remain situated close together because of the hydrogen bonding present between them. The DNA structure can be divided into two groove parts, termed the major and minor grooves, which curl around the molecule on opposite sides. This classification is based on the distance between the backbones; in the case of major grooves this distance is greater, while for minor grooves the situation is reversed (Fig. 1.6). [13]

A right-handed double helix is formed in the case where two strands turn around each other, and the backbone facing the observer moves in a downwards sense from the top right to bottom left. In this structure, the external hydrophilic backbone is shaped by the hydrophobic base pairs in the middle and the sugars together with the negatively charged phosphates (Fig. 1.7). [12]

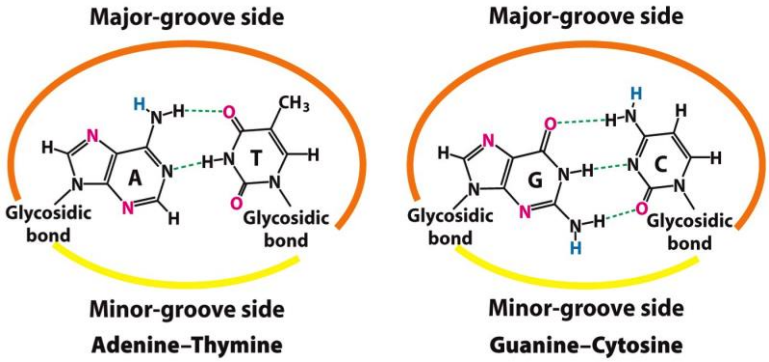

Fig. 1.6. Schematic representation of the major and minor groove sides of the DNA double helix. Taken from ref 216.

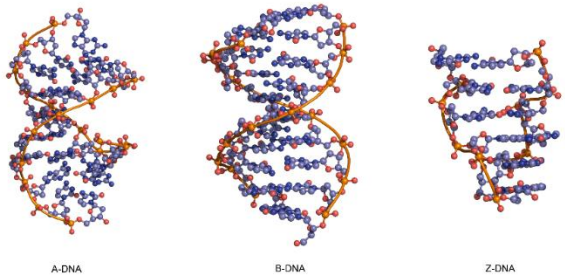

Fig. 1.7 Three-dimensional structures of A, B (right-handed) and Z (left-handed) DNA structures. Taken from ref 202.

The symmetrical grooves in double-stranded DNA are formed when the glycosidic bonds protrude at a 90-degree angle on both sides. [14] The role of glycosidic bonds is to attach the nucleic base to the sugar in the backbone, and the presence of an angle between the glycosidic bonds and the interface between the AT or GC pairs results in one of the faces of the base pair being larger than the other. [9,14] The basic proteins with the responsibility of DNA replication, transcription or modification are, in principle, bound to the major groove rather than the minor one. As a result of the position of DNA backbones and the wide angle, it is easier for the proteins to bind with the major groove sides.

As shown in Figure 1.8 there are three basic conformations of DNA helices: A-DNA, B-DNA and Z-DNA. [15]

Studies on the crystal form of oligonucleotide duplexes have confirmed that there are significant differences between the different DNA conformation structures in some basic parameters, which are classified in Table 1.1. [15]

Table 1.1. The average parameters of the three DNA conformations. Taken from ref 15.

Structural parameter	A-DNA	B-DNA	Z-DNA
Direction of helix	Right rotation	Right-handed	Left-handed
Residue per helical turn	11	10.5	12
Axial rise per residue	2.55 Å	3.4 Å	3.7 Å
Pitch (length) of the helix	28.2 Å	34 Å	44.4 Å
Base pair tilt	20°	-6°	7°
Rotation per residue	32.7°	34.3°	-30°
Diameter of helix	23 Å	20 Å	18 Å
Configuration dA, dT, dC	anti	anti	anti
of glycosidic bond dG	anti	anti	syn
Sugar pucker dA, dT, dC	C3' endo	C2' endo	C2' endo

The most common form of DNA is B-DNA, that is, the canonical right-handed DNA helix. Standard B-DNA comprises two antiparallel double helix strands. [15] This DNA conformation type has a wide major groove, making it suitable for binding with proteins that interact with the DNA. Furthermore, its narrow minor groove is a good target for small drug molecules to bind with DNA, such as distamycin. [16]

The A-form nucleic acid is a thicker right-handed DNA duplex with a shorter distance between its base pairs. A-form and B-form nucleic acids are particularly determined on the basis of the order of their base pairs inside the duplex: the B-form is characterised by the base-pairs being rather centred over the helical axis, while in the A-form the base pairs are closer to the major groove, which produces a ribbon-like helix with an open cylindrical core. [199]

The Z-DNA conformation, with its ‘zig-zag’ appearance, is fundamentally different to the other two forms of the duplex (Fig. 1.8). This structure comprises a strand coiling in a left-handed helix with the repetition of dinucleotide units. Furthermore, Z-DNA consists of an alternating purine-pyrimidine sequence (dCGCGCG); the zig-zag pattern results from the different conformation of these two nucleotides. [15,17]

Fig. 1.8. A comparison between the normal shape of B-DNA and the zig-zag form of Z-DNA. Taken from ref 15.

Generally, the vast majority of DNA double helices in eukaryote cells possess the B-form of a duplex in their genetic codes, while Z-DNA can only be found in some living cells. [18,19,20]

1.3 Modes of DNA interaction

In pharmacology, DNA is the most important target for anticancer metallodrugs to control gene expression. These drugs include transition metal compounds containing Ru, Co, Ni, Cu, Zn, Fe and other rare-earth compounds. [23]

There are several known mechanisms for the interaction between metallodrugs and DNA that have been discovered since the 1960s. [21,22] Considering the many possible binding sites on DNA that result from the varying electrochemical properties, size and complexity of nucleobases, two binding interaction modes can be demonstrated: irreversible, such as covalent binding, and reversible, such as intermolecular association. The main modes of DNA binding are classified as alkylation or covalent binding, groove binding (both major and minor forms), intercalation, and unique binding modes such as Y-junction, cruciform and hairpin, and G-quadruplex. [57]

1.3.1 Alkylation or covalent binding

Covalent binding is known as a common form of anticancer drug interaction with DNA. In general, covalent bonds are formed by strong electrophilic compounds that undergo chemical reaction with nucleophilic sites on the DNA structure. Alkylating agents can produce an irreversible bond with DNA nucleotides, consequently inhibiting the processes of transcription or replication and leading to cell death. [230]

The N(7) atom of guanine and N(3) atom of adenine are two active sites at the DNA base that react to alkylators. Nucleophilic substitution reactions can occur by both SN1 and SN2 mechanisms. For example, aziridines and alkyl sulphonates (such as methyl sulphonate or

busulphan and their analogues) react by an SN2 mechanism, while nitrogen mustard can cause the aziridinium ion to proceed to the SN1 mechanism (Fig. 1.9). [24]

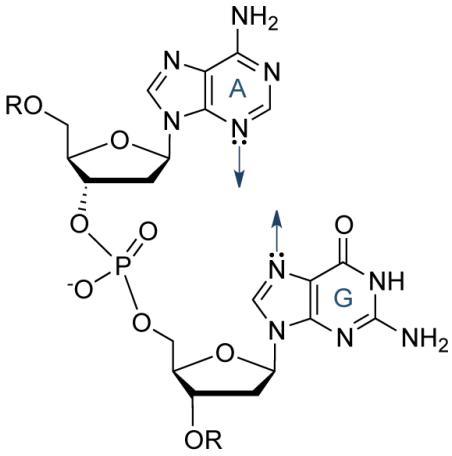

Fig. 1.9. The N(7) atom of guanine and N(3) atom of adenine as two active sites of the DNA base. Taken from ref 200.

Cisplatin (cis- [PtCl2(NH3)2]) is a famous anticancer metallodrug that is used to cure various types of cancer, such as ovarian and cervical cancer and melanomas, and is especially well-known for its use in curing over 90% of testicular cancers. Cisplatin is able to affect DNA by forming a strong coordination bond with nitrogen 7 of guanine and adenine in the DNA backbone (Fig. 1.10). [25,26]

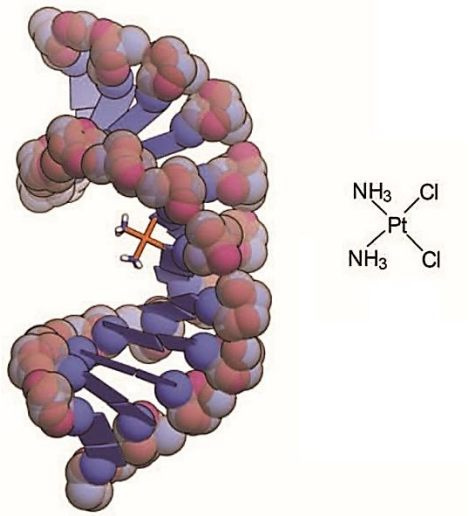

Fig. 1.10. 1,2-interastrand adduct formed between DNA and cisplatin. Taken from ref 74.

Published studies also illustrate the reaction of this compound with a vast range of biomolecules in various kinds of cells. [27] Furthermore, cisplatin (generally the clinical DNA covalent binder) as an metallo-organic drug has also shown good results in treating diseases other than cancers.

Other cisplatin analogues with a similar mode of interaction with DNA have been synthesised in recent decades, including carboplatin, heptaplatin and oxaliplatin. [27] These compounds were designed to avoid the negative side effects of cisplatin in cancer therapies (Fig. 1.11).

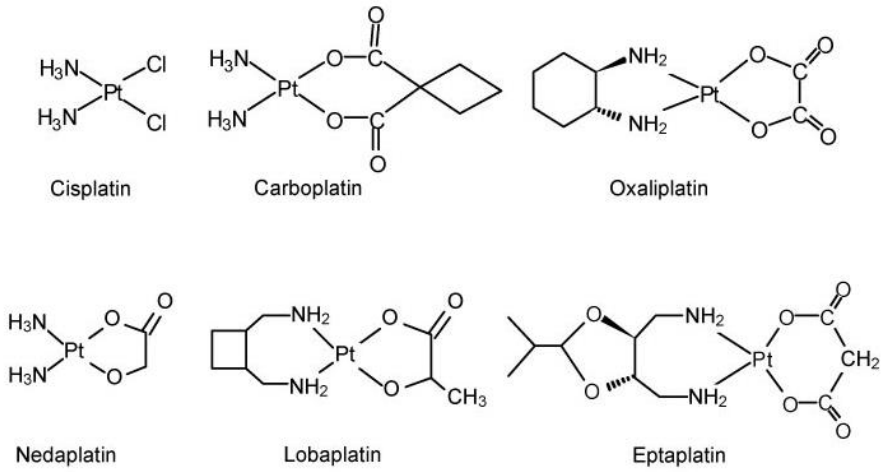

Fig. 1.11. The structures of three derivatives of cisplatin. Taken from ref 196.

Other non-platinum(II)–DNA covalent binders have also been designed in recent years. For instance, the titanium complex budotitane ([Ti(bzac)2(OEt)2] is one such well-known metallodrug with a very powerful anticancer property. Titanocene dichloride has also passed clinical trials. Hypothetically, this compound forms a covalent bond with DNA and is highly toxic to cancer cells. [29, 30]

1.3.2 Groove binding

DNA binding drugs generally act through one of the grooves of DNA, depending on their size and shape. Reversible electrostatic binding can occur by way of interaction between the positive sites of drugs and the negative sites of the phosphate backbone of the DNA helix. As a result of the fact that the major and minor grooves have different dimensions, to target them requires molecules with very diverse shapes. [32,33]

The difference in the dimensions of the two grooves is the reason for their differing interactions with various molecules. The width of the major groove is normally about 5.6 Å greater than that of the minor groove for the B-form ds-DNA sequence. [34]

1.3.2.1 Minor groove binders

The dimensions of the minor groove make it suitable for binding with small molecules, such as antibiotics; accordingly, this subject has become a research topic of high demand for scientists. In addition, the high binding affinity of the minor groove and its sequence specificity make it a more interesting mode of interaction than that of the intercalator binding mode. [221]

Minor groove binders are small molecules with a specific heterocyclic size and shape that can rotate freely. This property allows them to fit easily into the minor groove by the displacement of water. These molecules are useful in different areas of pharmacology, such as antiprotozoal, antiviral, antibacterial and antitumour. Although minor groove binder drugs are considered as an important class of antitumours in cancer therapy, only some are able to work as active anticancer agents in the body and to achieve good results in clinical therapy. [35]

Depending on their structure and potential sites, they are categorised into two different classes having either irreversible or reversible binds with DNA: the former class includes mitomycin C, anthramycin, CC-1065 and its synthetic analogues (carzelesin and adozelesin), enediyne antibiotics (neocarzinostatin, esperamicin A1 and calicheamicin g1), ecteinascidine derivative (ET-743) and bleomycin. These molecules cause permanent damage on DNA through irreversible binding with DNA nucleotides. The latter class includes distamycin A, diarylamines (DAPI, Berenil, and pentamidine), and bis-benzimidazoles such as Hoechst 33258. This group produces a reversible inhibition on DNA, and most of these compounds interact with AT-rich regions of DNA. [36,37]

One of these anticancer drugs, distamycin (3-[1-methyl-4-[1-methyl-4-[1-methyl-4-(formylamino)pyrrol-2-carboxamido]-pyrrol-2-carboxamid]pyrrol

carboxamid]propionamidin-hydrochlorid), is a natural pyrrole-amidine-antibiotic that possesses amino groups and three pyrrole rings, which can form a hydrogen bond with AT-rich regions of DNA as well as hydrophobic interactions. The terminal amidine group of the small molecule is basic and serves to attract the drug molecule to the negatively charged DNA phosphodiester backbone. The 2-amino group of guanine prevents distamycin from binding to the minor groove of GC base pairs by steric hindrance, thus conferring AT-selectivity on the drug molecule. In this way, distamycin inhibits transcription and increases the activity of topoisomerase II. Netropsin, another analogue of distamycin, has two *N*-methylpyrrole rings and demonstrates the same activities (Fig. 1.12). [38,39]

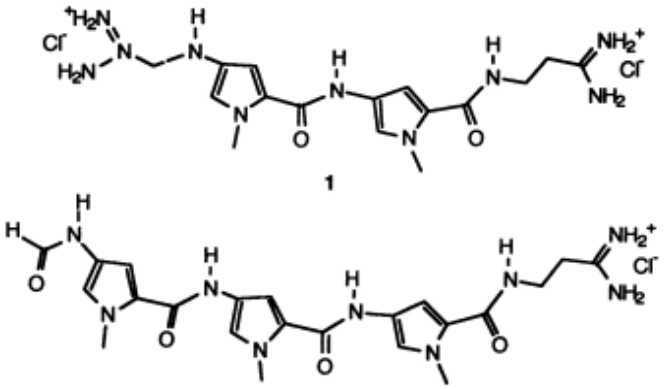

Fig. 1.12. DNA minor groove binding in oligopeptide netropsin (above) and distamycin (below). Taken from ref 204.

To increase DNA binding and the sequence selectivity of drugs, the semi-synthetic compound lexitropsin was synthesised as an analogue of distamycin and netropsin, to promote the relevant between similar units in the ligand and receptor. These polyamide molecules are designed to recognise the base sequence of DNA. The structure of lexitropsin, with three types of pyrrole units, imidazole and hydroxypyrrole give the full distinction of specific DNA base sequences (14–16 base pairs) (Fig. 1.13). [40, 41]

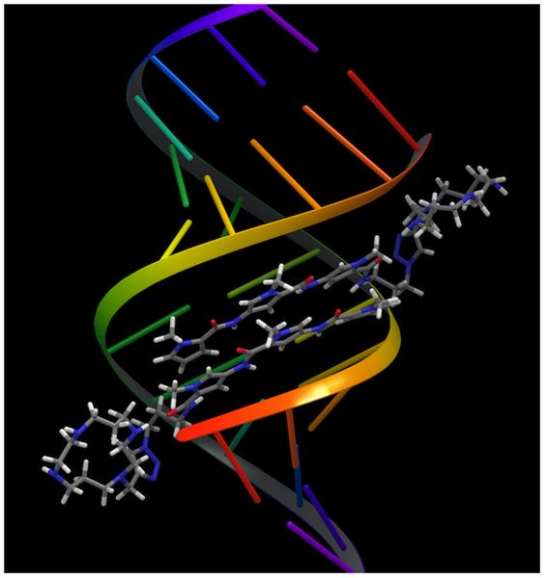

Fig. 1.13. Schematic representation of the interaction between lexitropsin and the AT-rich side of DNA. Taken from ref 38.

The di-nuclear zinc complex linked with azobenzene chromophore ligands, [Zn{meso-tetrakis-(N-methyl-4-pyridyl)porphine}]$^{4+}$, shows an affinity to the association in the DNA minor groove. The complex has been found to be self-associated between DNA minor groove strands and can cleave the DNA strands hydrolytically. This complex has two cis and trans isomers, which can be transformed into each other by photoisomerisation. However, only the cis isomer performs strand cleavage in the DNA minor groove (Fig. 1.14). [44,45]

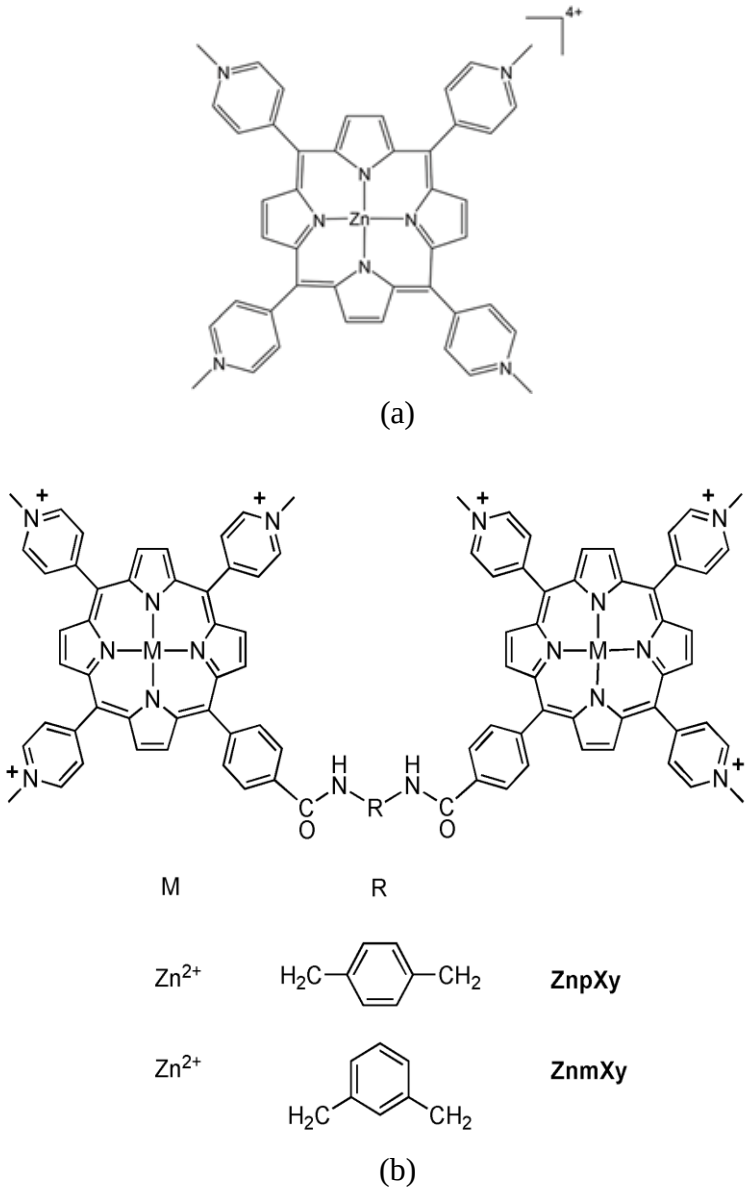

Fig. 1.14. a) The chemical structure of [Zn{meso-tetrakis-(N-methyl-4-pyridyl)porphine}]4+, the DNA groove binder; b) di-nuclear cis isomer of cationic porphyrins with different linkage factors represented (R). Taken from ref 215.

1.3.2.2 Major groove binders

While various metallodrugs that are minor groove binders have been studied during recent decades, limited reports exist of major groove binders in this category. Due to the fact that the major groove is wider than the minor groove, they are suitable for binding by DNA-protein interaction. On average, the major grooves represent 11.6 and 6.0 Å in B-form ds-DNA; this size is desirable for binding with small biomolecules such as proteins. [51] Therefore, the design of a special molecule with the ability to recognise the major groove of DNA with high binding affinity and sequence selectivity is desirable. The DNA transcript process could thus

be blocked by inhibiting the proteins binding with the major grooves of DNA, as a result of using major groove binder molecules. [51]

Metal-supramolecular compounds, depending on their size diversity, shape, the potential polarisability of their ligands and capability to form hydrogen bonds, can target the major groove differently. Transition metal complexes are known as interesting compounds with remarkable properties in terms of binding with DNA. Some examples include their varied coordination capacity to create a complex with different spatial geometry, various adjustable redox states to exhibit positive charges, and a vast range of other properties that make these compounds suitable for interaction with the DNA double helix in different modes. Because of their ability to utilise different binding modes to DNA (such as covalent and noncovalent binding), as well as their capacity for inducing DNA strand scission, these complexes can be applied as DNA probes and anticancer drugs. [32]

In recent decades, metal complexes have been considered because of their various possibilities, and have to be chosen from the list of transition metals (e.g. Rh, Ru, Os, Re, Pt, Cu, Co, Fe, Mn, and so on); in addition, various kinds of ligands can be investigated as photo nucleases. The properties of these ligands, such as their low energy and ability to form electronic bands in the visible region, are considered to be essential characteristics for metallodrug complex therapies. [32] For instance, rhodium complexes have been studied due to their DNA cleavage abilities; Rh(II) complexes containing polypyridyl aromatic ligands, [Rh(phen)2(phi)]3+, were designed and studied by Chow and Barton in 1992 as an anti double-strand DNA agent (Fig. 1.16). [51] This complex represents the ability to bind with the DNA helix in various modes according to its special stereochemistry, together with the properties of the aromatic ligands in a complex structure. It is important to note that this complex bind with the major groove by forming hydrogen bonds bond between the 9,10-phenanthrenequinone diimine (phi) groups of ligands with B-DNA, and with the hydrogen atom from C-3′at the intercalation site. [51]

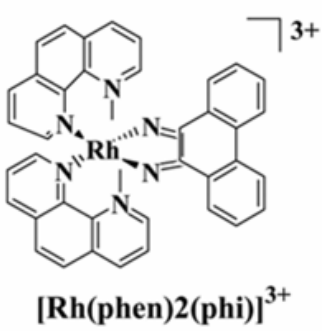

Fig. 1.16. The structure of Rh(phen)2phi3+, which targets openings in the DNA major groove. Taken from ref 51.

Copper complexes are mostly known as extensively studied examples of major groove binder compounds. The [Cu(ferrocenylmethylbis(2-pyridylmethylamine)(dppz)](ClO4) complex with two different ligands, ferrocenylmethylbis(2-pyridylmethylamine) and the dppz bind to the major groove of DNA, and exhibit photo-induced DNA cleavage properties under the light. (Fig. 1.18). [51] The results of photodynamic therapy (PDT) show that the complex shows DNA photo-cleavage under both visible (458 and 568 nm wavelengths) and red (647 nm wavelengths) laser light (Fig. 1.17). [51]

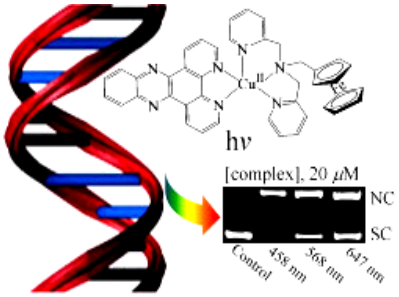

Fig. 1.17. Structure of the photo-interaction of [Cu(L)(dppz)](ClO4)2 complex with the DNA major groove. Taken from ref 46.

The diversity in the stereochemistry and physical properties of ligands in ruthenium(II) polypyridyl complexes are the reason why they are able to bind directly with both the major and minor grooves of DNA. [57] Research has shown that the major grooves of DNA are mostly occupied by compounds having a large size and adequate intercalation elements. One example of a ruthenium(II) complex is Λ-[Ru(3,4,7,8-tetramethyl-1,10-phenanthroline)$_3$]$^{2+}$ (Fig. 1.18), which has a tendency to intercalate on the GC-rich region of the major groove. [54]

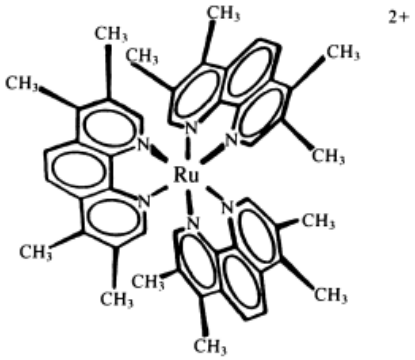

Fig. 1.18. The structure of Λ-[Ru(TMP)3]$^{2+}$, a major groove binder. Taken from ref 54.

The P and M isomers of the supramolecular iron complex [Fe2(L)3]$^{4+}$ (where L represents [μ-[4,4′-methylenebis[N-[(2-pyridinyl- κN)methylene]benzenamine-κN]]]) illustrates that the M enantiomer of the iron cylinder bonds with the major groove of DNA, and can induce dramatic intramolecular coiling. In contrast, the P enantiomer is unable to induce coiling, but can cover two phosphate backbones along the minor groove (Fig. 1.19). [55,56]

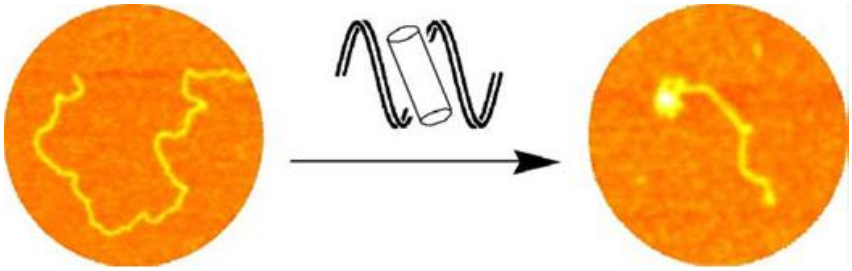

Fig. 1.19. Schematic representation of intramolecular DNA coiling induced by an iron triple helical cylinder. The picture demonstrates the AFM images of free linear plasmid DNA (on the left side of the picture) and the impact of the cylinder on linear DNA to make a small unexpected DNA coil (on the right side of the picture). Taken from ref 206.

The dinuclear ruthenium complexes [Ru2(1,10-phen)4L1]4+ and [Ru2(bpy)4L1]4+, where L1 represents (C5H4N)C=N(C6H4))2CH2), show a selective groove binding affinity when used in an enantiomerically pure form. [58] However, both phen complexes exhibit different activity when binding with DNA. The GC-rich sequence of DNA is the site of Δ, Δ-[Ru2(phen)4L1]$^{4+}$ interaction, and the AT-rich sequence is the target of another enantiomer. These represent different properties for DNA binding to iron cylinder helicates. [57]

1.3.3 Intercalation

The insertion of aromatic heterocyclic compounds (which are mostly flat, positively charged and planar) in between the base pairs of DNA's right-handed helix is called intercalation. After Lerman in 1961 [59], an extensive range of organic and inorganic chemical compounds have been designed as intercalator anticancer agents. In general, DNA intercalator agents act as anticancers by destroying the DNA transcription process and blocking cell division, leading to cell death. The π–π stacking interactions between DNA base pairs and the aromatic rings in drug structures are the factors that stabilise the insertion of the intercalator agents. Moreover, the combination of other types of interactions, such as van der Waals, hydrogen bonding and hydrophobic interactions, also plays a significant role in insertion stabilisation. [60] DNA unwinding takes place when the intercalator agents open a gap between the stacked base pair, which can occur in either major or minor grooves. Many metallo-intercalators as anticancers have been designed during recent years. It is important to note that these compounds commonly include anthracenes, phenanthrolines, acridines, anthraquinones, ellipticines and phenanthridines (Fig.1.20). [61]

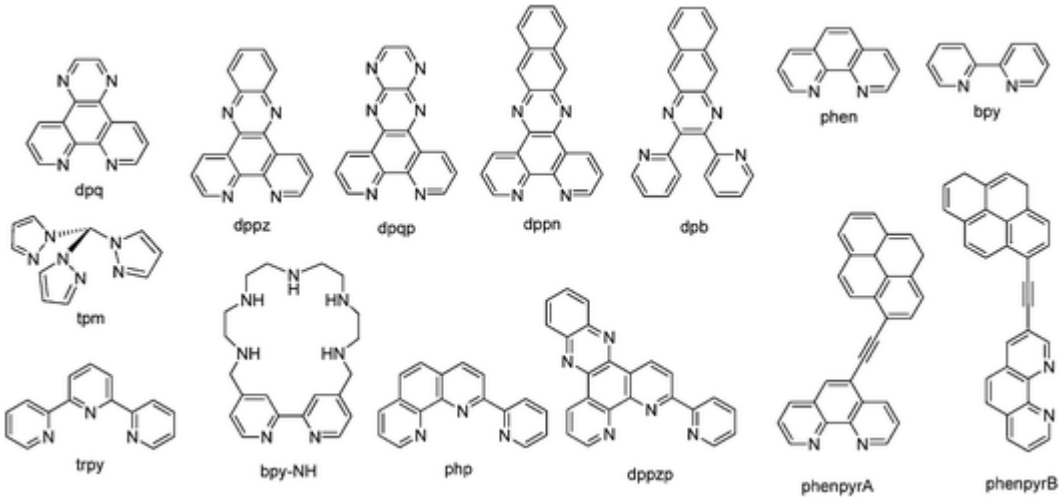

Fig. 1.20. The structure of various metallo-intercalator ligands. Taken from ref 207.

Notably, the aromatic ring systems play a significant role in modes of DNA interaction (see Figures 1.21 and 1.22). [61]

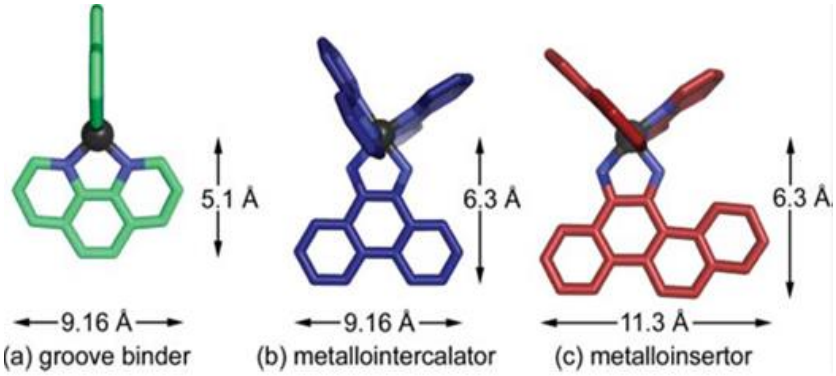

Fig. 1.21. Structural properties of: (a) groove binder; (b) metallo-intercalator; (c) metallo-insertor. Taken from ref 61.

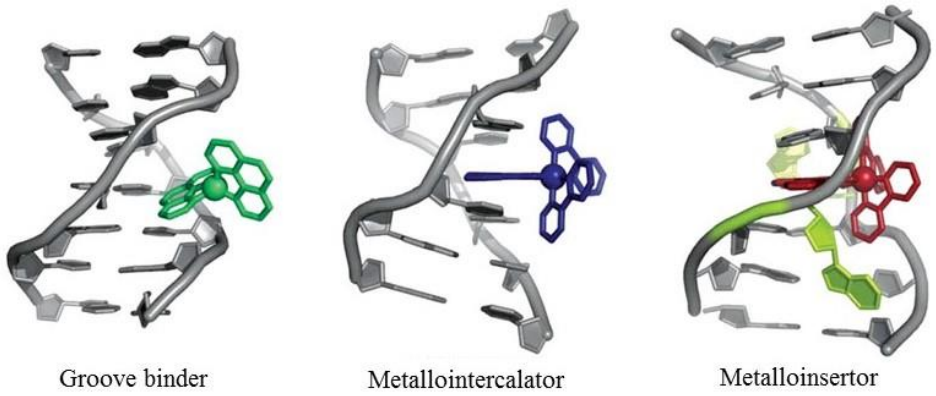

Fig. 1.22. Ligands with different aromatic ring systems represent different DNA modes of interaction. Taken from ref 64.

The first noncovalent DNA binding drug that has been widely used in cancer therapy is metallobleomycin. [62] This compound is part of the class of glycopeptide antibiotics, which was found in 1960. [62] A variety of metals, such as Cu(II), Zn(II) and Co(III), have been used as the central metal in the metallobleomycin structure, which forms an octahedral complex. Two octahedral forms and the positively charged tail of the complex are the reasons for the intercalation interaction with DNA (Fig. 1.23).

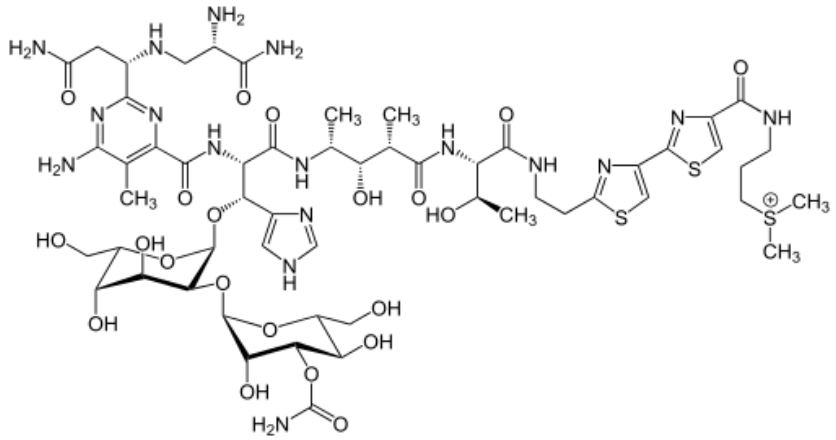

Fig. 1.23. A schematic representation of the bleomycin structure. Taken from ref 208.

One of the most important classes of metalloanticancers drugs are platinum complexes, which have displayed remarkable anticancer properties. The $[Pt(phen)(en)]^{2+}$complex with the general formula of $[Pt(IL)(AL)]^{2+}$ consists of two ligand parts: IL as an intercalating factor, and AL as a non-intercalating ancillary item. This complex generates DNA length and stiffness by intercalating into the DNA minor groove, particularly between the C3–G4 and T2–A5 base pairs (Fig. 1.24). [63–65]

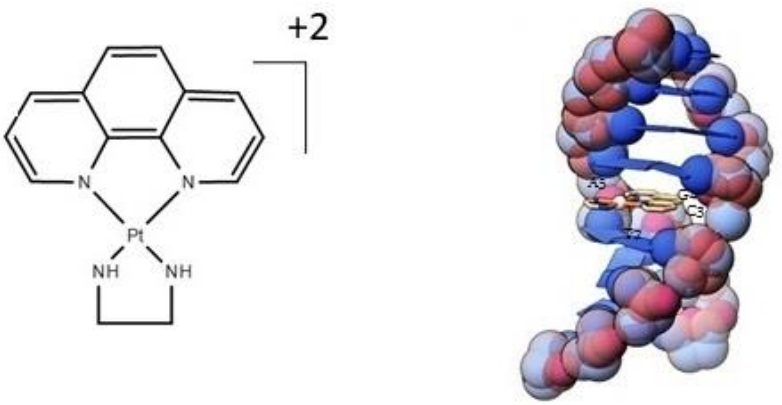

Fig. 1.24. The structure of $[Pt(phen)(en)]^{2+}$complex, and the molecular simulation of the complex intercalated with the DNA sequence $d(GTTGCAAC)_2$. Taken from ref 74,53.

The complex ligands play a significant role in complex biological activity, such as DNA affinity. For example, the positive charge of the complex causes the activation of both cellular uptake and DNA affinity. [66]

Octahedral ruthenium(II) complexes are known as effective anticancer active compounds, and have demonstrated low toxicity and fluorescence properties in therapies. For instance,

$[Ru(phen)3]^{2+}$ with two optical isomers (Λ/Δ) has shown significant biological activity against cancer cells (Fig. 1.25). Studies show that both chiral enantiomers function differently in cells, due to their optical properties. Furthermore, their spectral properties (i.e. their fluorescent properties) is dramatically increased after forming a bond to DNA, which makes them very attractive for application as DNA fluorescent probes. [67,68]

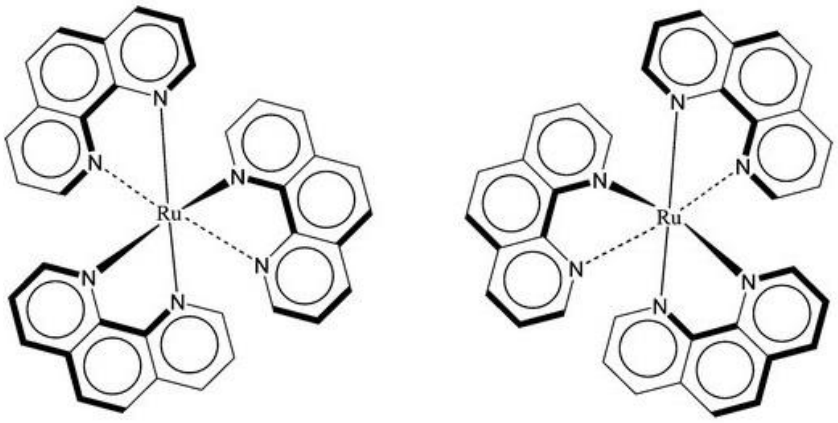

Fig. 1.25. The structures of two optical isomers (Λ/Δ) of [Ru(phen)3]2+. Taken from ref 208.

The type of metal in the metallo-intercalator compound plays an important role in its relative biological activity in terms of its binding affinity to DNA. Complexes of copper, zinc and nickel with the N4-tetradentate ligand, such as [M(N,N'-bis-5-(triethylammoniummethyl)-salicylidene-2,3-naphthalendiiminato)]n+, represent intercalating insertion with differing DNA binding affinity. When comparing the abovementioned metal complexes such as Ni, Zn, and Cu, it is evident that their spherical geometry is the key factor in their DNA affinity and insertion. As an example, square planar shapes, such as Ni complexes, are able to insert more deeply between DNA base pairs than octahedral shapes, such as Zn and Cu complexes. Copper complexes of phen and its derivatives have shown significant results in cancer treatment and as antibiotics. When an activating compound is present, DNA cleavage can occur by oxidising agents generated by the DNA-copper complex in cells. [69] For example, the [Cu(N-(9Hpurin-6-yl)benzenesulfphonamine)(phen)2] complex with two phenanthroline

parts, which formed effective bonds with the serinol bridge, caused considerable DNA cleavage in studied cells (Fig. 1.26). [70–72]

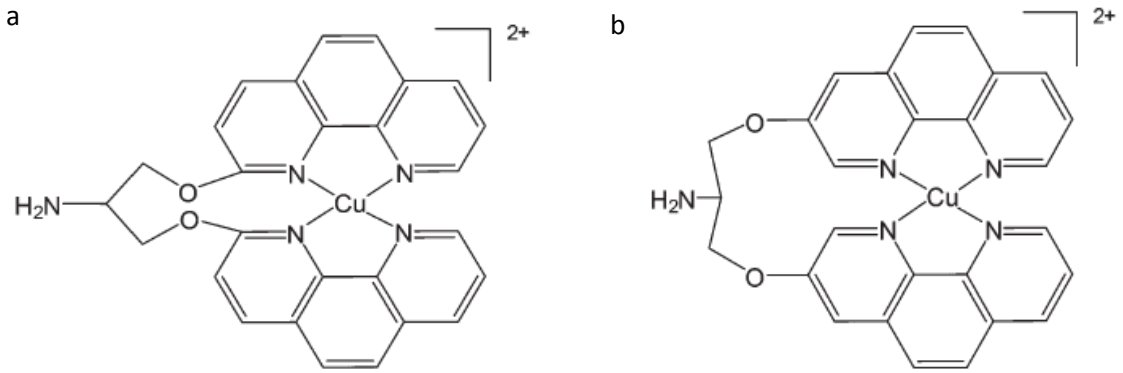

Fig. 1.26. The structures of two copper DNA intercalators: a) [Cu(3-clip-phen)]2+, and b) [Cu(2-clip-phen)]2+. Taken from ref 73.

A lot of research has been done on rhodium complexes that represent good results in cancer therapy based on their high selectivity on DNA sequences to linking and their ability of nuclease-cleaving. For an example the octahedral rhodium complex: Δ-[Rh(phi)(*R*,*R*-Me2trien)]3+ (where phi is 9,10-phenanthrenequinone diimine and *R*,*R*-Me2trien - 2R,9R-2,9-diamino-4,7-diazadecane) intercalates between GC base pairs of the DNA major groove by forming hydrogen bonds between the guanine parts and amine groups of the phi ligand (Fig. 1.27). [73]

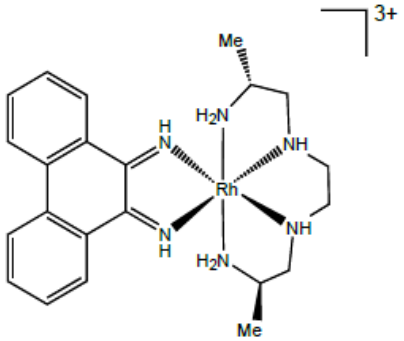

Fig. 1.27. The structure of Δ-[Rh(phi)(R,R-Me2trien)]3+. Taken from ref 73.

1.3.4 Y-junctions

Three-way junctions (3WJ), are not the simplest and most commonly occurring branched nucleic acids detected in abnormal DNA structures related to a genetic disease, such as

Huntington's disease. They have a special structure with three double helical arms, A, B and C, which are connected to one another at the junction point. This consists of some unpaired bases in at least one of the junction's hands. When one strand in a major groove (termed the third strand) forms a bond with the DNA double strand, the 3WJ is formed; an acidic pH is necessary at this point. [74] Y-junctions represent a lack of stability compared to DNA double helix strands, so they are suitable targets for metallodrugs to stall the DNA fork at a higher ratio than DNA duplexes. For instance, Hannon designed an iron cylinder with the formulation [Fe2{μ-[4,4′-methylenebis[N-[(2-pyridinyl-κN)methylene]benzenamine-κN]]}3] which flawlessly fits into the central cavity of the Y-junction structure. The iron cylinder can also block the centre of a 3WJ in RNA (Fig. 1.28). [75]

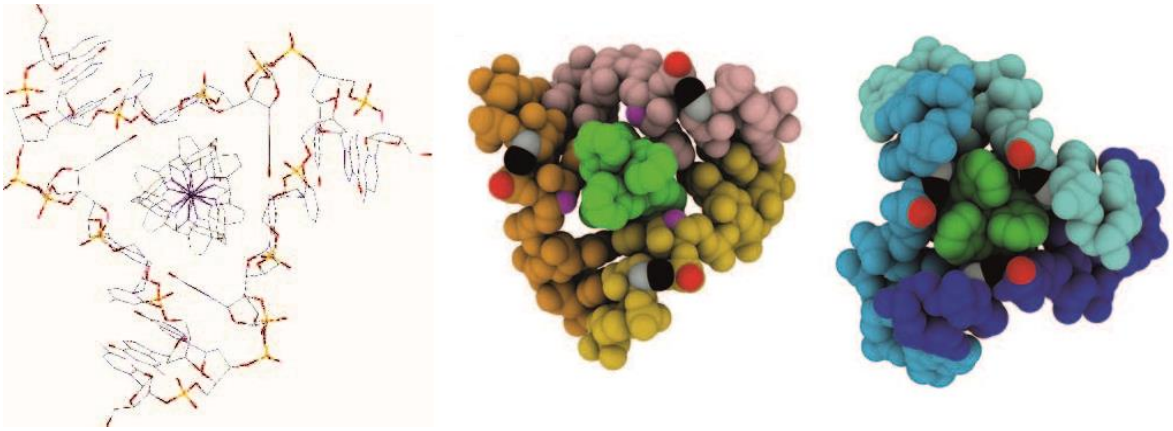

(a) (b) (c)

Fig. 1.28. a) The crystal structure of the cylinder's 3WJ interaction in RNA; space-filling models of the 3WJ blocked with a cylinder (shown in green) in: b) RNA and c) DNA. Taken from ref 74.

1.3.5 G-quadruplexes

G-quadruplex DNA or QDNA structures are forms of DNA and are rarely found in the telomeres and believed to be formed transiently in the promoter regions of genes in the human genome. G-quadruplexes are generated by self-assembly in Hoogsteen fashion, and consist of the basic G-quartet unit (four guanines of base pairs bonded together). Notably, metal ions play a key role in the structure's stability (Fig. 1.29). [76]

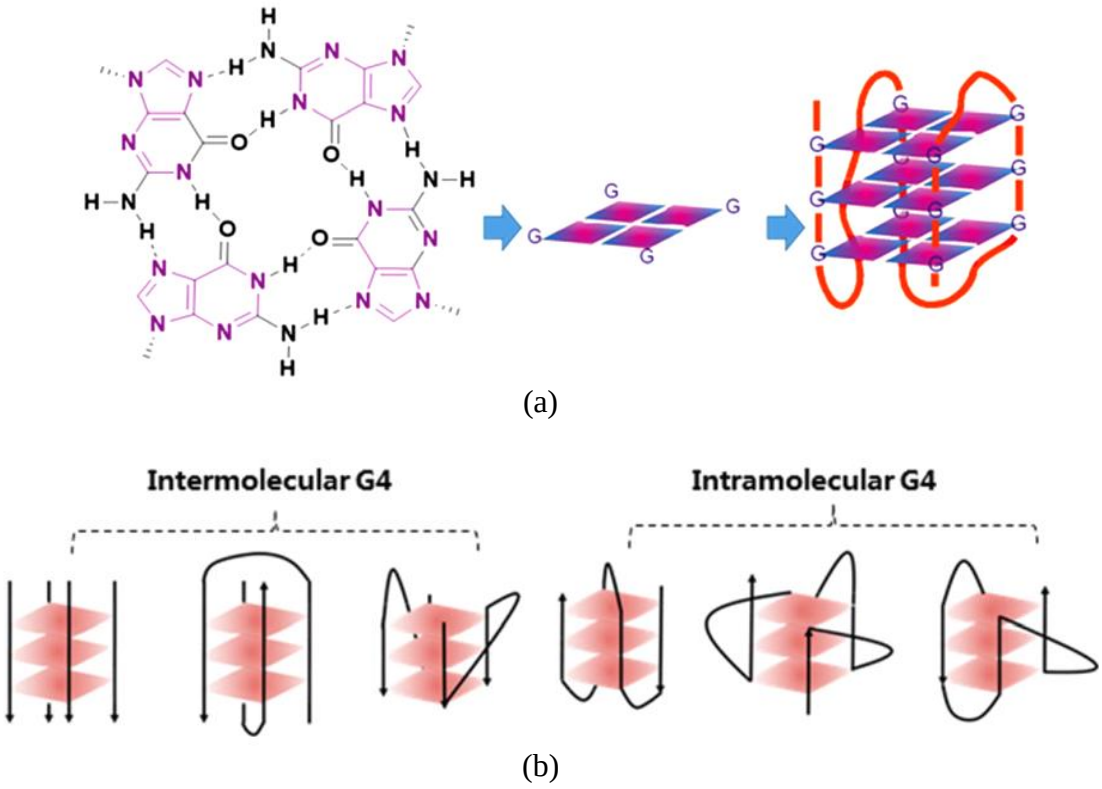

Fig. 1.29. a) Scheme of a G-quartet and the form of an intermolecular G-quadruplex structure; b) various representations of G-quadruplex arrangements, both intermolecularly and intramolecularly. Taken from ref 73.

The G-quadruplex form of DNA is a structure that can stall the terminal transferase or telomerase enzyme if the formation of QDNA occurs at the 3′ end of the telomeric DNA. [76]

The stabilisation of this structure is therefore a significant factor in cancer therapies. As mentioned above, metal ions play a key role in structure stability. Studies confirm that alkali metal cations such as Na^+ or K^+ can stabilise this structure by forming coordinated bonds with the oxygen atoms of guanine carbonyl in the central G-quartet channel (Fig 1.30). [77,78]

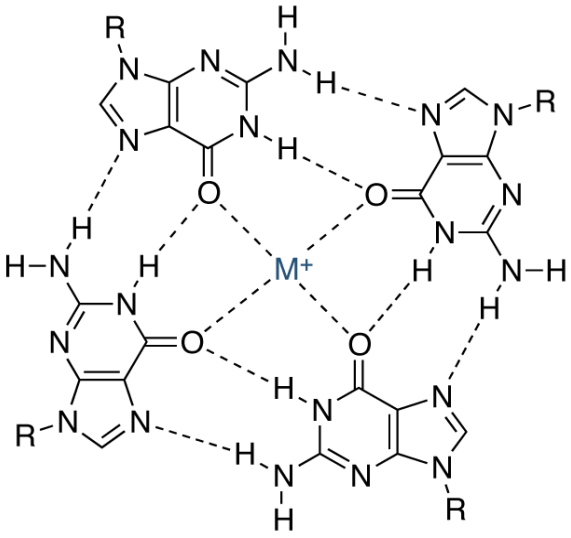

Fig. 1.30. Coordination bonds between oxygen atoms, hydrogen atoms and an alkali metal in the centre of the G-quartet channel, which improve the stability of the structure. Taken from ref 77.

Importantly, the activity of telomeric DNA of cancer cells, meaning that terminal transferase activity in cancer cells is high and reaches about 85%; however, it is silent in normal human cells. [79,80] The activity of telomerase guarantees maintaining the DNA of telomeric cancer cells. Moreover, DNA transcription is blocked when the G4 structure is formed in G-rich single strands. Thus, the inhibition of this enzyme and DNA transcription with the G-quartet structure key roles in cancer therapy. Small molecule ligands in the structure of anticancer drugs can interact, stabilise or selectively cleave the hTel G4 structure or its promoter, in order to treat the targeted cancer cells (without the side effects caused by drug toxicity in normal cells). [81]

However, cisplatin as a famous anticancer is classified as a small metallodrug that can interact with the G4 structure and cause cell apoptosis. Cisplatin is not a targeted selective drug, and causes severe side effects due to its interaction with various biomolecules in cells besides the G-quartet structure. Many investigations of metallodrugs targeting the G4 structure have been initiated recently. For example, a variety of ligands have been used in the structures of drug complexes, such as metallophthalocyanines, metallocorroles, metal–salphen, metal–salen, metal–phenanthroline and their derivatives. [82]

The Au III in metalloporphyrin complexes, gold(III)–TMPyP4 (Fig. 1.31), is one compound that has shown good results in stabilising hTel G4, and is also known as a strong telomerase inhibitor. This complex can inhibit the telomerase enzyme with a good inhibition rate of 57%

by blocking the PCR (Polymerase chain reaction)amplification of a G4 sequence. The toxicity of this anticancer in normal nasopharyngeal cells is IC50 > 50 μM. [82]

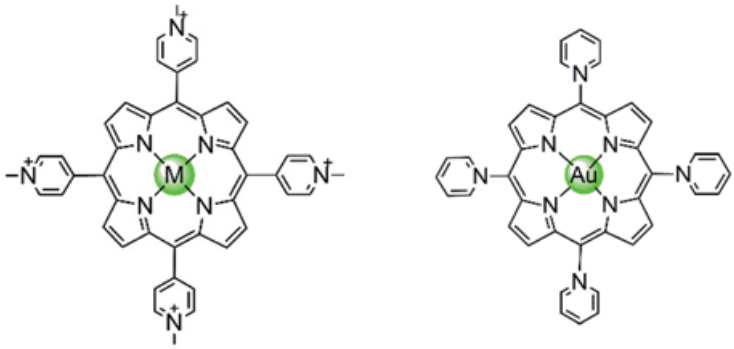

(a) **(b)**

Fig. 1.31. a) A scheme of the total structure of metal-TMPyP4 as kinds of G-quartet ligands; b) the structure of gold(III)–TMPyP4 complex. aken from ref 81.

Meso-methylpyridinium-substituted Mn(III)–corrole, as a type of metallocorrole complex, has a high toxicity in cancer cells, with values of 2.37 and 1.52 μM. This water-soluble complex can stabilise hTel and c-myc G-quadruplex DNA with the desired shape and electron concentration (Fig. 1.32). [73–85]

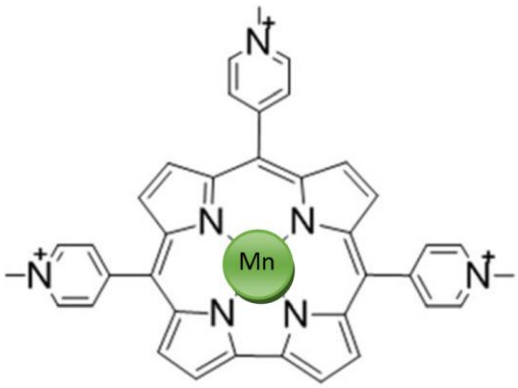

Fig. 1.32. Structure of the Mn(III)–corrole complex, with cationic side arms as G-quartet ligands. Taken from ref **81**.

Cylinders are a new class of G4-targeted chiral binders. Their properties have been recently studied as anticancers in biological systems; for example, the ability of selective QDNA interaction with a bimetallic triple helical cylinder of Ni was studied by Qu et al. (Fig. 1.33). [86]

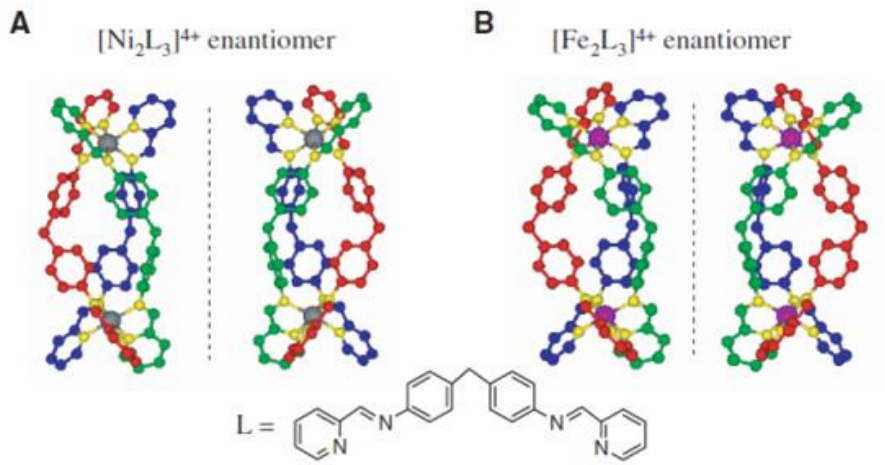

Fig. 1.33. a) Structures of the M-enantiomer (left) and P-enantiomer (right) of the [Ni2L3]4+ cation; b) structures of the M-enantiomer (left) and P-enantiomer (right) of the [Fe2L3]4+ cation. Taken from ref 209.

While both cylinders can stabilise hTel G4 DNA or telomeric QDNA, the P-enantiomer is more active in binding with the G4 structure. The cell can be protected from the endonuclease enzyme when the cylinder forms bonds with hTel G4, as a result of the electrostatic interaction generated by the metal's positive ion charge in the cylinder structure (Fig. 1.34). [86]

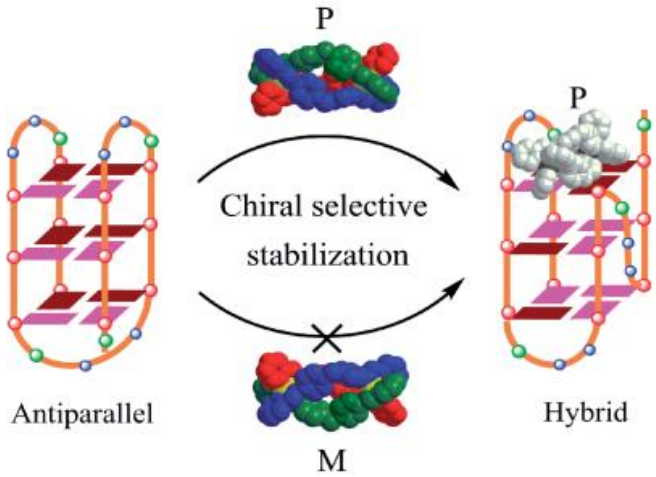

Fig. 1.34. The selective recognition of the supermolecular cylinder of telomeric G-quadruplex DNA. Taken from ref 209.

1.4 Metal complexes and their therapeutic effects

For centuries, metals have had medical applications. [57] More recently, modern metallodrugs have also demonstrated excellent results in treating various kinds of diseases, such as cancers. Their properties can be investigated using a variety of methods, such as: a) by in vitro study,

to survey their effects on targeted live cells and tissues; and b) by in vivo study with xenograft tumour models.

Organometallic compounds, which are the combination of classic inorganic compounds with organic ligands, have thus become a new field of research in chemistry.

One of the most extensively researched topics is metallodrugs, which aim to bind to DNA in a non-coordinative manner. This is because noncovalent DNA interactions with various functions have been already seen in nature. [87]

Metal complexes are known as compounds with high potential to engage in interactions with different biological targets in vivo. Metallodrugs can form different kinds of interactions with intracellular targets, such as irreversible (covalent) and reversible (noncovalent) bindings. For instance, titanocene dichloride $[Ti(CP)_2(Cl)_2]$ is known as one of the most famous anticancer drugs has successfully passed its clinical trial. This complex can form covalent binding to DNA. [88,89] Although the square planar structure of titanocene is similar to that of cisplatin, the hydrolysis of halide ligands within this complex (in order to bind to DNA) happens outside the cells. Accordingly, a multinuclear complex can be formed as an active product. [90]

Two zinc and cobalt complexes can interact with DNA (by noncovalent binding) through associations inside the DNA groove. For example, cis-$[Co(en)_2(bpy)_2]^{+3}$ exhibits toxicity in cancer cells with separation in DNA strands after association within the minor groove. [71,72]

Because copper and zinc are naturally present in the human body and have a critical influence upon cellular functions, they have been extensively used as DNA nucleases in medicinal chemistry. [93]

The zinc complex [Zn(L)2]2+, L is 2,6-bis(1-phenyl-1H-benzo[d]imidazol-2yl)pyridine (bpbp) (Fig. 1.35) was recently reported. This complex shows high toxicity against various cell lines, such as the IC50 2.9 -0.3 μM value in MCF-7 cells. It's important to note that the p53 gene, which is activated in response to any intracellular stresses such as DNA damage, can induce cell apoptosis. In this case, the activation of the p53 gene following DNA cleavage generated by intercalation of $[Zn(L)2]^{2+}$ complex through the DNA structure can thus theoretically cause cell apoptosis. [94,95]

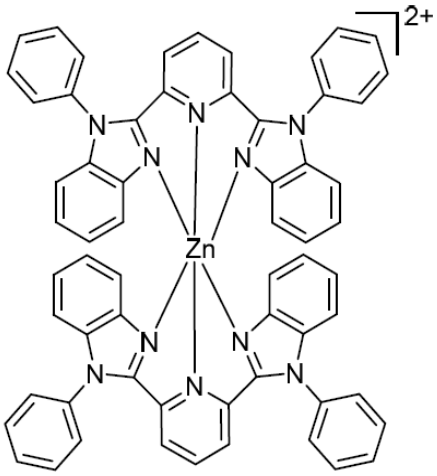

Fig. 1.35. The structure of the $[Zn(bpbp)2]^{2+}$complex. Taken from ref 73.

The natural bioavailability of copper, in addition to its role in angiogenesis and increased uptake in cancerous tissues, has resulted in its wide range of applications in medicinal inorganic chemistry, and more specifically in antibacterial and anticancer agents for many years. [96,97] There are some properties that make copper complexes suitable as important anticancer agents. As it has a variety of different coordination numbers, copper is able to form complexes with various geometries that can interact with similar molecules in different manners. [100,102] Moreover, the intercalation of copper complexes through the DNA structure with the ability of DNA cleavage (independent of oxidising agents) plays a critical role in DNA damage and cell death. [100,101]

While there are a variety of copper complexes with the capability of anticancer activities, its phenanthroline complexes have shown low-micromolar activity against many different cancer cells, such as SKOV3. Figure 1.36 presents the structure of phenanthroline copper complexes and the possibility of its different ligands. [214]

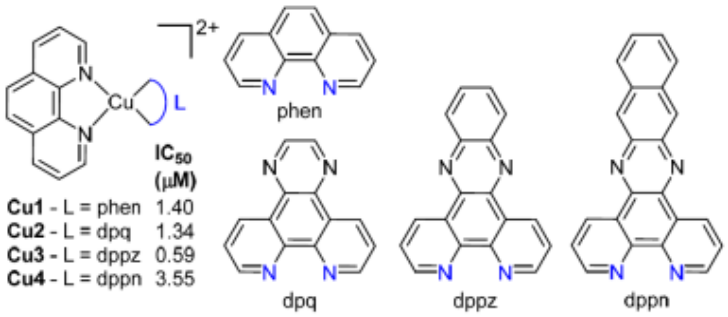

Fig. 1.36. The structure of the [Cu(phen)(L)] complex with different ligands. Taken from ref 214.

1.4.1 Platinum-based anticancers

One of the most famous metal anticancer drugs that has been sold to treat various kinds of cancers is cisplatin, the so-called ‘DNA paradigm’. The discovery of cisplatin by Rosenberg et al. in 1965 laid the foundation for the current developments in organometallic drugs as anticancers. [104] Cisplatin can show great results in curing various kinds of cancers, specifically testicular cancer (with a 90% cure rate). [105] Over time, this compound has represented successful clinical treatment, thus making it the first popular platinum anticancer drug.

In recent years, other platinum complexes have been introduced to the pharmaceutical market as new targeted cancer therapy medicines, such as carboplatin, lobaplatin, oxaliplatin and nedaplatin. These compounds are used in 50% of all cancer chemotherapies.

Cisplatin analogues can bind to DNA and stop the replication process, and thus the cause of cell death. [106,107] Although cisplatin and its analogues react with various parts of cells’ biomolecules, DNA remains an important target. [108,109]

1.4.1.1 DNA as a target of cisplatin

Research has shown that uptaking cisplatin through cells occurs by a passive diffusion process, or sometimes by active transportation. In addition, cisplatin’s labile chloride ligands are a cause of cisplatin–DNA binding in cells (Fig. 1.37). Normally, neutral cisplatin molecules undergo hydrolysis inside cells due to the fact that cells have a very low concentration of chloride ions (2–20 mM), in spite of the high concentration of chloride ions (100 mM) in arteries. Replacing chloride ions with water can generate the positive charge needed for cisplatin to facilitate favourable interactions with polyanionic nucleic acids. [110] The $[Pt(NH3)2Cl(OH2)]^{+}$ complex is formed during this process and plays a significant role in forming a bond with DNA, mostly with certain nitrogen atoms of purine bases in DNA at the N^{7} position. These free positions of nitrogen do not bind to other DNA bases, so they are free to form a bond with cisplatin. Accordingly, the DNA double helix is opened and the transcription process is subsequently inhibited. The failure of DNA transcription activates proteins in the network of intracellular signals called DNA damage response, in order to repair the damage. Finally, cell apoptosis occurs after repeated failure to repair damage. [111]

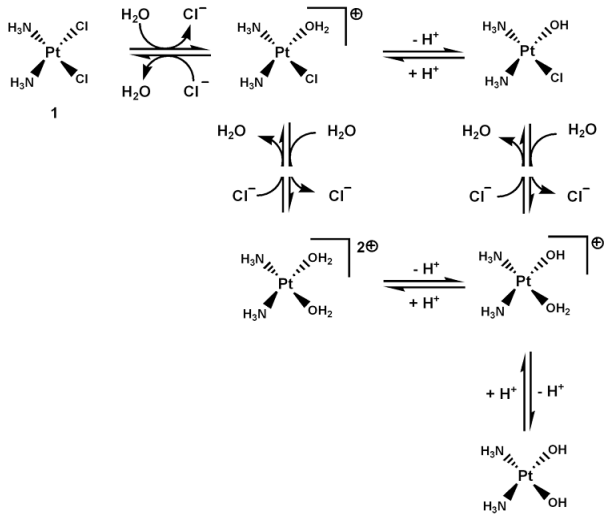

Fig. 1.37. The intracellular hydrolysis mechanism of cisplatin. Taken from ref 111.

As shown in Figure 1.39, cisplatin can impact on cancerous cells in several ways: by targeting DNA, RNA, mitochondria, sulphur-containing enzymes such as metallothionein nucleotide acids, and proteins. [112]

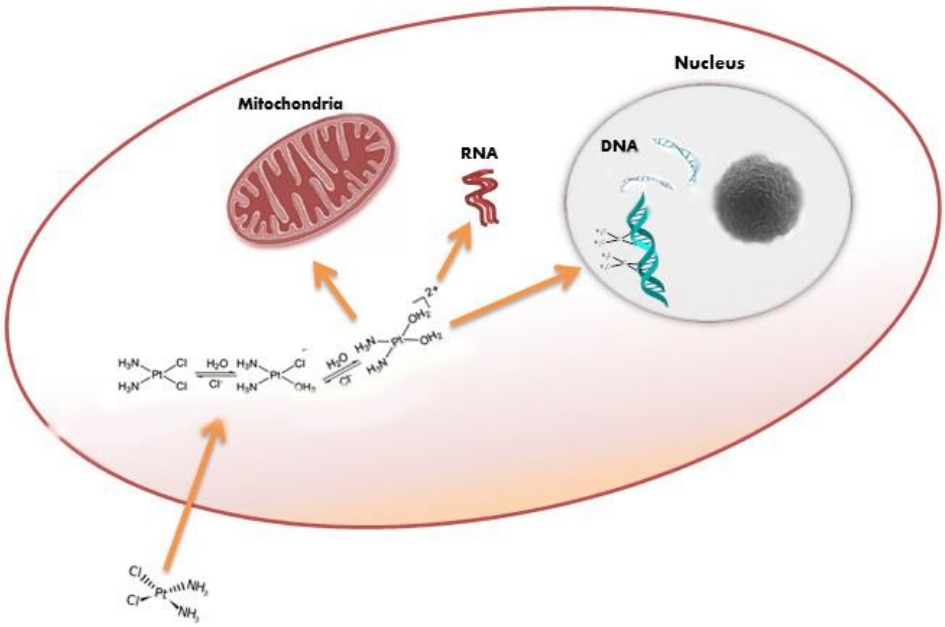

Fig. 1.39. A scheme of cisplatin hydrolysis inside the treated cell and its three possible apoptotic pathways through targeting DNA, RNA, and mitochondria.

The toxicity of cisplatin arises from crosslinking cellular DNA, which can repress DNA replication and transcription, thus causing apoptosis. The geometry of cisplatin is an

important characteristic that has an impact on its anticancer activities. Diamminedichloroplatinum has two cis and trans geometric isomers; unwinding of the helix occurs when the cis configuration forms intra-strand crosslinks with DNA, causing transcription to stall and consequently cell apoptosis. Transplatin (the trans isomer) degrades quickly in vivo and does not work as an anticancer. Because of the separate strand crosslinking (1,2-interastrand and 1,3-interastrand) performed by transplatin, it can be repaired easily, in contrast to cisplatin (Fig.1.40). [113] Moreover, the square planar form of a platinum(II) complex helps to better bind with DNA strands, and Cl- substitution in a complex with the nitrogen of the DNA base occurs more easily in cisplatin than in transplatin. [114, 115] The bond formed between DNA and cisplatin is irreversible.

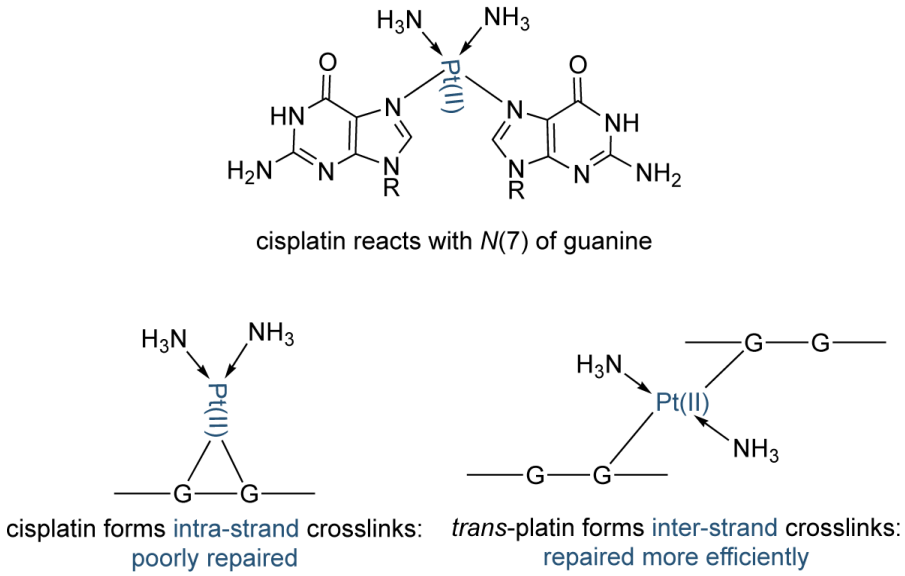

Fig. 1.40. A schematic representation of the difference between cisplatin and transplatin in binding with guanine-7 of DNA strands. This illustrates the possibility of cisplatin forming intra-strand crosslinks, and transplatin forming inter-strand crosslinks. Taken from ref 200.

There are various forms of DNA adduction with cisplatin, such as 1,2-intrastrand crosslinking, interstrand crosslinking, monofunctional adduction, and protein–DNA crosslinking, all of which are presented in Figure 1.41. [115]

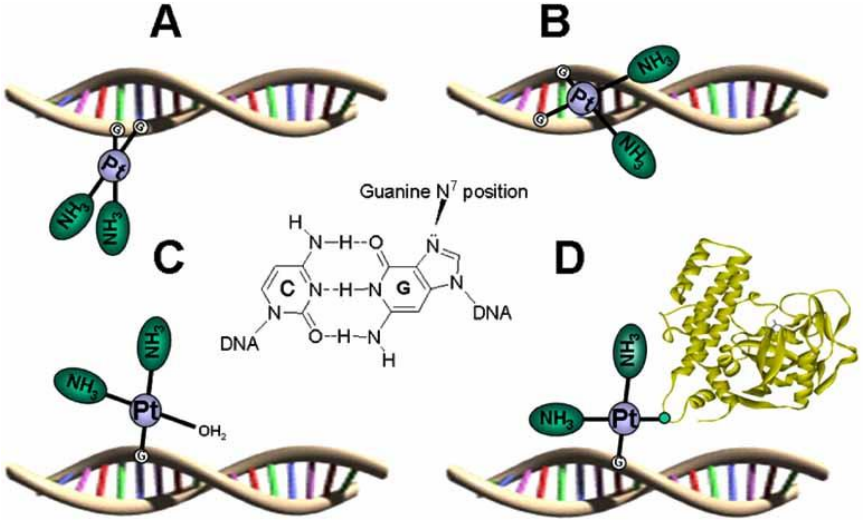

Fig. 1.41. a) 1,2-intrastrand crosslinking; b) interstrand crosslinking; c) monofunctional adduction; d) protein–DNA crosslinking. Taken from ref 224.

Interstrand crosslinks can also be generated between DNA and cisplatin between two Gs on opposite sides of the duplex. It has been shown in the literature that most crosslinks are formed as 65% 1,2(GpG) and 25% 1,2(APG). [116] Furthermore, it has been confirmed that the intrastrand crosslink between cisplatin and N_7 atoms of guanine in the DNA structure (1,2 strand DNA adduct) can change the DNA structure to bend at 45º. One theory claims that the toxicity of cisplatin is caused by this bending form of the double helix, particularly towards the major groove. [117]

DNA repair occurs on the 1,3interastrand crosslink with higher efficiency than at the 1,2 strand DNA adduct with high mobility group proteins; this is another reason for cisplatin's toxicity in cancerous cells. [18,119] A low concentration of these high mobility group proteins, in order to perform excision repair, is observed in healthy cells (Fig. 1.42). [18,120]

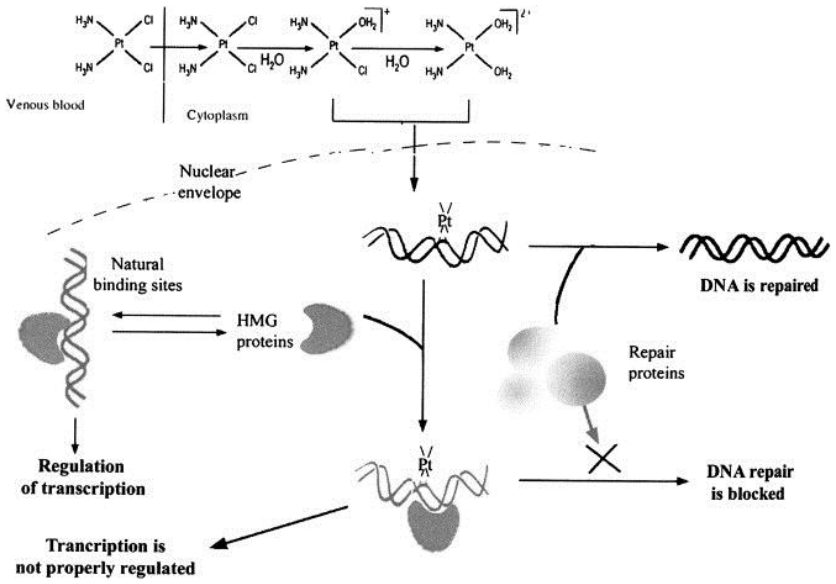

Fig. 1.42. Scheme of the cancer cell apoptosis process under exposure to cisplatin. Taken from ref 231.

Various cancer cells, such as ovarian carcinoma, non-small human lung carcinoma and breast adenocarcinoma, are resistant to cisplatin. There are a number of reasons for this resistance: an ineffective drug dose, cell success in platinum DNA adduct repair, the disabling of cisplatin following adduction to the sulphur enzyme, and deactivation of the programmed cell suicide pathway. [121]

Cisplatin's mechanism of action on mitochondria has not yet been determined clearly; however, there is some evidence that the interaction between cisplatin and mitochondria DNA could be the reason for cell death. Meanwhile, the interaction of cisplatin with enzymes (which contain sulphur) is known to be a reason for cell resistance to cisplatin. [112]

DNA is regarded as an important target in cancerous cells therapy in many studies. For example, the research of Lippard et al. on HeLa cells [121,105] determined that 22 platinum atoms are bound per DNA molecule, in contrast to one platinum atom per mRNA, one per 30 rRNA, one per 1,500 tRNA and one per 1,500 protein molecules. These explain why cancer cell lines show wide ranges of response and different patterns of sensitivity to cisplatin.

Incidentally, the interaction of cisplatin with RNA has received far less attention in the literature, although recent research is more focussed on this interaction. There are two reasons why it plays a less significant role than the interaction between cisplatin and DNA. First, damaged RNA by cisplatin can be easily repaired. Second, the covalent binding interaction

between RNA and cisplatin does not show considerable toxicity against cancer cells in vitro. The results represent just 0.1–10% of RNA damage in studied cells. [122]

The use of Pt(II) anticancer drugs is limited due to their severe side effects, such as nephrotoxicity, neurotoxicity, ototoxicity, nausea and vomiting. [123] To avoid these drawbacks of cisplatin, scientists have decided either to use other generations of cisplatin analogues, or to create effective non-platinum anticancer compounds such as iron, titanium, rhodium and ruthenium complexes. [124] Because of their special properties, these transition metals can form complexes with the vast majority of biomolecules as ligands, and can also form specific interactions to DNA. These characteristics make them very good alternatives for cisplatin. [125,126]

1.4.1.2 Iron-based anticancers

Iron is an essential element which plays a significant role in biological processes such as DNA synthesis. It displays two common oxidation states (+2 and +3), and the transformation between the two forms of iron (Fe^{+2} and Fe^{+3}) via electron transformation is the reason that it is a significant element in biological reactions. Moreover, iron unusually exhibits higher oxidation states: Fe(V), Fe(VI), Fe(VII) and Fe(VIII), which can play significant roles as catalysers in biological oxidation reactions. [127, 128] Accordingly, iron complexes have been extensively studied for over a decade as effective anticancers in biological systems.

With regards to their outstanding biological roles, interest in using iron complexes as an anticancer has grown since the early years of the new millennium. Ferrocenium picrat and ferrocenium trichloroacetate salts are two of the very first iron complexes used to treat cancers (Fig. 1.43). [129]

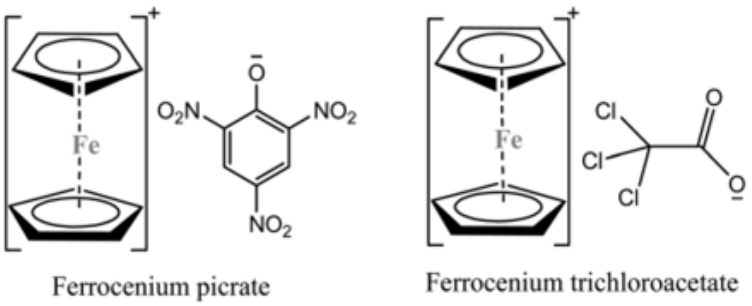

Fig. 1.43. The structure of ferrocenium picrate and ferrocenium trichloroacetate. Taken from ref 129.

One of the most important characteristics of anticancer drugs is tumour-specific treatment (i.e. their tumour-specific action). This ability to act selectively towards molecular targets is the cause of reduced side effects in chemotherapy.

Two thiosemicarbazone-based iron(III) complexes, 5-methyl-3-formylpyrazole-N(4)-dimethylthiosemicarbazone and 5-methyl-3-formylpyrazole-N(4)-diethylthiosemicarbazone, were reported by Ghosh et al. [130] to demonstrate considerable toxicity in HeLa cells. These iron complexes with pyrazolyl thiosemicarbazones ligands are able to interrupt and block DNA synthesis (Fig. 1.44). [130]

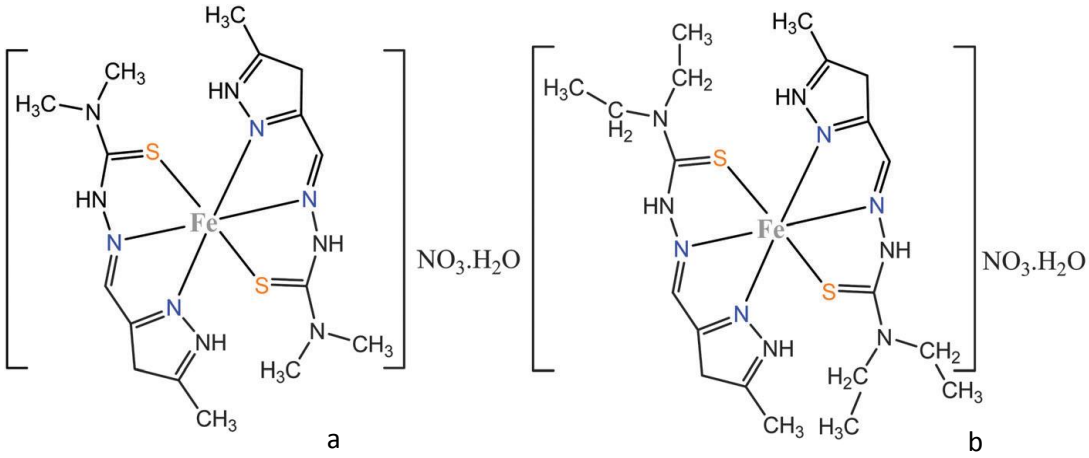

Fig. 1.44. Structures of iron complexes; a) 5-methyl-3-formylpyrazole-N(4)-dimethylthiosemicarbazone, and b) 5-methyl-3-formylpyrazole-N(4)-diethylthiosemicarbazone. Taken from ref 129.

The ligand type present in the complex has an important role in the biological properties of metallodrugs. Salen ligands and derivatives, such as alkoxyl, hydroxy-, alkyl- or trihalomethyl, are known as effective ligands which possess considerable anticancer properties. Moreover, iron complexes containing monodentate azole-derived ligands demonstrate intense toxicity against various cancer cell lines such as HeLa, A549, A2780, MCF-7, G-361 and HOS. The toxicity of these compounds as anticancers in cancer cells are far more significant than that of cisplatin in those cells. Figure 1.45a presents one of these complexes, which displays severe toxicity against the ovarian carcinoma human cell line (A2780) with an IC50 value of 58 nM, while cisplatin produces a value of about 13 µM. [131]

There are many iron(II/III) complexes with several coordination bonds with chelating ligands which play the role of anticancer agents in therapies. Intracellular reactive oxygen species (ROS) are generated by iron chelate complexes, and providing a deoxyribonucleotide is the cause of DNA damage. Consequently, these complexes deactivate the human ribonucleotide reductase and interrupt DNA synthesis and repair (Fig. 1.45b). [132]

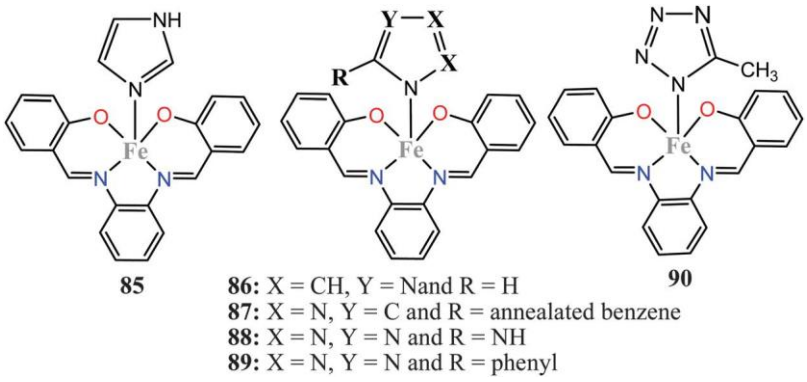

(a)

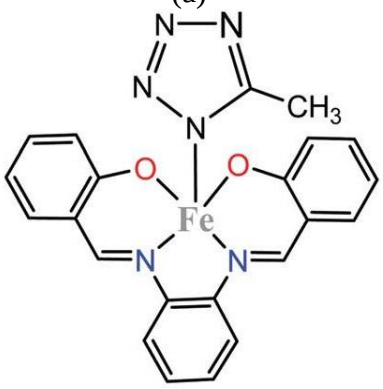

(b)

Fig. 1.45. a) Iron(II/III) salophen complexes (85–90) containing monodentate azole-derived; b) the structure of iron(II/III) salophen complex. Taken from ref 131,136.

In this class, iron(II) bleomycin complex (Fig. 1.46) is one of the most successful anticancers that has passed clinical trials to treat testicular carcinoma with high cure rates. [134,135] The complex is made by coordinating five nitrogen atoms of bleomycin glycopeptide to an iron(II) ion, as the metal centre of the complex. Bleomycin possesses amines, pyrimidine and imidazole functional groups in its structure, and is thus an effective N-terminal metal-binding domain. [133,142]

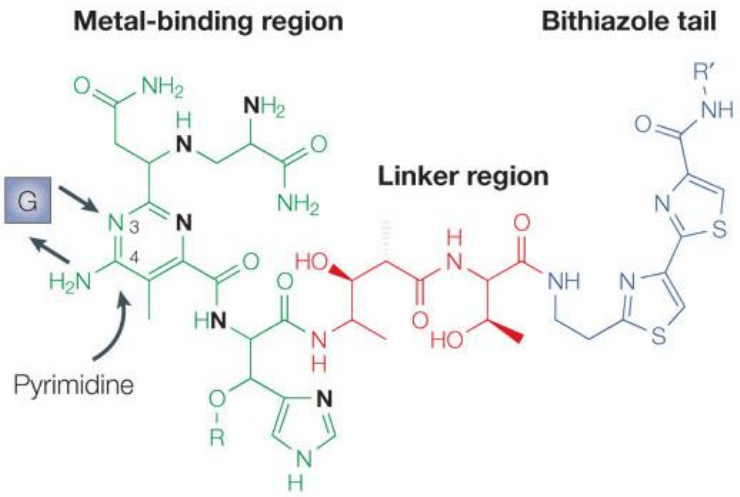

Fig. 1.46. Structures of bleomycin A, representing the variety of the molecule's functional domains. Taken from ref 132.

Apoptotic cell death occurs following DNA damage produced by the bleomycin–FeIII_OOH complex. This structure is produced by coordinating iron and dioxygen, which subsequently provides superoxide ($O_2^{\bullet-}$) as a kind of reactive oxygen species (ROS) and a factor of DNA destruction. [136]

The ferrous-triapine complex (Fig. 1.47) is another example of this anticancer class which plays a significant role as hRRM2/hRRM1 and p53R2/hRRM1 inhibitors in vitro. [137]

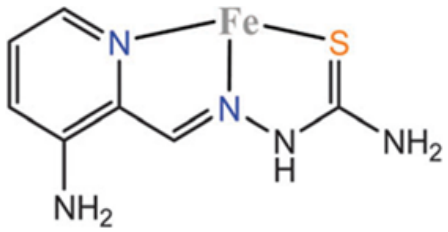

Fig. 1.47. Ferrous-triapine complex structure. Taken from ref 129.

Iron multinuclear complexes with more than one metal centre linked to DNA display different modes of DNA binding, such as DNA crosslinking, bisintercalation and DNA–protein crosslinking, which make them interesting as anticancer agents.

The cytotoxicity of iron(III) complexes with the total formula $[Fe(salen)(\mu\text{-}L)]_n$ have been studied in different cancer cell lines such as A549, HeLa, HOS, G361, MCF-7, A2780 and A2780cis. L was one of the heterocyclic ligands including nitrogen with free donor electrons

such as imidazole, 5-methyltetrazole, 5-aminotetrazole, 1,2,4-triazole, benztriazole and 5-phenyltetrazole. These complexes demonstrate high toxicity against all of the aforementioned cancer cell lines. For instance, $[Fe(salen)(\mu\text{-atz})]_n$ and $[Fe(salen)(\mu\text{-phtz})]_n$ complexes exhibit IC50 values of 0.39 ± 0.05 µM and 0.40 ± 0.17 µM against A2780, respectively. However, on average this value is 0.2-0.5 µM against A2780 cells (Fig. 1.48). [138]

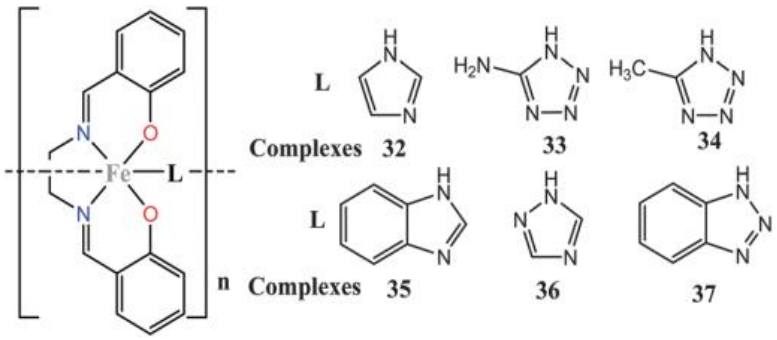

Fig. 1.48. The structure of [Fe(salen)(µ-phtz)]n complex and its possible optional ligands. Taken from ref 129.

It is also important to note that some iron complexes have been defined as effective DNA strand cleavage agents with promising anticancer activities. For example, tris(diimine)iron(II) complexes, rac-[Fe(diimine)3](ClO4)2, have been reported as this class of anticancer. Complexes with different diimine ligands display different toxicity against MCF-7 cells; the complex with 2,2¢-bipyridine (bpy) as a diimine ligand has an IC50 value of 32 µM, while 2,5,6-dimethyl-1,10-phenanthroline (5,6-dmp), dipyrido[3,2-d:2¢,3¢-f]quinoxaline (dpq) and 1, 1,10-phenanthroline (phen) have values of 0.8, 20, and 28 µM, respectively (Fig. 1.49). [139]

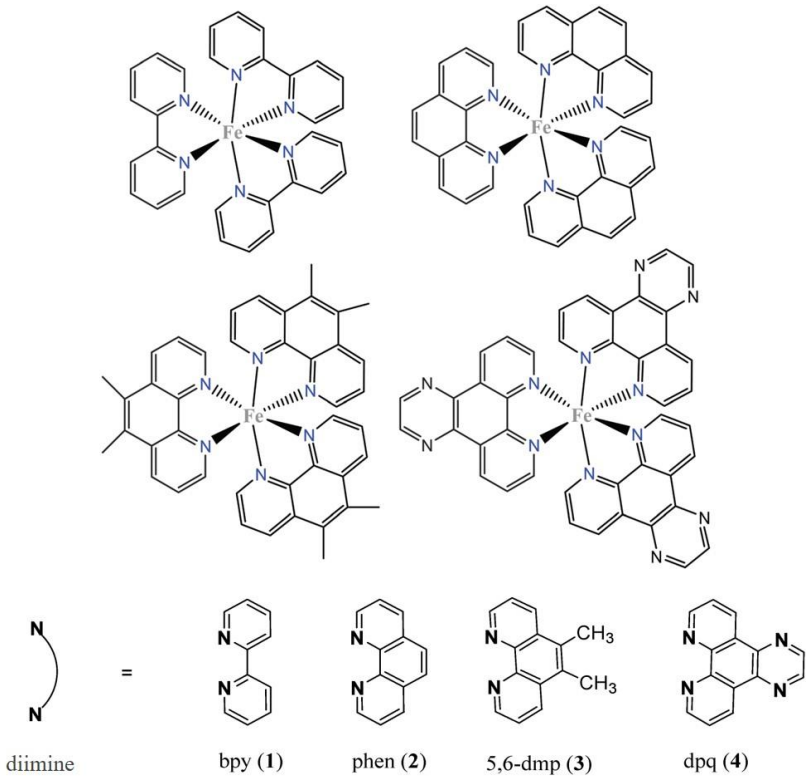

Fig. 1.49. The chemical structures of tris(diimine)iron(II) complexes with different possible ligands. Taken from ref 210.

On the other hand, they display interaction with circulating tumour DNA, and cell apoptosis occurs following DNA cleavage after oxidative DNA binding. [140]

1.4.1.3 Ruthenium-based anticancers

During the past decade, extensive research has been carried out to find a good alternative to platinum complexes for synthesising anticancer drugs. Organoruthenium complexes have been found to be some of the most effective non-platinum complexes, and show very good results at treating cancerous cells. Ruthenium compounds have displayed various types of interaction with DNA, such as covalent binding, intercalation, bisintercalation and groove binding. According to the research of Fruehauf and Zeller in 1991 [141], the toxicity of ruthenium complexes is dependent on their ability to bind to DNA. Inhibition of DNA replication, possession of mutagenic activity, DNA repair and decreased RNA synthesis all arise from the way that ruthenium compounds bind with DNA.

Ruthenium complexes perform the nontoxic transport of iron with high stability in vivo and in vitro, with special properties such as a lower toxicity than other chemotherapeutic agents.

Ruthenium complexes can also imitate the biological activities of iron, especially in binding with significant targets such as DNA. In addition, the low toxicity of these compounds makes them a suitable alternative to platinum anticancer drugs, particularly in those cells that are resistant to cisplatin. [142]

The antitumour property of cisplatin is related to its ability to damage DNA arising from the square-planar shape of the cisplatin complex. Owing to the octahedral structures of ruthenium(II) and (III), the functions of these complexes as antitumours should differ from that of cisplatin.

The range of oxidation states of ruthenium (Ru^{II}, Ru^{III} and Ru^{IV}) is one of its advantages compared to platinum. This redox activation is most important in transferring electrons in order for metal-based drugs to play their anticancer role. In addition, ruthenium can form a stable complex with an anticipated structure and the ability of substitution rate. The imine sides of biomolecules are known as excellent selective targets to bind to ruthenium inside cells, in order to generate its anticancer capability. [146]

There are two ruthenium(III) complexes that have entered clinical trial regulations: NAMI-A (imidazolium trans-[tetrachlorido(imidazole)(dimethylsulphoxide) ruthenate(III)) [147] and KP1019 (indazolium trans-[tetrachloridobis(1H-indazole)ruthenate(III)] [149], which affect the process of metastasising to prevent secondary cancers by presenting notably low toxicity. [148,150] These compounds both perform covalent binding to DNA, despite having different mechanisms of action, and both have special characteristics to avoid tumour metathesis in their own ways (Fig. 1.50). [151–152]

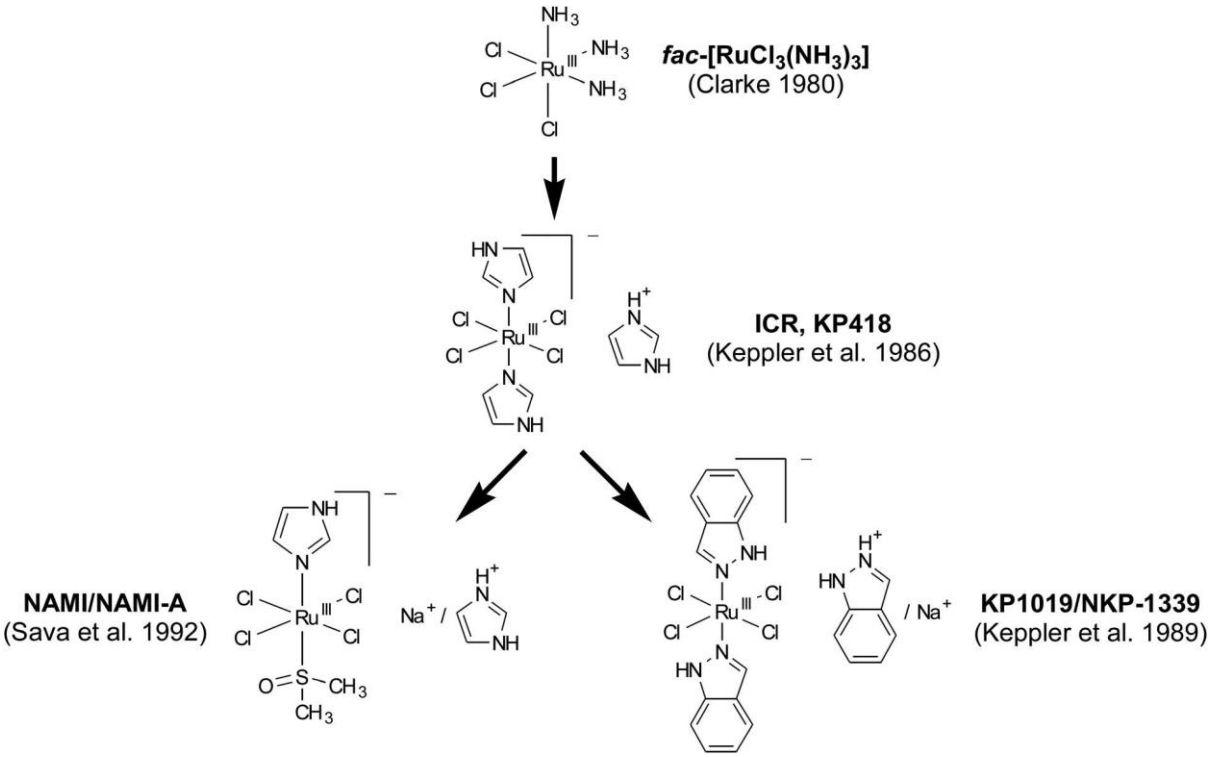

Fig. 1.50. Genealogy of ruthenium anticancer drugs from 1980 till the discovery of NAMI-A (the subject of clinical evaluation). Taken from ref 149.

There are some ruthenium(II) complexes (including 2,2'-bipyridine) that, as ligands with low toxicity, work as anticancer agents. These structures display fluorescent properties that make them suitable for spectroscopic studies. [153] For instance, the ruthenium complex $[Ru(phen)2(dppz)]^{2+}$ is used as a fluorescent DNA probe in drug delivery studies. Since this complex exhibits fluorescent ability in vivo, after binding to DNA it can become a very good choice for study. Moreover, the mode of intercalation of this ligand through DNA can vividly alter its fluorescent properties. [154, 155], and the size and charge of ligands has a direct influence on intercalating the octahedral metal complex in interaction with DNA. [156]

Recently, Chen *et al.* reported the ruthenium(II) complex with the anticancer property of causing mitochondrial dysfunction. The complex has a structure of $[Ru(MeIm)4(L)]2^{+}$ (where MeIm is 1-methylimidazol and L is 2-(4-chlorophenyl)-1H-imidazo[4,5-f] [1,10]phenanthroline, Ru4, or 2-phenyl-1H-imidazo[4,5-f] [1,10]phenanthroline, Ru5) and was studied in the A549 cell line at the G0/G1 phase. Apoptosis, involving ROS accumulation and Bcl-2 and caspase family activation, occurred as a result of interrupting mitochondrial activity. [157] The toxicity of this complex is comparable with cisplatin in a vast range of cell lines, such as HeLa cells. Its IC50 value against HeLa cells is 27 and 25 μM for Ru4 and Ru5, respectively, compared to a value of 15 μM for cisplatin (Fig. 1.51).

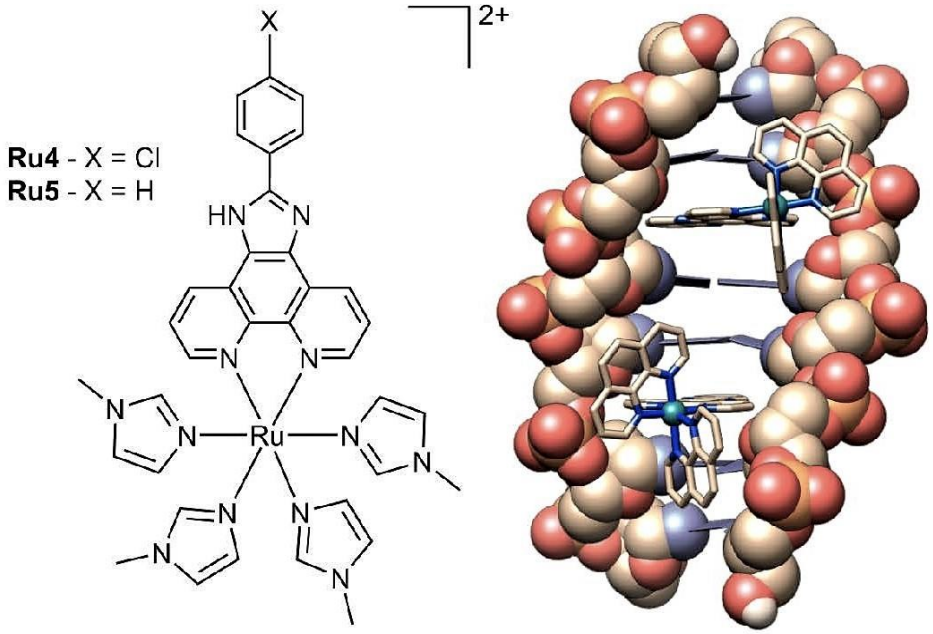

Fig. 1.51. The structure of the ruthenium polypyridil complex, and the X-ray crystal structure of rac-[Ru(phen)2(dppz)]$^{2+}$ bound to DNA sequence d(ATGCAT)$_2$. Taken from ref 73.

Their DNA affinity can be improved by increasing the number of metal centres, ruthenium herein, to enhance the pharmacological activity of drugs accordingly. For example, the complex [{Ru(dpq)2}2μ-(phen-5-SOS-5-phen)]$^{4+}$ exhibits a DNA affinity about 1,000 times greater than that of [Ru(dpq)2(phen)]$^{2+}$ and is in the intercalation class of DNA interactions (Fig. 1.52). [73]

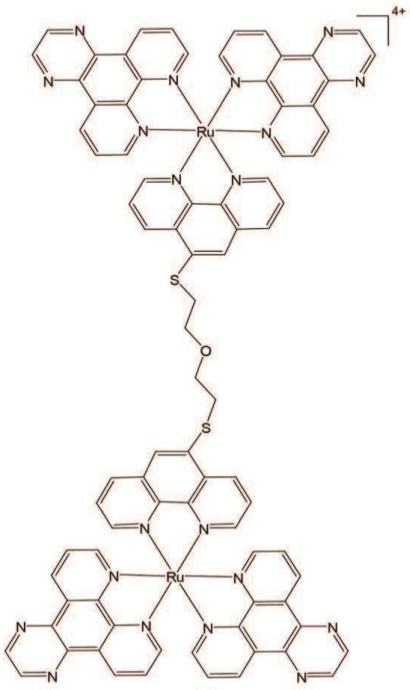

Fig. 1.52. Chemical structures of the ruthenium bisintercalators [{Ru(dpq)2}2μ-(phen-5-SOS-5-phen)]4+. Taken from ref 73.

The ruthenium porphyrin complex [Ru(phen)2MPyTPP] exhibits a high affinity for binding to the DNA telomere G-quadruplex by noncovalent π–π stacking interaction. [73] Furthermore, Zheng *et al.* reported that the Ru(II) complexes demonstrate a high affinity for binding to c-myc G4 DNA in groove binding mode, and that cell apoptosis can subsequently occur. [158] [Ru(III)(salan)(PPh3)Cl] complex is a new DNA groove binder compound which has shown good results in treating ovarian and breast cancers.

Following intracellular activation by reduction, ruthenium compounds with anticancer activity enter tumours and bind to cellular DNA. However, this is only the case where the lone pair electron on nitrogen has a tendency to undergo metal ion coordination. Subsequently, most often the histidyl imidazole side in protein and the N7 site of imidazole in the ring of the purine nucleotide are coordinated selectively by the ruthenium core of the complex. Because of differing ligand geometry between their complexes, ruthenium compounds show different ability to bind DNA and different cytotoxicity subsequently. [159]

Binding between octahedral ruthenium compounds and guanine in DNA chains can provide crosslinking that manifests as a bend in the DNA structure. In this way, the ligands of

ruthenium complexes play a key role in DNA interaction and form strong bonds with DNA strands or with different biomolecules. Accordingly, ruthenium complexes exhibit superior abilities to form strong chemical bonds with a vast range of electronegativity and electron density. [160]

Moreover, there is a theory that ruthenium(III) works in a similar way to prodrugs in cells. They can be activated after metabolism to an active form of pharmaceutical medicine within the body. Therefore, they are less toxic in general than cisplatin. [163,162] It is worth noting that the property of reduction (Ru III to Ru II) in vivo plays a significant role for coordinating more quickly to DNA, and is termed activation by reduction. The difference between normal and tumour cell metabolism is the key to understanding why ruthenium complexes have such an important function as anticancers. Due to the fact that the tumour growth process is so fast, oxygen and nutrition are used up quickly in these cells. As a result, cancer cells often witness dramatic hypoxia as their required energy is made from glycolysis. [163,164] Lactic acid resulting from glycolysis metabolism reduces the pH of cells and alters the electrochemical potency. The reduction of Ru III to Ru II is made easier under acidic conditions inside tumours. There is evidence that Ru II can form a stronger bond to DNA than Ru III, so Ru III activation by a reduction in tumour cells (by hypoxia) plays a key role in the toxicity of ruthenium(III) complexes in cancer therapy. In contrast, the transformation of Ru II to Ru III through an oxidation reaction rarely occurs in cancer cells. [165–167]

1.5 Metallo-supermolecular helices

Helices are special structures found in biological systems, in vital biomolecules such as proteins with an alpha-helical shape, DNA with its double-strand helical structure, and triple-strand helical collagen proteins. Helical structures are formed by organic ligands with different coordinating binding sites (capable atoms) that can make a helical axis by coordination to metal ions. Visually, it seems that metal ions are wrapped by ligands. Helicates are formed by self-assembly; the subunits must be pre-designed, and they therefore play a key role in the formation of the helical structure. The planar structure of metal helicates depends on the metal coordination number and the number of ligand binding sites. These structures are designed with a variety of ligand numbers (one, two and three) and different metal ions. [168]

In recent decades, a vast range of metal helicates have been synthesised using different metals and ligands such as rhodium, copper, silver, iron and ruthenium. The silver core with a slight helical twist was reported by Constable *et al.* in 1988 [162]; this helicate includes a single strand, 2,2’:6’,2”:6”,2”’:6”’,2””-quinquepyridine (La) with five nitrogens as electron donors which bind to silver(I) to shape the compact single-strand helicate. [169]

Many double and triple metal helicates have been recently designed. Metal ions in a double-strand helix mostly represent four-coordinate geometry, but iron(II), nickel(II) and ruthenium(II) are good examples of double-strand helicates that form six-coordinate metal centres. Meanwhile, triple-stranded helicates are generally formed by using three-, six- or nine-coordinate metal ions. For instance, the synthesis of triple-strand complexes was reported by Zhang and Dolphin in 2010 [170], who reported multinuclear octahedral bis(dipyrromethene) complexes with Fe^{+3} and Co^{+3} as nuclear metal ions, and helicates with a racemic mixture. [170]

The helical ruthenium complex designed by Piguet et al. consists of the ligand Lh, as shown in Figure 1.53a. This ligand, with its various nitrogen atoms, is capable of donating several electrons to ruthenium to make a double- or triple-strand cylinder. A self-assembled heteronuclear helical cylinder is formed as a result (Fig. 1.53b). [171]

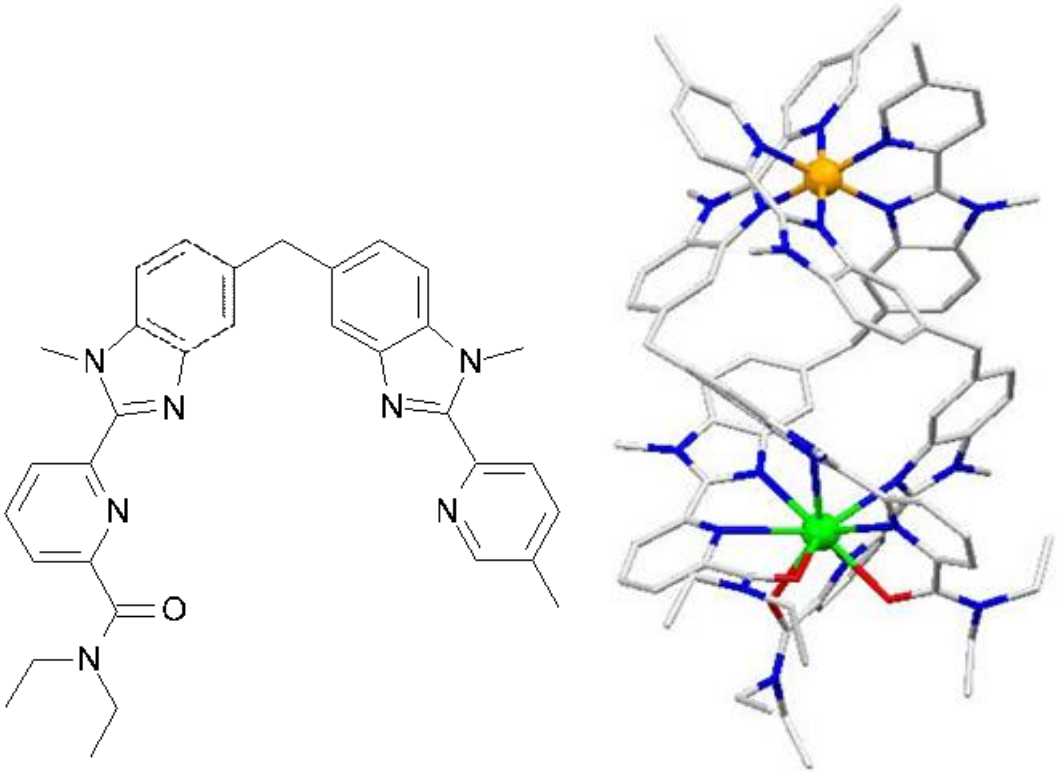

(a) (b)

Fig. 1.53. a) The ligand Lh; b) Piguet's heteronuclear helicate. Taken from ref 101.

The supermolecular metal helicates are known as important compounds that possess significant anticancer properties in various cancer cell lines. Direct interaction with DNA is considered as the most important property of smart anticancer drugs, which these complexes represent.

1.5.1 Cylinders

Special helicates with a DNA major groove binding affinity were designed and synthesised by Hannon's group [194] in order to treat various kinds of targeted diseases, in an effective, nongenotoxic and clever way. The pyridylimine ligands (L) (Fig. 1.54) are basic elements of helicates with the ability to bind with various kinds of transition metals, such as Fe(II), Co(II), Ni(II), Zn(II) and Ru(II), to make a special helicate called a cylinder. [172–174]

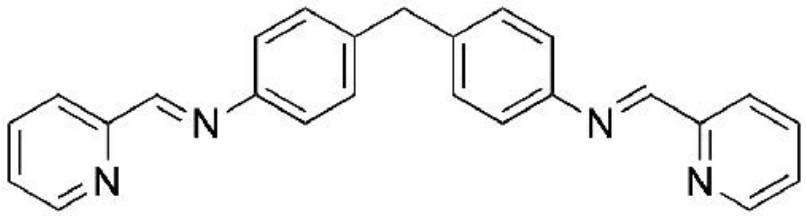

Fig. 1.54. The chemical structure of pyridylimine ligands (L). Taken from ref 194.

This ligand is synthesised by the reaction between bis(4-aminophenyl)methane and 2-formylpyridine in ethanol conditions for two hours. The formation of a tetracationic dinuclear triple-stranded helicate with the formulation $[M_2(L)_3]^{4+}$ can be synthesised by a one-pot reaction. This cylinder includes three strands of the ligand wrapped around the metal centre. The scheme of this reaction is shown in Figure 1.55.

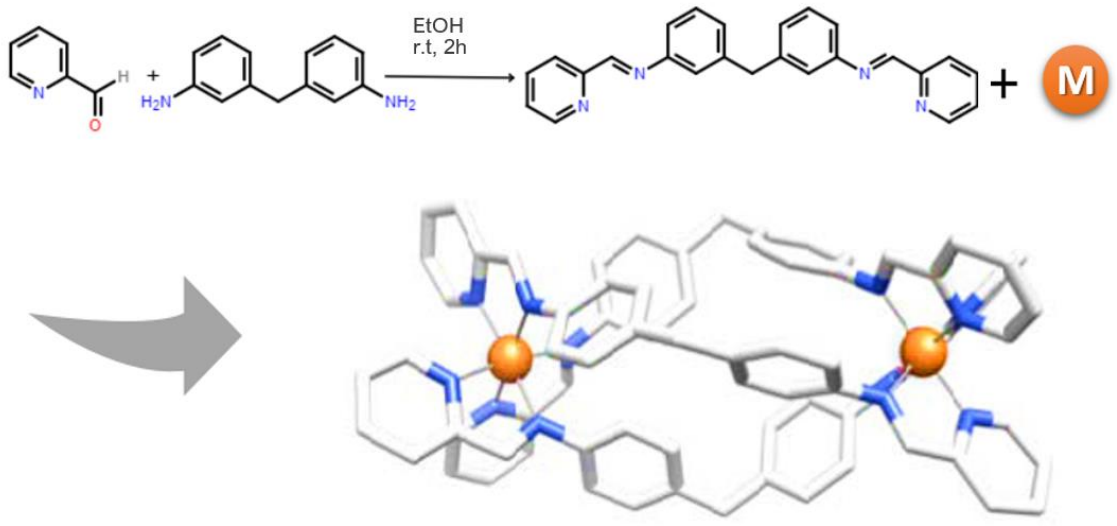

Fig. 1.55. Schematic representation of supramolecular cylinder [Fe2L3]4+ synthesis in two steps (L = C 25 H 20 N 4).

This complex synthesis produces a racemic mixture of chiral cylinders, M (minus, anticlockwise) and P (plus, clockwise) enantiomers. Both enantiomers interact with DNA with a minor difference in their DNA binding and coiling abilities. [175]

The iron cylinder is one of the most interesting helical cylinders, and produces very good results as an antitumour in many cancer cell lines. The toxicity of this complex has been studied for various diseases in vitro during recent decades. [176] The formulation of iron supramolecular cylinders comprises two iron ions that wrap with three ligand strands and represent a tetra-cationic charge; $[Fe_2L_3]^{4+}$ exhibits a helical structure. The iron cylinder is formed easily in a one-pot reaction and, as mentioned above, the racemic mixture of the two enantiomers (M and P) results from synthesis. The two right-handed and left-handed enantiomers (P: positive, M: negative twisted) are shown in Figure 1.56. [176]

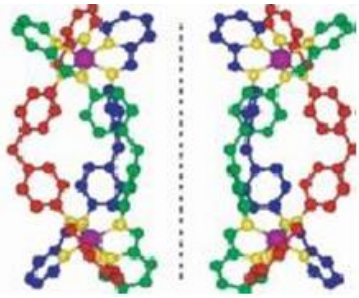

Fig. 1.56. The 3D structures of the two iron cylinder enantiomers, M -[Fe 2 L 3] 4+ and P -[Fe 2 L 3] 4+. Taken from ref 215.

Surveying the modes of interaction of these enantiomers with DNA demonstrates that both P and M enantiomers form strong bonds with DNA, but due to their different chirality, they bind to DNA by different modes. H^1NMR and circular dichroism (CD) spectroscopy show that the M enantiomer selects the major groove to bind with normal sequences of alternating purines and pyrimidines of DNA, while the P enantiomer may adopt the minor groove, spanning the two phosphate backbones. [177] Consequently, the M enantiomer of the cylinder forms a more effective noncovalent bond with DNA than the P enantiomer.

The octahedral spherical shape of the iron and ruthenium complexes and the possibility of ligand coordination to form noncovalent bonds with DNA are considered to be important characteristics of these cylinders. The free nonbonding pair electrons of nitrogen atoms in the ligand structure enable hydrogen bonding to the DNA base pairs. Indeed, the π- stacking interactions with DNA bases are enabled if the M enantiomer is used for study. There are a number of varied studies based on the biological activities of cylinders and their interaction modes with DNA. [57,183]

The iron cylinder shape and size is designed to be similar to the size of a zinc finger protein. The correct size of this structure is 2 nm in length and 1 nm in diameter, which makes it a good fit into the major groove. [178,179] This similarity to DNA-binding protein motifs make it a good option as a DNA replication inhibitor in order to disrupt cell growth, resulting in cell death. [180]

Research outcomes have demonstrated the difference between cisplatin and iron cylinders in their mode of action in biological systems. So,Y-shaped junctions are found endogenously in cells in the form of DNA replication forks. [181] Research has shown that human telomeric G-quadruplex DNA binding is possible with the dinuclear iron(II) cylinder. [182]

These molecules bind noncovalently and strongly to the major groove of DNA due to dramatic binding and intramolecular coiling. The main factor that forms strong noncovalent binding to DNA is the contribution between the cationic metal centres of complexes with the anionic part of DNA strands. The binding ability of the ruthenium cylinder was studied by the spectrophotometry technique, and its binding constant value was measured at over 10^7 M^{-1}. [183]

The triple helical cylinder can not only bind with the major groove, but can also recognise the Y-shaped junctions in DNA and 3WJs in RNA intracellularly, and bond strongly with the

heart of junctions. The cylinder can also induce unexpected and dramatic intramolecular DNA coiling, which gives rise to small coils of DNA; accordingly, DNA is bent by about 45º. [184,185]

Studies on the biological activity of [Fe2L3]Cl4 (L=$C_{25}H_{20}N_4$) reveal that this metal complex has an impact on reducing mitochondrial activity in cancer cells. As a result, blocking of the cell cycle and cell apoptosis subsequently occur. [187,188] The iron cylinder exhibits toxicity in various kinds of cancer cells in vitro, and can potentially be used to inhibit HIV-1 by blocking Tat–TAR RNA as a key element of the transaction.

$[Fe_2L_3]$ Cl_4 has also been reported as an antibiotic that is active against E. coli through binding with DNA molecules as a crucial target of therapies. The same study also presented a 3D model of the iron cylinder that targets the heart of the DNA 3WJ and blocks its core cavity (Fig. 1.57). [186]

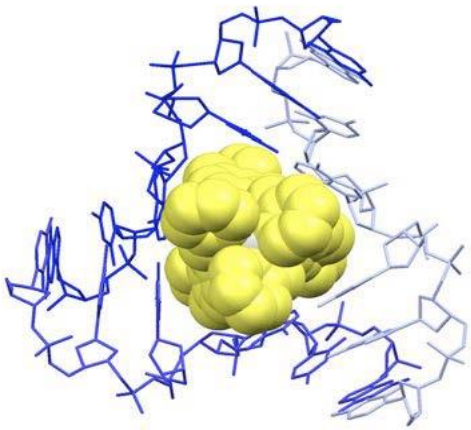

Fig. 1.57. The crystal structure of an iron(II) triple-helicate bound to the junction point of a DNA 3WJ (PDB ref. 2ETO). Taken from ref 186.

A variety of cancer cell lines have been treated by three helical iron cylinder complexes, such as HBL100, T47D, SKOV3, HL-60 and MRC5, in previous studies. [188] The toxicity of the iron cylinder is similar to that of carboplatin against those cancer cells, so it could be used as a cisplatin alternative. Moreover, the iron cylinder is a nongenotoxic metallodrug anticancer that can exhibit fewer general side effects in therapies. Two incubation times and the amount of the drug administered can also play important roles in cytotoxicity on super helical cylinders. [188]

The Hannon group have been working on a range of helical systems by designing them with different metals and ligands, and are studying their biological effects mainly on DNA in vitro. Obviously, these compounds represent different biological activities (such as interaction with DNA) in the studied cells, depending on their shape and spherical structure. For instance, both ruthenium and iron triple-stranded helices exhibit similar structural characteristics [189,190], while the cobalt(III) cylinder ($[Co_2(L)_3]^{4+}$) displays antimicrobial activity against both Staphylococcus aureus and Escherichia coli microorganisms. [191] Moreover, copper helices have a slight difference in size and shape to the iron cylinder and are active in the synthesis of the nuclease enzyme, which is responsible for breaking the bonds between nucleotides in nucleic acids. [192]

Meanwhile, there is a variety of research on synthesising novel metallohelices by designing new ligands and examining their properties through binding with DNA. To this end, hetero atoms can be used as a bridge between the two aromatic cycles to change the properties of cylinders as well as their resulting affinity for DNA binding and interaction.

Results show that these ligands can bind to DNA in the same way. A decrease in the thermal stability of the ligand unit occurs when oxygen is used as a link between the two phenyl parts. [222, 223] In contrast, when sulphur is used instead of oxygen, it causes a significant increase in ligand thermal stability. [223]

The novel chiral derivative of the iron cylinder has been synthesised by adding arginine units to the ligand sites, and the cylinder's anticancer properties were subsequently studied in different cancer cell lines. These investigations confirmed that the arginine units promoted cylinder cytotoxicity in A2780 ovarian cancer cells. [193]

This nongenotoxic cylinder can form noncovalent bonds to the Y-shaped DNA junction and stall DNA replication, thus driving cells to death. In this regard, arginine plays a significant role as an activating part of this anticancer.

The cellular uptake of supermolecular anticancers is an important challenge in the delivery of these drugs. Arginine, as an amino acid involved in direct protein contacts with DNA and RNA, plays a key role in improving cellular uptake. Peptides with cell-penetrating ability have been applied to improve the cellular and nuclear uptake of ruthenium polypyridyl complexes depending on their lysine- and arginine-rich sides and poly-arginine tails. [193] In addition, DNA binding and the activity of the cylinder have been changed significantly

through the effect of grafting arginine residues of the cylinder structure onto the cylinder core. [193]

Although Fe(II) supramolecular cylinders have produced very good results in the treatment of various kinds of diseases such as cancers and HIV [194], these compounds have low stability in an aqueous solution; this is known to be their disadvantage. Drug stability in aqueous solution is considered to be a significant characteristic of drugs applied to biological systems. Accordingly, the ruthenium(II) analogue of the iron(II) cylinder is chosen to study for treating various cancers in Hannon's group. [195] The high stability of the ruthenium cylinder ($[Ru_2L_3]^{4+}$) in both aqueous solution and biological media is the reason for its selection as an alternative to iron in the cylinder structure. [195]

Fluorescence, CD, LD and X-ray studies are used to characterise the ruthenium(II) cylinder $[Ru_2L_3]^{4+}$ which has the same structure as the iron(II) cylinder, and expresses the same coiling and binding modes to DNA. [183]

There are some differences between the iron and ruthenium cylinders in their activities inside cells. For instance, these helical cylinders possess differing cytotoxicity against the same cancerous cell lines; the difference in their cytotoxic activity against ovarian and breast (T47D and HBL100) cancer cell lines is notable. [197] In addition, under the influence of a UV-vis light beam, the ruthenium cylinder has different effects on DNA strands to the iron cylinder, causing the DNA strand to break. As a result, DNA cleavage occurs in a sequence-dependent fashion at the guanine bases. This is in contrast to the iron cylinder, despite the two cylinders' DNA binding and coiling properties being comparable. [196]

Using ruthenium(II) instead of iron(II) in the triple-stranded helicate structure can produce some difficulties in assembling the cylinder. [195] The synthesis of the ruthenium cylinder analogue is a challenge, especially during the purification steps. The resulting low yield of the pure cylinder complex (~ 1%) after some purification steps is its drawback. [195]

The amounts of the ruthenium and iron supramolecular cylinders play a significant role in their biological effects. A low concentration of the applied cylinder can cause cell growth and multiplication inhibition, and disturbs cell nature growth; conversely, to some extent a higher concentration of cylinders can drive cells to self-destruction. [198] These results are not independent of the concentration of the cylinder samples used as a drug, rather the amount of compound in cells are essential hereupon. [198] Ultimately, the type of cancer cells and the cell uptake play a key role in therapies.

1.6 References

1. Boyle, Peter. "Global burden of cancer." The Lancet (1997): SII23.
2. https://www.cancer.org/content/cancer/en/treatment/understanding-your-diagnosis/advanced-cancer/treating-bone-metastases.html
3. Lodish, H., Berk, A., Zipursky, S.L., Matsudaira, P., Baltimore, D. and Darnell, J., 2000. Molecular cell biology 4th edition. National Center for Biotechnology InformationÕs Bookshelf.
4. https://www.cancer.gov/about-cancer/treatment/types/targeted-therapies/targeted-therapies-fact-sheet
5. Hoelder, Swen, Paul A. Clarke, and Paul Workman. "Discovery of small molecule cancer drugs: successes, challenges and opportunities." Molecular oncology 6.2 (2012): 155-176.
6. Frezza, M., Hindo, S., Chen, D., Davenport, A., Schmitt, S., Tomco, D. and Ping Dou, Q., 2010. Novel metals and metal complexes as platforms for cancer therapy. Current pharmaceutical design, 16(16), pp.1813-1825.
7. Dasari, Shaloam, and Paul Bernard Tchounwou. "Cisplatin in cancer therapy: molecular mechanisms of action." European journal of pharmacology 740 (2014): 364-378.
8. Dahm, Ralf. "Discovering DNA: Friedrich Miescher and the early years of nucleic acid research." *Human genetics* 122.6 (2008): 565-581.
9. Lodish, Harvey, and S. Lawrence Zipursky. "Molecular cell biology." *Biochemistry and Molecular Biology Education* 29 (2001): 126-133.
10. Elson D, Chargaff E (1952). "On the deoxyribonucleic acid content of sea urchin gametes". Experientia. 8 (4): 143–145. doi:10.1007/BF02170221.
11. Chargaff, E., Lipshitz, R. and Green, C., 1952. Composition of the desoxypentose nucleic acids of four genera of sea-urchin. J Biol Chem, 195(1), pp.155-160.
12. Neidle, Stephen, Laurence H. Pearl, and Jane V. Skelly. "DNA structure and perturbation by drug binding." *Biochemical Journal* 243.1 (1987): 1.
13. Wang, Difei, Nikolai B. Ulyanov, and Victor B. Zhurkin. "Sequence-dependent Kink-and-Slide deformations of nucleosomal DNA facilitated by histone arginines bound in the minor groove." *Journal of Biomolecular Structure and Dynamics* 27.6 (2010): 843-859.

14. https://en.wikibooks.org/wiki/Structural_Biochemistry/Nucleic_Acid/DNA/DNA_structure
15. Werner, A., F. Kuipers, and H. J. Verkade. "Madame Curie Bioscience Database [Internet], DNA: Alternative Conformations and Biology " (2000).
16. Ohyama, Takashi. *DNA conformation and transcription*. Springer US, 2005.
17. Herbert, Alan, and Alexander Rich. "The biology of left-handed Z-DNA." Journal of Biological Chemistry 271.20 (1996): 11595-11598.
18. G. L. Wang, L. A. Christensen, K. M. Vasquez, Proc. Natl. Acad. Sci. U. S. A. 2006, 103, 2677.
19. M. Balaz, M. De Napoli, A. E. Holmes, A. Mammana, K. Nakanishi, N. Berova, R. Purrello, Angew. Chem., Int. Ed. 2005, 44, 4006.
20. J. R. Bothe, K. Lowenhaupte, H.M.Al- Hashimi, J. Am. Chem. Soc. 2011, 133, 2016.
21. B. Rosenberg, L. van Camp, and T. Krigas, "Inhibition of cell division in Escherichia coli by electrolysis products from a platinum electrode," Nature, vol. 205, no. 4972, pp. 698–699,1965.
22. B. Rosenberg, L. VanCamp, J. E. Trosko, and V. H. Mansour,"Platinum compounds: a new class of potent antitumouragents," Nature, vol. 222, pp. 385–386, 1969.
23. Benjamin Garbutcheon-Singh, K., P Grant, M., W Harper, B., M Krause-Heuer, A., Manohar, M., Orkey, N. and R Aldrich-Wright, J., 2011. Transition metal based anticancer drugs. Current topics in medicinal chemistry, 11(5), pp.521-542.
24. Holland, James F. "Cancer medicine." (1982).
25. Chia VM, Quraishi SM, Devesa SS, Purdue MP, Cook MB, McGlynn KA. International trends in the incidence of testicular cancer, 1973-2002. Cancer Epidemiol Biomarkers Prev. 2010; 19:1151-9.
26. Greenlee RT, Hill-Harmon MB, Murray T, Thun M. Cancer statistics, 2001. CA Cancer J Clin. 2001; 51:15-36. Erratum in: CA Cancer J Clin 2001; 51:144
27. N. J. Wheate, S. Walker, G. E. Craig and R. Oun, Dalton Trans., 2010, 39, 8113–8127.
28. Melendez E. Titanium complexes in cancer treatment. Crit Rev Oncol Hematol 2002;42:309–315.
29. Toney JH, Marks TJ. Hydrolysis chemistry of the metallocene dichlorides M(ç5-C5H5)2Cl2, M = Ti, V, Zr. Aqueous kinetics, equilibria, and mechanistic implications for a new class of antitumor agents. J AmChem Soc 1985;107:947–953.

30. Köpf H, Grabowski S, Voigtlander R. Spectrometric and preparative studies on the hydrolysis of titanocene dichloride. J Organomet Chem 1981;216:185–190.
31. Kim, Byung J., Trevor W. Hambley, and Nicole S. Bryce. "Visualising the hypoxia selectivity of cobalt (III) prodrugs." *Chemical Science* 2.11 (2011): 2135-2142.
32. S. Arnott, Nature, 1986, 320, 313.
33. C. Oguey, N. Foloppe and B. Hartmann, PLoS One, 2010,5, e15931.
34. Paul, Ananya, and Santanu Bhattacharya. "Chemistry and biology of DNA-binding small molecules." *Current Science (Bangalore)* 102.2 (2012): 212-231.
35. Wilson, W.D., Tanious, F.A., Mathis, A., Tevis, D., Hall, J.E. and Boykin, D.W., 2008. Antiparasitic compounds that target DNA. Biochimie, 90(7), pp.999-1014.
36. http://www.sciencedirect.com/science/article/pii/S0968089699002230
37. http://www.annualreviews.org/doi/pdf/10.1146/annurev.bb.24.060195.002335
38. Lo, A.T., Salam, N.K., Hibbs, D.E., Rutledge, P.J. and Todd, M.H., 2011. Polyamide-scorpion cyclam lexitropsins selectively bind at-rich dna independently of the nature of the coordinated metal. PloS one, 6(5), p.e17446.
39. Cai, Xuemei, Phillip J. Gray, and Daniel D. Von Hoff. "DNA minor groove binders: back in the groove." *Cancer treatment reviews* 35.5 (2009): 437-450.
40. Baraldi, P.G., Bovero, A., Fruttarolo, F., Preti, D., Tabrizi, M.A., Pavani, M.G. and Romagnoli, R., 2004. DNA minor groove binders as potential antitumor and antimicrobial agents. Medicinal research reviews, 24(4), pp.475-528.
41. https://de.wikipedia.org/wiki/Distamycin
42. Y. Ishikawa, N. Yamakawa and T. Uno, Molecules, 2008,13, 3117–3128.273
43. V. G. Barkhudaryan, G. V. Ananyan, Y. B. Dalyan and S. G. Haroutiunian, J. Porphyrins Phthalocyanines, 2014,18, 594–599.
44. Y. Ishikawa, N. Yamakawa and T. Uno, Molecules, 2008,13, 3117–3128.
45. V. G. Barkhudaryan, G. V. Ananyan, Y. B. Dalyan and S. G. Haroutiunian, J. Porphyrins Phthalocyanines, 2014, 18, 594–599.
46. Y. Jenkins, A. E. Friedman, N. J. Turro and J. K. Barton,Biochemistry., 1992, 31, 10809–10816.
47. C. M. Dupureur and J. K. Barton, J. Am. Chem. Soc., 1994,116, 10286–10287.
48. T. Hard, C. Hiort and B. Nordén, J. Biomol. Struct. Dyn.,1987, 5, 89–96.
49. B. Nordén and F. Tjerneld, FEBS Lett., 1976, 67, 368–370.

50. Wu, L.; Reymer, A.; Persson, C.; Kazimierczuk, K.; Brown, T.;Lincoln, P.; Nordén, B.; Billeter, M. Initial DNA Interactionsof the Binuclear Threading Intercalator Λ,Λ-[μ-bidppz(bipy)4Ru2](4+): An NMR Study with [d(CGCGAATTCGCG)]2. Chemistry,Eur. J. 2013, 19, 5401-5410.
51. Neidle, Stephen. "DNA minor-groove recognition by small molecules." *Natural product reports* 18.3 (2001): 291-309.
52. Chow, C. S. and Barton, J. K., Transition metal complexes as probes of nucleic acids. *Methods Enzymol*., 1992, **212**, 219–242.
53. Maity, Basudev, Mithun Roy, and Akhil R. Chakravarty. "Ferrocene-conjugated copper (II) dipyridophenazine complex as a multifunctional model nuclease showing DNA cleavage in red light." *Journal of Organometallic Chemistry* 693.8 (2008): 1395-1399.
54. Mei, H. Y.; Barton, J. K. Tris(tetramethylphenanthroline)rutheni um(II): a chiral probe that cleaves A-DNA conformations. Proc. Nat. Ac. Sci. 1988, 85, 1339-43.
55. Meistermann, I., Moreno, V., Prieto, M.J., Moldrheim, E., Sletten, E., Khalid, S., Rodger, P.M., Peberdy, J.C., Isaac, C.J., Rodger, A. and Hannon, M.J., 2002. Intramolecular DNA coiling mediated by metallo-supramolecular cylinders: differential binding of P and M helical enantiomers. Proceedings of the National Academy of Sciences, 99(8), pp.5069-5074.
56. Hannon, M.J., Moreno, V., Prieto, M.J., Moldrheim, E., Sletten, E., Meistermann, I., Isaac, C.J., Sanders, K.J. and Rodger, A., 2001. Intramolecular DNA Coiling Mediated by a Metallo- Supramolecular Cylinder. Angewandte Chemie, 113(5), pp.903-908.
57. García-Ramos, J.C., Galindo-Murillo, R., Cortés-Guzmán, F. and Ruiz-Azuara, L., 2013. Metal-based drug-DNA interactions. Journal of the Mexican Chemical Society, 57(3), pp.245-259.
58. McDonnell, U., Kerchoffs, J.M., Castineiras, R.P., Hicks, M.R., Hotze, A.C., Hannon, M.J. and Rodger, A., 2008. Synthesis and cytotoxicity of dinuclear complexes containing ruthenium (II) bipyridyl units linked by a bis (pyridylimine) ligand. Dalton Transactions, (5), pp.667-675.
59. Johann, Timothy W., and Jacqueline K. Barton. "Recognition of DNA by octahedral coordination complexes." *Philosophical Transactions of the Royal Society of London A: Mathematical, Physical and Engineering Sciences* 354.1706 (1996): 299-324.

60. Wheate, N.J., Brodie, C.R., Collins, J.G., Kemp, S. and Aldrich-Wright, J.R., 2007. DNA intercalators in cancer therapy: organic and inorganic drugs and their spectroscopic tools of analysis. Mini reviews in medicinal chemistry, 7(6), pp.627-648.
61. Zeglis, Brian M., Valerie C. Pierre, and Jacqueline K. Barton. "Metallo-intercalators and metallo-insertors." *Chemical Communications* 44 (2007): 4565-4579.
62. Lippard, Stephen J. "Metals in Medicine." Bioinorganic Chemistry. Mill City: University Science Books, 1994. 505-583
63. S. J. Lippard, P. J. Bond, K. C. Wu and W. R. Bauer,Science, 1976, 194, 726–728.
64. H. M. Berman and P. R. Young, Annu. Rev. Biophys.Bioeng., 1981, 10, 87–114.
65. D. Jaramillo, D. P. Buck, J. G. Collins, R. R. Fenton,F. H. Stootman, N. J. Wheate and J. R. Aldrich-Wright,Eur. J. Inorg. Chem., 2006, 4, 839–849.
66. Wani, W.A., Baig, U., Shreaz, S., Shiekh, R.A., Iqbal, P.F., Jameel, E., Ahmad, A., Mohd-Setapar, S.H., Mushtaque, M. and Hun, L.T., 2016. Recent advances in iron complexes as potential anticancer agents. New Journal of Chemistry, 40(2), pp.1063-1090.
67. Härd, Torleif, Catharina Hiort, and Bengt Nordén. "On the Use of Chiral Compounds for Probing the DNA Handedness: Z to B Conversion in Poly (dGm5dC) Upon Binding of Fe (phen) 3 2+ and Ru (phen) 3 2+." *Journal of Biomolecular Structure and Dynamics* 5.1 (1987): 89-96..
68. Nordén, Bengt, and Folke Tjerneld. "Binding of inert metal complexes to deoxyribonucleic acid detected by linear dichroism." *FEBS letters* 67.3 (1976): 368-370.M. Pitié, C. J. Burrows and B. Meunier, Nucleic Acids Res.,2000, 28, 4856–4864.
69. J. L. García-Giménez, M. González-Álvarez, M. Liu-González, B. Macías, J. Borrás and G. Alzuet, J. Inorg. Biochem.,2009, 103, 923–934.
70. A. Robertazzi, A. V. Vargiu, A. Magistrato, P. Ruggerone,P. Carloni, P. d. Hoog and J. Reedijk, J. Phys. Chem. B,2009, 113, 10881–10890.
71. A. Robertazzi, A. V. Vargiu, A. Magistrato, P. Ruggerone,P. Carloni, P. d. Hoog and J. Reedijk, J. Phys. Chem.B,2009, 113, 10881–10890.
72. K. E. Erkkila, B. P. Hudson, J. K. Barton, D. C. Rees, *Nat. Struct. Biol.*2000, *7*, 117.
73. Pages, B.J., Ang, D.L., Wright, E.P. and Aldrich-Wright, J.R., 2015. Metal complex interactions with DNA. Dalton Transactions, 44(8), pp.3505-3526.

74. Phongtongpasuk, S., Paulus, S., Schnabl, J., Sigel, R.K., Spingler, B., Hannon, M.J. and Freisinger, E., 2013. Binding of a Designed Anti- Cancer Drug to the Central Cavity of an RNA Three- Way Junction. Angewandte Chemie International Edition, 52(44), pp.11513-11516.
75. R. H. Shafer and I. Smirnov, Biopolymers, 2000, 56, 209–227.
76. H. J. Lipps and D. Rhodes, Trends Cell Biol., 2009, 19,414–422.
77. J. Bidzinska, G. Cimino-Reale, N. Zaffaroni and M. Folini,Molecules, 2013, 18, 12368–12395.
78. L. Oganesian and T. M. Bryan, BioEssays, 2007, 29, 155–165.
79. M. A. Blasco, Eur. J. Cell Biol., 2003, 82, 441–446.
80. S. Balasubramanian and S. Neidle, Curr. Opin. Chem.Biol., 2009, 13, 345–353.
81. Cao, Q., Li, Y., Freisinger, E., Qin, P.Z., Sigel, R.K. and Mao, Z.W., 2017. G-quadruplex DNA targeted metal complexes acting as potential anticancer drugs. Inorganic Chemistry Frontiers, 4(1), pp.10-32.
82. B. Fu, D. Zhang, X. Weng, M. Zhang, H. Ma, Y. Ma and X. Zhou, Chem. – Eur. J., 2008, 14, 9431–9441.
83. Z. Gershman, I. Goldberg and Z. Gross, Angew. Chem., Int. Ed., 2007, 46, 4320–4324.
84. J. Bendix, H. B. Gray, G. Golubkov and Z. Gross, Chem. Commun., 2000, 1957–1958.
85. H. Yu, X. Wang, M. Fu, J. Ren and X. Qu, Nucleic Acids Res., 2008, 36, 5695–5703.
86. Bruijnincx, Pieter CA, and Peter J. Sadler. "New trends for metal complexes with anticancer activity." *Current opinion in chemical biology* 12.2 (2008): 197-206.
87. B. K. Keppler and M. Hartmann, Met.-Based Drugs, 1994,1, 145–150.
88. M. Tacke, L. T. Allen, L. Cuffe, W. M. Gallagher, Y. Lou, O. Mendoza, H. Mueller-Bunz, F.-J. K. Rehmman and N. Sweeney, J. Organomet. Chem., 2004, 689, 2242–2249.
89. M. Tacke, L. P. Cuffe, W. M. Gallagher, Y. Lou,O. Mendoza, H. Mueller-Bunz, J. P. Rehmann and N. Sweeney, J. Inorg. Biochem., 2004, 98, 1987–1994.
90. F. Caruso, M. Rossi, C. Opazo and C. Pettinari, Bioinorg. Chem. Appl., 2005, 3, 317–329.
91. H. Prakash, A. Shodai, H. Yasui, H. Sakurai and S. Hirota, Inorg. Chem., 2008, 47, 5045–5047.

92. Osredkar, J., and N. Sustar. "Copper and zinc, biological role and significance of copper/zinc imbalance." *J Clinic Toxicol S* 3.2161 (2011): 0495.
93. Liu, S.; Cao,W.; Yu, L.; Zheng, W.; Li, L.; Fan, C.; Chen, T. Zinc(II) complexes containing bis-benzimidazole derivatives as a new class of apoptosis inducers that trigger DNA damage-mediated p53 phosphorylation in cancer cells. Dalton Trans. 2013, 4, 5932–5940.
94. Haribabu, J.; Jeyalakshmi, K.; Arun, Y.; Bhuvanesh, N.S.P.; Perumal, P.T.; Karvembu, R. Synthesis, DNA/protein binding, molecular docking, DNA cleavage and in vitro anticancer activity of Nickel(II) bis(thiosemicarbazone) complexes. RSC Adv. 2015, 5, 46031–46049.
95. Finney, L.; Vogt, S.; Fukai, T.; Glesne, D. Copper and angiogenesis: Unravelling a relationship key to cancer progression. Clin. Exp. Pharmacol. Physiol. 2009, 36, 88–94.
96. Wende, C.; Lüdtke, C.; Kulak, N. Copper complexes of N-donor ligands as artificial nucleases. Eur. J.Inorg. Chem. 2014, 2014, 2597–2612.
97. Brewer, G.J., Dick, R.D., Grover, D.K., LeClaire, V., Tseng, M., Wicha, M., Pienta, K., Redman, B.G., Jahan, T., Sondak, V.K. and Strawderman, M., 2000. Treatment of metastatic cancer with tetrathiomolybdate, an anticopper, antiangiogenic agent: Phase I study. Clinical Cancer Research, 6(1), pp.1-10.
98. Pass, H.I.; Brewer, G.J.; Dick, R.; Carbone, M.; Merajver, S. A Phase II trial of tetrathiomolybdate after surgery for mlignant mesothelioma: Final results. Ann. Thorac. Surg. 2008, 86, 383–390.
99. Lu, J.; Sun, Q.; Li, J.L.; Jiang, L.; Gu, W.; Liu, X.; Tian, J.L.; Yan, S.P. Two water-soluble Copper(II) complexes:Synthesis, characterization, DNA cleavage, protein binding activities and in vitro anticancer activity studies.J. Inorg. Biochem. 2014, 137, 46–56.
100. Lu, J.; Sun, Q.; Li, J.L.; Jiang, L.; Gu, W.; Liu, X.; Tian, J.L.; Yan, S.P. Two water-soluble Copper(II) complexes:Synthesis, characterization, DNA cleavage, protein binding activities and in vitro anticancer activity studies.J. Inorg. Biochem. 2014, 137, 46–56.
101. Liu, Y.H.; Li, A.; Shao, J.; Xie, C.Z.; Song, X.Q.; Bao, W.G.; Xu, J.Y. Four Cu(II) complexes based onantitumor chelators: Synthesis, structure, DNA

binding/damage, HSA interaction and enhanced cytotoxicity.Dalton Trans. 2016, 45, 8036–8049.

102. Molphy, Z.; Prisecaru, A.; Slator, C.; Barron, N.; McCann, M.; Colleran, J.; Chandran, D.; Gathergood, N.; Kellett, A. Copper phenanthrene oxidative chemical nucleases. Inorg. Chem. 2014, 53, 5392–5404.

103. Rosenberg, Barnett, and Loretta Vancamp. "Platinum compounds: a new class of potent antitumour agents." *Nature* 222 (1969): 385-386.

104. Zhang, Christiana Xin, and Stephen J. Lippard. "New metal complexes as potential therapeutics." *Current opinion in chemical biology* 7.4 (2003): 481-489.

105. Suzanne E. Howson1, Albert Bolhuis2, Viktor Brabec3, Guy J. Clarkson1, Jaroslav Malina3, Alison Rodger1 and Peter Scott1* NATURE CHEMISTRY | VOL 4 | JANUARY 2012

106. 2 B. Rosenberg, L. Van Camp, J. E. Trosko and V. H. Mansour, Nature, 1969, 222, 385–386. 3

107. Pil, P., Lippard, S. J. In Encyclopedia of Cancer, J. R. Bertino, Ed. Academic Press: San Diego, CA, 1997, Vol. 1, pp. 392-410.]

108. 33 S. Ishida, J. Lee, D. J. Thiele and I. Herskowitz, Proc. Natl. Acad. Sci. U. S. A., 2002, 99, 14298–14302.

109. Lu, Q-B. "Molecular reaction mechanisms of combination treatments of low-dose cisplatin with radiotherapy and photodynamic therapy." *Journal of medicinal chemistry* 50.11 (2007): 2601-2604.

110. D. Wang and S. J. Lippard, Nat. Rev. Drug Discovery, 2005, 4, 307–320.

111. Esteban-Fernández, D., Moreno-Gordaliza, E., Cañas, B., Palacios, M.A. and Gómez-Gómez, M.M., 2010. Analytical methodologies for metallomics studies of antitumor Pt-containing drugs. Metallomics, 2(1), pp.19-38.

112. V. Cepeda, M. A. Fuertes, J. Castilla, C. Alonso, C. Quevedo and J. M. Perez, Anti-Cancer Agents Med. Chem., 2007, 7, 3–18

113. R. A. Alderden, M. D. Hall and T. W. Hambley, J. Chem. Educ., 2006, 83, 728–734.

114. E. Wong and C. M. Giandomenico, Chem. Rev., 1999, 99, 2451–2466

115. A. Pasini and F. Zunino, Angew. Chem., Int. Ed. Engl., 1987, 26, 615–624.

116. Eastman, A. (1986), Reevaluation of interaction of cis-dichloro(ethylenediamine)

117. Anti-Cancer Agents in Medicinal Chemistry, 2007, Vol. 7, No. 1

118. González, V.M.; Fuertes, M.A.; Alonso, C.; Pérez, J.M. Mol. Pharmacol., 2001, 59, 657.

119. Fisher, David E. "Apoptosis in cancer therapy: crossing the threshold." *Cell* 78.4 (1994): 539-542.

120. Dhar, Shanta, and Stephen J. Lippard. "Mitaplatin, a potent fusion of cisplatin and the orphan drug dichloroacetate." *Proceedings of the National Academy of Sciences* 106.52 (2009): 22199-22204.

121. Dasari, Shaloam, and Paul Bernard Tchounwou. "Cisplatin in cancer therapy: molecular mechanisms of action." *European journal of pharmacology* 740 (2014): 364-378.

122. Leng, M.; Locker, D.; Giraud-Panis, M.J.; Schwartz, A.; Intini, F.P.; Natile, G.; Pisano, C.; Boccarelli, A.; Giordano, D.; Coluccia, M. Mol. Pharm., 2000, 58, 1525.

123. Giaccone, G. Drugs, 2000, 59, U4.

124. P. C. A. Bruijnincx and P. J. Sadler, Curr. Opin. Chem. Biol., 2008, 12, 197–206.

125. E. Meggers, Curr. Opin. Chem. Biol., 2007, 11, 287–292.

126. Wang, Kehua, and Enjun Gao. "Recent advances in multinuclear complexes as potential anticancer and DNA binding agents." *Anti-Cancer Agents in Medicinal Chemistry (Formerly Current Medicinal Chemistry-Anti-Cancer Agents)* 14.1 (2014): 147-169.

127. I. Romero-Canelon and P. J. Sadler, Inorg. Chem., 2013, 52, 12276–12291.

128. P. Kopf-Maier, H. Kopf and E. W. Neuse, J. Cancer Res. Clin. Oncol., 1984, 108, 336–340.

129. Wani, W.A., Baig, U., Shreaz, S., Shiekh, R.A., Iqbal, P.F., Jameel, E., Ahmad, A., Mohd-Setapar, S.H., Mushtaque, M. and Hun, L.T., 2016. Recent advances in iron complexes as potential anticancer agents. New Journal of Chemistry, 40(2), pp.1063-1090.

130. U. Ghosh, S. K. Seth and T. Kar, Polyhedron, 2012, 34, 1–12.

131. J. Vanco, Z. Sindelar, Z. Dvorak and Z. Travnicek, J. Inorg. Biochem., 2014, 142C, 92–100.

132. Chen, Jingyang, and JoAnne Stubbe. "Bleomycins: towards better therapeutics." *Nature Reviews Cancer* 5.2 (2005): 102-112.

133. L. M. Mir, O. Tounekti and S. Orlowski, Gen. Pharmacol., 1996, 27, 745–748.

134. H. Umezawa, Antimicrob. Agents Chemother., 1965, 5, 1079–1085.

135. Kwong, W.L., Lok, C.N., Tse, C.W., Wong, E.L.M. and Che, C.M., 2015. Anti- Cancer Iron (II) Complexes of Pentadentate N- Donor Ligands: Cytotoxicity, Transcriptomics Analyses, and Mechanisms of Action. Chemistry-A European Journal, 21(7), pp.3062-3072.

136. J. Shao, B. Zhou, A. J. Di Bilio, L. Zhu, T. Wang, C. Qi,J. Shih and Y. Yen, Mol. Cancer Ther., 2006, 5, 586–592.

137. Dvořák, Z., Štarha, P., Šindelář, Z. and Trávníček, Z., 2012. Evaluation of in vitro cytotoxicity of one-dimensional chain [Fe (salen)(L)] n complexes against human cancer cell lines. Toxicology in Vitro, 26(3), pp.480-484.

138. Ramakrishnan, S., Suresh, E., Riyasdeen, A., Akbarsha, M.A. and Palaniandavar, M., 2011. DNA binding, prominent DNA cleavage and efficient anticancer activities of tris (diimine) iron (II) complexes. Dalton Transactions, 40(14), pp.3524-3536.

139. Kwong, W.L., Lok, C.N., Tse, C.W., Wong, E.L.M. and Che, C.M., 2015. Anti- Cancer Iron (II) Complexes of Pentadentate N- Donor Ligands: Cytotoxicity, Transcriptomics Analyses, and Mechanisms of Action. Chemistry-A European Journal, 21(7), pp.3062-3072.

140. Frühauf, S., and W. J. Zeller. "New platinum, titanium, and ruthenium complexes with different patterns of DNA damage in rat ovarian tumor cells." *Cancer research* 51.11 (1991): 2943-2948.

141. Chen, Jingyang, and JoAnne Stubbe. "Bleomycins: towards better therapeutics." *Nature Reviews Cancer* 5.2 (2005): 102-112.

142. Brabec, Viktor, and Olga Nováková. "DNA binding mode of ruthenium complexes and relationship to tumor cell toxicity." *Drug Resistance Updates* 9.3 (2006): 111-122.

143. Clarke, Michael J. "Ruthenium metallopharmaceuticals." Coordination Chemistry Reviews 236.1 (2003): 209-233.

144. J Vincent and S Love, Biochim. Biophys. Acta, 2011, DOI: 10.1016/j.bbagen.2011.07.003

145. Clarke, Michael J. "Ruthenium metallopharmaceuticals." *Coordination Chemistry Reviews* 236.1 (2003): 209-233.

146. Trondl, R., Heffeter, P., Kowol, C.R., Jakupec, M.A., Berger, W. and Keppler, B.K., 2014. NKP-1339, the first ruthenium-based anticancer drug on the edge to clinical application. Chemical Science, 5(8), pp.2925-2932.

147. Hannon, Michael J. "Metal-based anticancer drugs: from a past anchored in platinum chemistry to a post-genomic future of diverse chemistry and biology." *Pure and Applied Chemistry* 79.12 (2007): 2243-2261.

148. Panja, A., Matsuo, T., Nagao, S. and Hirota, S., 2011. DNA cleavage by the photocontrolled cooperation of ZnII centers in an azobenzene-linked dizinc complex. Inorganic chemistry, 50(22), pp.11437-11445.

149. Sava, G., Clerici, K., Capozzi, I., Cocchietto, M., Gagliardi, R., Alessio, E., Mestroni, G. and Perbellini, A., 1999. Reduction of lung metastasis by ImH [trans-RuCl4 (DMSO) Im]: mechanism of the selective action investigated on mouse tumors. Anti-Cancer Drugs, 10(1), p.129.

150. E. Antonarakis and A. Emadi, Cancer Chemother. Pharmacol., 2010, 66,1 –9.

151. C. G. Hartinger, M. A. Jakupec, S. Zorbas-Seifried, M. Groessl, A. Egger, W. Berger, H. Zorbas, P. J. Dyson and B. K. Keppler, Chem. Biodiversity, 2008, 5, 2140–2155.

152. C. G. Hartinger, S. Zorbas-Seifried, M. A. Jakupec, B. Kynast, H. Zorbas and B. K. Keppler, J. Inorg. Biochem., 2006, 100, 891–904.

153. T. W. Johann and J. K. Barton, Philos. Trans. R. Soc. London, A, 1996, 354, 299–324.

154. I. Haq, P. Lincoln, D. Suh, B. Nordén, B. Z. Chowdhry and J. B. Chaires, J. Am. Chem. Soc., 1995, 117, 4788–4796.

155. Vos, Johannes G., and John M. Kelly. "Ruthenium polypyridyl chemistry; from basic research to applications and back again." *Dalton Transactions* 41 (2006): 4869-4883.

156. Chen, L.; Peng, F.; Li, G.; Jie, X.; Cai, K.R.; Cai, C.; Zhong, Y.; Zeng, H.; Li, W.; Zhang, Z.; et al. The studies ont he cytotoxicity in vitro, cellular uptake, cell cycle arrest and apoptosis-inducing properties of rutheniummethylimidazole complex [Ru(MeIm)4(p-cpip)]2+. J. Inorg. Biochem. 2016, 156, 64–74.

157. Ren, J., Wang, J., Han, L., Wang, E. and Wang, J., 2011. Kinetically grafting G-quadruplexes onto DNA nanostructures for structure and function encoding via a DNA machine. Chemical Communications, 47(38), pp.10563-10565.

158. Gray, Harry B., and Jay R. Winkler. "Electron transfer in proteins." *Annual review of biochemistry* 65.1 (1996): 537-561.

159. Chavarot, M., Ménage, S., Hamelin, O., Charnay, F., Pécaut, J. and Fontecave, M., 2003. "Chiral-at-metal" octahedral ruthenium (II) complexes with achiral ligands: a new type of enantioselective catalyst. Inorganic chemistry, 42(16), pp.4810-4816.

160. L. Messori, P. Orioli, D. Vullo, E. Alessio, E. Iengo, Eur. J.Biochem. 267 (2000) 1206.

161. M.J. Clarke, F. Zhu, D. Frasca, Chem. Rev. 99 (1999) 2511.

162. M.J. Clarke, in: B.K. Keppler (Ed.), Metal Complexes in Cancer Chemotherapy, VCH, Weinheim, 1993, pp. 129_/157.

163. B.D. Palmer, W.R. Wilson, S.M. Pullen, J. Med. Chem. 33(1990) 112.

164. J.E. Biskupiak, K.A. Krohn, J. Nucl. Med. (1993) 411.

165. D. Miklavcic, G. Sersa, S. Novakovic, J. Bioelect. 9 (1990) 133.

166. J.A. Marchant, T. Matsubara, P.C. Ford, Inorg. Chem. 16(1977) 2160.

167. Meistermann, I., Moreno, V., Prieto, M.J., Moldrheim, E., Sletten, E., Khalid, S., Rodger, P.M., Peberdy, J.C., Isaac, C.J., Rodger, A. and Hannon, M.J., 2002. Intramolecular DNA coiling mediated by metallo-supramolecular cylinders: differential binding of P and M helical enantiomers. Proceedings of the National Academy of Sciences, 99(8), pp.5069-5074.

168. G.M. Coleman, J.W. Gesler, E.A. Shirley, J.R. Kuempel, Inorg.Chem. 12 (1973) 1036.

169. E. C. Constable, M. G. B, Drew, G. Forsyth, M. D. Ward, J. Chem. Soc., Chem. Commun., 1988, 22, 1450-1451.

170. Zhang, Zhan, and David Dolphin. "Synthesis of triple-stranded complexes using bis (dipyrromethene) ligands." *Inorganic chemistry* 49.24 (2010): 11550-11555.

171. S. Torelli, D. Imbert, M. Cantuel, G. Bernardinelli, S. Delahaye, A. Hauser, J. C. G. Bunzli, C. Piguet, Chem. Eur. J., 2005, 11, 3228-3242.

172. M. J. Hannon, V. Moreno, M. J. Prieto, E. Moldrheim, E. Sletten, I. Meistermann, C. J. Isaac, K. J. Sanders, A. Rodger, Angew. Chem., Int. Ed. 2001, 40, 880.

173. M. J. Hannon, C. L. Painting, A. Jackson, J. Hamblin, W. Errington, Chem. Commun. 1997,1807.

174. G. I. Pascu, A. C. G. Hotze, C. Sanchez- Cano, B. M. Kariuki, M. J. Hannon, Angew. Chem., Int.Ed. 2007, 46, 4374.

175. M. J. Hannon and M. Coll, Angew. Chem., Int. Ed., 2006, 45, 1227;D. R. Boer, J. M. C. A. Kerckhoffs, Y. Parajo, M. Pascu, I. Uson, P. Lincoln, M. J. Hannon and M. Coll, Angew. Chem., Int. Ed., 2010, 49, 2336.

176. Meistermann, I., Moreno, V., Prieto, M.J., Moldrheim, E., Sletten, E., Khalid, S., Rodger, P.M., Peberdy, J.C., Isaac, C.J., Rodger, A. and Hannon, M.J., 2002. Intramolecular DNA coiling mediated by metallo-supramolecular cylinders: differential binding of P and M helical enantiomers. Proceedings of the National Academy of Sciences, 99(8), pp.5069-5074.

177. Hotze, A. C., Hodges, N. J., Hayden, R. E., Sanchez-Cano, C., Paines, C., Male, N., Tse, M. K., Bunce, C. M., Chipman, J. K., Hannon M. J. (2008) Supramolecular iron cylinder with unprecedented DNA binding is a potent cytostatic and apoptotic agent without exhibiting genotoxicity. Chem Biol. 15 (12): 1258-1267.

178. Tuna, F., Lees, M. R., Clarkson, G. J., Hannon, M. J. (2004) Readily Prepared Metallo-Supramolecular Triple Helicates Designed to Exhibit Spin-Crossover Behaviour. Chem. Eur. J. 10 (22): 5737 –5750.

179. I. Meistermann, V. Moreno, M. J. Prieto, E. Moldrheim, E. Sletten, S. Khalid, P. M. Rodger, J. C. Peberdy, C. J. Isaac, A. Rodger, M. J. Hannon, Proc. Natl. Acad. Sci. U. S. A. 2002, 99, 5069.

180. Hotze, A.C., Hodges, N.J., Hayden, R.E., Sanchez-Cano, C., Paines, C., Male, N., Tse, M.K., Bunce, C.M., Chipman, J.K. and Hannon, M.J., 2008. Supramolecular iron cylinder with unprecedented DNA binding is a potent cytostatic and apoptotic agent without exhibiting genotoxicity. Chemistry & biology, 15(12), pp.1258-1267.

181. a) G. I. Pascu, A. C. G. Hotze, C. Sanchez-Cano, B. M. Kariuki,M. J. Hannon, Angew. Chem. 2007, 119, 4452 – 4456; Angew.Chem. Int. Ed. 2007, 46, 4374 – 4378; b) A. C. G. Hotze, N. J.Hodges, R. E. Hayden, C. Sanchez-Cano, C. Paines, N. Male,M. K. Tse, C. M. Bunce, J. K. Chipman, M. J. Hannon, Chem.Biol. 2008, 15, 1258 – 1267; c) A. J. Pope, C. Bruce, B. Kysela,M. J. Hannon, Dalton Trans. 2010, 39, 2772 – 2774.

182. Meistermann, Isabelle, et al. "Intramolecular DNA coiling mediated by metallo-supramolecular cylinders: differential binding of P and M helical

enantiomers." *Proceedings of the National Academy of Sciences* 99.8 (2002): 5069-5074.

183. J. Malina, M. J. Hannon and V. Brabec, Chem.–Eur. J., 2007, 13,3871. A. Oleksy, A. G. Blanco, R. Boer, I. Uson, J. Aymami, A. Rodger,

184. M. J. Hannon and M. Coll, Angew. Chem., Int. Ed., 2006, 45, 1227;D. R. Boer, J. M. C. A. Kerckhoffs, Y. Parajo, M. Pascu, I. Uson, P. Lincoln, M. J. Hannon and M. Coll, Angew. Chem., Int. Ed., 2010, 49, 2336.

185. Richards, A.D., Rodger, A., Hannon, M.J. and Bolhuis, A., 2009. Antimicrobial activity of an iron triple helicate. International journal of antimicrobial agents, 33(5), pp.469-472.

186. Hotze, A.C., Hodges, N.J., Hayden, R.E., Sanchez-Cano, C., Paines, C., Male, N., Tse, M.K., Bunce, C.M., Chipman, J.K. and Hannon, M.J., 2008. Supramolecular iron cylinder with unprecedented DNA binding is a potent cytostatic and apoptotic agent without exhibiting genotoxicity. Chemistry & biology, 15(12), pp.1258-1267.

187. L. Cardo, V. Sadovnikova, S. Phongtongpasuk, N. J. Hodges, M. J.Hannon, Chem. Commun. 2011, 47, 6575–6577.

188. L. J. Childs, J. Malina, B. E. Rolfsnes, M. Pascu, M. J. Prieto, M. J. Broome, P. M. Rodger, E. Sletten, V. Moreno, A. Rodger, M. J. Hannon,*Chem. Eur. J.* 2006, *12*, 4919.

189. G. I. Pascu, A. C. Hotze, C. Sanchez-Cano, B. M. Kariuki, M. J. Hannon,Angew. Chem. Int. Ed. 2007, 46, 4374.

190. Vasdev, R.A., Preston, D., Scottwell, S.Ø., Brooks, H.J., Crowley, J.D. and Schramm, M.P., 2016. Oxidatively Locked [Co2L3] 6+ Cylinders Derived from Bis (bidentate) 2-Pyridyl-1, 2, 3-triazole "Click" Ligands: Synthesis, Stability, and Antimicrobial Studies. Molecules, 21(11), p.1548.

191. Ducani, C., Leczkowska, A., Hodges, N.J. and Hannon, M.J., 2010. Noncovalent DNA- Binding Metallo- Supramolecular Cylinders Prevent DNA Transactions in vitro. Angewandte Chemie International Edition, 49(47), pp.8942-8945.

192. Cardo, L., Sadovnikova, V., Phongtongpasuk, S., Hodges, N.J. and Hannon, M.J., 2011. Arginine conjugates of metallo-supramolecular cylinders prescribe helicity and enhance DNA junction binding and cellular activity. Chemical Communications, 47(23), pp.6575-6577.

193. Malina, Jaroslav, Michael J. Hannon, and Viktor Brabec. "Iron (II) supramolecular helicates interfere with the HIV-1 Tat–TAR RNA interaction critical for viral replication." *Scientific Reports* 6 (2016).

194. Pascu, G.I., Hotze, A.C., Sanchez- Cano, C., Kariuki, B.M. and Hannon, M.J., 2007. Dinuclear Ruthenium (II) Triple- Stranded Helicates: Luminescent Supramolecular Cylinders That Bind and Coil DNA and Exhibit Activity against Cancer Cell Lines. Angewandte Chemie, 119(23), pp.4452-4456.

195. Jaroslav Malina1, Michael J. Hannon2 & Viktor Brabec1,3 2016

196. J. Malina, M. J. Hannon, V. Brabec, *Chem. Eur. J.* 2008, *14*, 10408.

197. G. I. Pascu, A. C. Hotze, C. Sanchez-Cano, B. M. Kariuki, M. J. Hannon,*Angew. Chem. Int. Ed.* 2007, *46*, 4374.

198. Ho, P. Shing, and Megan Carter. *DNA structure: alphabet soup for the cellular soul*. INTECH Open Access Publisher, 2011.

199. http://www.atdbio.com/content/5/Nucleic-acid-structure

200. https://en.wikipedia.org/wiki/DNA

201. http://www.atdbio.com/content/5/Nucleic-acid-structure

202. Liu, W.P., Ye, Q.S., Yu, Y., Chen, X.Z., Hou, S.Q., Lou, L.G., Yang, Y.P., Wang, Y.M. and Su, Q., 2008. Novel lipophilic platinum (II) compounds of salicylate derivatives. Platinum Metals Review, 52(3), pp.163-171.

203. Chen, Yong-Huang, and J. William Lown. "DNA minor groove binding of cross-linked lexitropsins: experimental conditions required to observe the covalently linked WPPW (groove wall-peptide-peptide-groove wall) motif." *Biophysical journal* 68.5 (1995): 2041-2048.

204. Ishikawa, Yoshinobu, Naoki Yamakawa, and Tadayuki Uno. "Binding of cationic bis-porphyrins linked with p-or m-xylylenediamine and their zinc (II) complexes to duplex DNA." *Molecules* 13.12 (2008): 3117-3128.

205. Giaccone, Giuseppe. "Clinical perspectives on platinum resistance." *Drugs* 59.4 (2000): 9-17.

206. Georgiades, Savvas N., and Ramon Vilar. "Interaction of metal complexes with nucleic acids." *Annual Reports Section" A"(Inorganic Chemistry)* 106 (2010): 481-503.

207. https://en.wikipedia.org/wiki/Bleomycin

208. Richards, Adair D., and Alison Rodger. "Synthetic metallomolecules as agents for the control of DNA structure." *Chemical Society Reviews* 36.3 (2007): 471-483.

209. Yu, H., Wang, X., Fu, M., Ren, J. and Qu, X., 2008. Chiral metallo-supramolecular complexes selectively recognize human telomeric G-quadruplex DNA. Nucleic acids research, 36(17), pp.5695-5703.

210. D. Plazuk, S. Top, A. Vessie `res, M. A. Plamont, M. Huche, J. Zakrzewski, A. Makal, K. Woz´niak and G. Jaouen, Dalton Trans., 2010, 39, 7444–7450.

211. O.Buriez,J.M.Heldt,E.Labbe ´,A.Vessie `res,G.Jaouenand C. Amatore, Chemistry, 2008, 14, 8195–8203.

212. http://www.richardwheeler.net/contentpages/image.php?gallery=Scientific_Illustration&img=Ruthenium_and_Transferrin&type=png

213. Trondl, R., Heffeter, P., Kowol, C.R., Jakupec, M.A., Berger, W. and Keppler, B.K., 2014. NKP-1339, the first ruthenium-based anticancer drug on the edge to clinical application. Chemical Science, 5(8), pp.2925-2932.

214. Deo, K.M., Pages, B.J., Ang, D.L., Gordon, C.P. and Aldrich-Wright, J.R., 2016. Transition Metal Intercalators as Anticancer Agents—Recent Advances. International journal of molecular sciences, 17(11), p.1818.

215. Yu, H., Wang, X., Fu, M., Ren, J., Qu, X. (2008) Chiral metallo-supramolecular complexes selectively recognize human telomeric G-quadruplex DNA. Nucleic Acids Research, 36 (17): 5695-5703

216. http://www.madsci.org/posts/archives/2010-03/1268774308.Gb.r.html

217. Matsui, T., Miyachi, H., Shigeta, Y. and Hirao, K., 2012. Metal-Assisted Proton Transfer in Guanine-Cytosine Pair: An Approach from Quantum Chemistry. In Some Applications of Quantum Mechanics. InTech.

218. Suárez, R.M., Bosch, P., Sucunza, D., Cuadro, A.M., Domingo, A., Mendicuti, F. and Vaquero, J.J., 2015. Targeting DNA with small molecules: a comparative study of a library of azonia aromatic chromophores. Organic & biomolecular chemistry, 13(2), pp.527-538.

219. Howson, S.E., Bolhuis, A., Brabec, V., Clarkson, G.J., Malina, J., Rodger, A. and Scott, P., 2012. Optically pure, water-stable metallo-helical ‘flexicate’assemblies with antibiotic activity. Nature chemistry, 4(1), pp.31-36.

220. Parajó, Y., Malina, J., Meistermann, I., Clarkson, G.J., Pascu, M., Rodger, A., Hannon, M.J. and Lincoln, P., 2009. Effect of bridging ligand structure on the thermal

stability and DNA binding properties of iron (II) triple helicates. Dalton Transactions, (25), pp.4868-4874.

221. Fahmy, H. A., and O. A. Gharib. "Effect of Low Radiation Dose on Cisplatin Induced Hepato-Testicular Damage in Male Rats." (2014).

222. Strebhardt, Klaus, and Axel Ullrich. "Paul Ehrlich's magic bullet concept: 100 years of progress." Nature Reviews Cancer 8.6 (2008): 473-480.

223. Colvin M. Alkylating Agents. In: Kufe DW, Pollock RE, Weichselbaum RR, et al., editors. Holland-Frei Cancer Medicine. 6th edition. Hamilton (ON): BC Decker; 2003. Available from: https://www.ncbi.nlm.nih.gov/books/NBK12772/

224. http://www.sciencedirect.com/topics/page/NAMI-A

CHAPTER 2

Methods and Experimental Details

2.1 Synthesis of iron cylinder $[Fe_2L_3]Cl_4$

2.1.1 Synthesis of ligand

In this work, all the required chemical agents were provided by Sigma Aldrich (UK). No further purification was carried out.

In order to prepare the ligand to make the iron cylinder, 3 g (15.2 mmol) of N,N'-bis(pyridin-2-ylmethylene)-4,4‟‟-diaminodiphenylmethane was mixed with 2.80 g (30 mmol) of pyridine-2-carboaldehyde in 50 ml ethanol at room temperature. [1] The mixture was stirred for 12 hours to completion. The yellow precipitate was filtered by vacuum filtration and was recrystallised from ethanol to achieve a purified compound. The resulting product was dried under vacuum.

Yield: (4.9 g, 80%)

ESI MS: m/z 399 [(C25H20N4) + Na]+.

1H NMR (CD2Cl2): δ 8.72 (2H, d, J = 3.8 Hz, H6), δ 8.6 (2H, s, Hi), δ 8.23 (2H, d, J = 7.5 Hz, H3), δ 7.85 (2H, td, J = 7.3 Hz, H4), δ 7.40 (2H, t, J = 7.2 Hz, H5), δ 7.29 (8H, m, HPh), δ 4.1 (2H, s, CH2).

2.1.2 Synthesis of cylinder

0.96 g (4 mmol) iron(II) chloride tetrahydrate was added to 2.72 g (6 mmol) ligand in 160 ml methanol and stirred for 2–3 hours under reflux. The purple solution was cooled to room temperature and purple iron cylinder precipitate $[Fe2L_3]Cl_4$ was separated from solution by vacuum filtration. The resulting product was dried under vacuum and purified with methanol and diethyl ether. [1] Yield: (3.83 g, 88%)

ESI MS: m/z 310 [Fe2(C25H20N4)3]4+.

1H NMR (MeOD): δ 9.2 (2H, s, Hi), δ 8.71 (2H, d, J = 7.0 Hz, H3), δ 8.49 (2H, t, J = 6.5 Hz, H4), δ 7.87 (2H, t, J = 6.1 Hz, H5), δ 7.48 (2H, d, J = 4.2 Hz, H6), δ 6.99 (4H, s, Ha/b), δ 5.6 (4H, s, Ha/b), δ 4.13 (2H, s, CH2).

The purity of the iron cylinder could have changed over time because of its low stability in storage at room temperature or in solution. Taking this into consideration, the synthesis of the iron cylinder was repeated every 3–4 months and a fresh solution was used in each test. The 2,500 µM stock solution of iron cylinder in sterilised water was prepared for each test.

2.2 Synthesis of ruthenium cylinder $[Ru_2L_3]$ $[PF_6]_4$

2.2.1 Synthesis of cis-dichlorotetrakis (dimethylsulphoxide) ruthenium

To synthesise the ruthenium halide complex, 0.2 g of $RuCl_3$ was dissolved in 5 ml of DMSO in a 50 ml two-neck flask. The mixture was stirred under an N_2 atmosphere for 10 mins. After 10 mins, the solution heated under reflux for 5 mins. The N_2 atmosphere was established during the process. 50% of the DMSO was removed after 5 mins by changing the condenser's application. After reducing the solvent by this process, the solution was cooled to room temperature, 20 ml acetone was added to the reaction, and a yellow precipitate suddenly appeared. It was filtrated by vacuum filtration and washed with cold acetone (10 ml in 2 portions). The resulting product was dried under vacuum. Yield: 78%

2.2.2 Synthesis of cylinder

The ruthenium cylinder $[Ru_2L_3](PF_6)_4$ was synthesised under an argon atmosphere to protect the reaction from oxidation. The yield of the reaction is not high, so oxidation can block the intended reaction or reduce the expected yield, with an increase in unexpected side products. To synthesise the ruthenium cylinder, 0.968 g cis-$[Ru(dmso)_4Cl_2]$ (2 mmol) was added to 30 ml ethylene glycol and stirred to produce a clear solution, to which 1.12 g ligand L (3 mmol) was added slowly.

The system was set under an argon atmosphere; the neutral gas was purged on top of the solution and the oxygen was removed from the vessels by creating a vacuum. The reaction was heated under reflux for 5 days to completion. The reaction progress was controlled with TLC as it progressed. A brown-orange solution resulted over time. The reaction was cooled to room temperature and filtrated from celite. A saturated methanolic solution of NH_4PF_6 (20 ml) was made and added to the cold reaction mixture in 5 min. The mixture was stirred on an ice bath for 30 mins, followed by storage in a freezer for 24 hours. The brown-orange precipitate was vacuum filtrated and washed with cold methanol, diethyl ether and petroleum ether. To remove solvent from the product, the wet precipitate was dried under vacuum for 2 days (resulting in 3.5 g of compound). The TLC was obtained from the impure product with the standard sample of ruthenium cylinder to detect the exact place of the cylinder on alumina paper, and to find the place of the side products. The alumina plate was used for extraction of

the ruthenium cylinder from the impure compound. A mixture of CH_3CN, H_2O and KNO_3 (saturated, aqueous) was used as a mobile phase in a ratio of 20:1:1. 50 mg of compound was dissolved in 10 ml acetonitrile, and mixed to produce a clear solution. The concentrated solution was applied onto an alumina plate and placed into a large tank for 1 hour. The second orange band, considered as a ruthenium cylinder band, was scraped from the plate and split from the alumina powder by resolving in methanol. The alumina powder and excess potassium nitrate was extracted under vacuum filtration in this step. The filtrated product was washed with cold ethyl acetate and methanol, and dried under vacuum. [2]
4.015 mg, yield: 1%
TOF MS ES^+ d(CH3CN): m/z (%): 333.08 (100, [Ru2L3]4+), 492.42 (32, {[Ru2L3][PF6]}3+), 811.12 (10, {[Ru2L3][PF6]2}2+).
1H NMR, [Ru2L3](PF6)4 (300 MHz, CD3CN): d = 8.82 (s, 1H, Him), 8.5 (d, J = 3 Hz, 1H, H3), 8.29 (t, J = 3,1H,H4), 7.7 (ddd, J = 5.2, 1H, H5), 7.55 (d, J = 5.2 Hz, 1H, H6), 6.98 (d, J = 6.5 Hz, 2H, HPh), 5.69 (d, J = 6.2 Hz, 2H, HPh), 4 ppm (s, 1H, CH2 spacer).
UV/Vis (CH3CN): lmax [nm] (e [m_1cm_1]): 485(24,200), 445 (17,600), 320 (45,500), 270 (71,300)

2.3 Cell culture

The U2OS cell line culturing method is described below. All cell culture must be undertaken in microbiological safety cabinet using aseptic technique to ensure sterility.

2.3.1 Cell line

Currently, knowledge about protein expression in the human osteosarcoma U2OS cell line and the effect of cylinders is very limited, despite its extensive applications in the field of biomedical research. [3]
U2OS (ATCC number HTB-96): osteosarcoma; bone sarcoma from the tibia of a human female.

2.3.2 Complete media preparation

Gibco® by life technologies™ 16600-082 McCoy's 5A Medium (modified) [+] L-glutamine is a general purpose medium which enhances the spreading of various primary cells and also

supports the growth of primary mammalian cells derived from normal bone marrow, skin, spleen, kidney, lung, rat embryos and other tissues.
McCoy's 5A (modified) Medium was supplemented with foetal bovine serum (10% v/v), penicillin (100 U/ml), streptomycin (100 µg/ml) and L-glutamine (2 mM). The complete media was stored in the fridge at 4 °C. [5]

2.3.3 Cell cultures

The U2OS (osteosarcoma) cell line was removed from storage at -80°C and pre-warmed to thaw in a 37 °C water bath. In addition, PBS and complete McCoy's 5A Medium were also warmed at 37 °C.
Thawed cells were resuspended in 10 ml of PBS in 10 ml falcon tubes, and were then centrifuged at 1,500 rpm at 25°C for 5 mins to remove the growth medium containing DMSO. The pellet was resuspended in 200 µl fresh medium and then transferred to 25 ml of complete media in a 75 cm^3 tissue culture flask with a vented cap (T75) (Costar). Cells were incubated at 37 °C in a 5% CO_2, 95% air incubator to grow (Sanyo, MCO-17A). The media was changed every 2 days and cells were passaged every 2 or 3 days and split cultured when they reached 85% confluence. [4]

2.3.4 Subculturing of U2OS cells

Once cells were confluent, they were passaged. Complete media, trypsin-EDTA (Gibco®) and 0.01 M phosphate buffered saline (PBS) (Sigma-Aldrich) were warmed in a 37 °C water bath. The aspirated growth media was taken carefully from the culture flask and washed with 10 ml of PBS to ensure that the entire surface was cleaned from the old media. PBS was removed from the cultured flask and 2–3 ml of trypsin (depending on cell confluence) was added to the flask. The flask was incubated at 37 °C for 2–5 min, before it was tapped to dislodge the cells and checked under the microscope to ensure the cells detached more than 70–90% confluent. fresh media was added (8 ml if 2 ml trypsin was used, and 7 ml if 3 ml trypsin was used, in order to produce a maximum 10 ml mixture).
To inhibit the trypsin and the contents of the flask, they were transferred to a 15 ml falcon tube. The cell suspension was centrifuged for 5 mins at 1,500 rpm at room temperature, and the supernatant was discarded. Suspended cells in 200 µl of fresh media and cells were mixed gently. The cell suspension was split into two 100 µl parts, and 15 ml of fresh media was

added to each part in a new T75 flask. Both flasks were incubated in an incubator at 37 ºC and 5% CO2. [4,5]

2.3.5 Storage of U2OS cells

Extra cells (2–5×10^6 cells/ml) after two or three episodes of re-culturing were frozen to maintain an appropriate stock of viable cells. Cells were checked for bacterial, yeast or fungal contamination under a microscope. The old media was removed and trypsinised by a standard protocol, as described in section 2.3.4. Cells were resuspended in new media and were then centrifuged at 1,500 rpm at 4 °C for 5 min.

Supernatant was removed and the pellet was immediately resuspended with 1 ml of frozen media containing 5% DMSO in vials. The vials were placed on ice and labelled with name, date and cell type. They were stored overnight in a freezer at -80 °C, then transferred to a liquid nitrogen tank. [5]

2.3.6 Maintenance of cell cultures (in T_{75} flasks)

Cell cultures were maintained in T_{75} flasks containing 15 ml of fresh media. These flasks were placed in a humidified incubator at 37 °C and 5% CO2. The flasks were examined daily under the microscope for signs of contamination and general cell morphology.
Every 2 days, the old media was removed from the T_{75} flask. 10 ml of PBS was added to the flask and then removed to eliminate any dead cells. 15 ml of complete media was then added to the flask, and the flask was placed back into the incubator. [5]

2.3.7 Cell counting

To count cells, the hemocytometer and cover slip were cleaned, thoroughly dried and assembled. As described in section 2.3.4, cells were washed with PBS and trypsinised for 2 mins, then centrifuged to split the pellet. The pellet was resuspended in 1×10^3 µl media. Cell dilution (1:10) was performed by the addition 10 µl of the suspension to 90 µl of fresh media in an Eppendorf. 20 µl of dilution suspension was then pipetted under the edge of each of the two counting chambers, and allowed the cell suspension to be drawn into the counting chamber by capillary action. The hemocytometer was then placed under a microscope and cells were viewed at 100× magnification. The cells were checked at the central grid of the

device and the number of any viable cells in each square was recorded. The average number of cells was calculated and multiplied by the dilution factor.
If the cells have not been diluted, this factor is 10^4 cells/ml. Any dilution of the sample after removal from the cell suspension (such as when using vital stain) needs to be included in the calculation. The number of cells was calculated according to the following equation:
Cell density (cells/ml) = number of cells counted × dilution factor (10) × 10^4. [5]

2.3.8 Cell viability

To count viable cells, 0.4% trypan blue solution in PBS was made, and the solution was incubated for 2–5 mins before loading. The cell suspension was mixed 1:1 with 0.4% trypan blue solution. Dark blue cells were detected as unviable cells and cell viability was calculated as the number of unstained cells divided by the total number of cells, and expressed as a percentage. [5]

2.4 MTT-based cytotoxicity assay

2.4.1 Survey of the cytotoxicity effect of synthesised metallodrugs on U2OS cells

Subconfluent monolayer U2OS cells maintained in a T75 flask were trypsinised to collect the cells in growth medium. The suspension was centrifuged (5 min at 1,500 rpm) to pellet the cells and removed the supernatant. To count the viable cells, cells were resuspended in 1,000 µl of medium. A Neubauer haemocytometer was used to count the cells. Cells were diluted to 2.5–10×10^4 cells/ml. The cell suspension was then transferred to a 9 cm petri dish and 200 µl of the suspension was added to each well of a flat-bottomed 96-well plate. Seeding the cells began from column number 2 and ended with column number 11, 8 wells columns number 1 and 12 were used as control lines in each plate. The plate was left in the incubator at 37 °C and 5% CO2 for 24 hours, to ensure that there were enough adherent cells on the wells' surface. [5]

2.4.2 Preparation of drugs

To survey the toxicity of iron and ruthenium cylinders in U2OS cell lines, 2,500 µM stock solutions of each iron and ruthenium cylinder, as well as cisplatin as a standard, were made.

To make fresh stock solution of the iron cylinder, 9.101 mg of cylinder powder was solved in 2 ml of deionised autoclaved water and was mixed to homogenise completely. 1.5 mg of cisplatin was solved in 2 ml of deionised millipore autoclave water and mixed carefully to create a homogenised solution, which was used fresh.

A stock of ruthenium cylinder was prepared using Beer-Lambert's law and a UV spectrometer. 2 mg of the cylinder was solved in 500 µl of acetonitrile, and the λmax was used to establish the concentration of ruthenium cylinder in acetonitrile by applying the Beer-Lambert equation for concentration. Acetonitrile was vacuumed from the solution and mixed with DMSO-water (1:1) to have a 2,500 µM stock solution.

2.4.3 Evaluating the cytotoxic effects of ruthenium and iron cylinder treatment

Following incubation for adherent cells, the medium was removed very carefully from each well in columns 2 to 11, and 200 µl of fresh medium (warmed up to 37 °C) was added to each well from columns 2 to 11. Cells were then treated with various concentrations of iron cylinder and cisplatin in water (0, 5, 10, 15, 20, 25, 75 and 150 µM) in plate 1, and with ruthenium cylinder and cisplatin (0, 5, 10, 15, 20, 25, 75 and 150 µM) in DMSO (or in the mixture of DMSO and water to have less than 1% DMSO in each wells) in plate 2. Water and DMSO were applied as a positive control in plates 1 and 2, respectively. Two plates were wrapped in plastic sheets and left in an incubator in 5% CO2 at 37 °C for 72 hours (2–3 PDTs).

Following incubation, wells were washed with 37 °C warmed PBS three times to remove the drugs completely, and 200 µl complete growth medium was then added to columns 1–12. The MTT (3-[4,5-dimethylthiazol-2-yl]-2,5-diphenyltetrazolium bromide) solution was prepared in PBS (5 mg/ml). 50 µL of MTT was added to every well in columns 1–11.

The plates were incubated for 2 hours in a humidified atmosphere at 37 °C. Following incubation, the media was removed from each well and the remaining purple MTT-formazan crystals were dissolved by adding 200 µL of DMSO to every well in columns 1–12. DMSO (200 µl) was also added to the empty column 12 to serve as a blank. The absorbance was recorded immediately (because the product is unstable) with a plate reader at an absorbance setting of 570 nm (BIO-TEK, FL600, with KC4 software). The converting of MTT into formazan occurs after cell death, so the colour transformation from yellow (MTT) to purple (formazan) is the best marker to define the viable cells. Reading was done from column 1–12; columns 1 and 12 contained medium and MTT but no cells, to blank the plate reader. The

percentages of viable cells were calculated using the average absorbance of the two readings (DMSO was blank adjusted, with the control set to 100%).

2.5 Imaging microscopy

Confocal microscopy was used to examine the effects of cylinders on U2OS cells, and to establish where they have an influence on DNA. [6]

2.5.1 Live cell microscopy

2.5.1.1 Qualitative analysis

Live cell imaging allows real time monitoring of cell treatment. Cultured U2OS cells were trypsinised and 2×10^5 cells were counted and placed in each dish for live-cell imaging. Petri dishes with covered glass bottoms were used for live-cell imaging (35 mm glass-bottom dish, dish size 35 mm, well size 20 mm, cover glass (0.085–0.115 mm). 200 µl of fresh media was added to each dish and incubated overnight until cells were adherent. Cells were labelled with Hoechst 33258 before carrying out microscopy. 500 µl of 5 mg/L Hoechst solution was added to each dish and they were incubated for 20 mins at 37 °C. Dishes were removed from the incubator and wrapped in aluminium foil immediately. They were then taken to a dark room under a hood; Hoechst was removed completely from MatTeks and cells were washed twice with 1 ml of warmed PBS. 200 µl of media was added to each dish, and they were wrapped again. A Nikon Eclipse Ti epifluorescence microscope (40x oil-objective) was used for fluorescent imaging of U2OS cells. Cells were treated with various concentrations of ruthenium and iron cylinders (0, 15, 25, 50 and 100 µM) under a hood. Images were taken every 30 mins (before and after the treatment) from each concentration of cylinder and DMSO (6 samples treated with cylinders, 2 negative control samples and 3 positive control samples with DMSO) for 2 hours. The laser was turned off following image capture to prevent photo-bleaching. The samples were maintained at 37 °C by means of a heated stage under a CO_2 atmosphere. The process was also performed with confocal microscopy in the Z-plane.

2.5.1.2 Quantitative analysis

8×10^4 cells were counted and cultured in 200 µl fresh media in each wells of multi- well MatTeks (8-well cell culture slides, 12 × 5 × 2.5 inch). MatTeks were incubated overnight till cells attached to surface. 40 µl of 5 mg/L Hoechst solution was added to each dish and incubated them for 20 mins at 37°C. Dishes were removed from incubator and wrapped in aluminium foil immediately. Dishes were taken to dark room under hood, Hoechst was removed completely from MatTeks and cells were washed with 300 µl warmed PBS twice with multiple gun. 200 µl of media was added in each dish and they were wrapped again. Nikon Eclipse Ti epifluorescence microscope (40x oil-objective) was used to do fluorescent imaging from U2OS cells. Cells were treated with various concentrations of ruthenium and iron cylinders: two wells were assigned to negative controls; two wells were allocated to positive control with 2 µl DMSO; two wells were allocated to positive controls with autoclaved deionised water; and 4 other wells were assigned to ruthenium cylinder and iron cylinder. Cells were treated with 50 µM concentration of each cylinder in 200 µl of media (ruthenium cylinder was used from 5000 µM stock solution in DMSO and iron cylinder was used from 5000 µM stock solution in water). Images were captured before the treatment and every hour after the treatment for 3 hours. The laser was turned off following image capture to prevent photo-bleaching. The samples were maintained at 37 °C by means of a heated stage under a CO_2 atmosphere. Images were analysed after captured with ImageJ/FIJI programs.

2.5.2 Fixed-cell microscopy

Cell staining is a technique that can be used to better visualise cells and cell components under a microscope. To perform fixed-cell microscopy, 10×10^6 U2OS cells per well were cultured on glass microscope slides, which were placed into multi-well microscopy dishes (three 8-well microscopy dishes), and 1 ml fresh medium was added to each well. Dishes were incubated overnight. The next day, adherent cells were washed with warm PBS once, and 200 ml fresh medium and 40 µl of 5 mg/L Hoechst solution was added to each well. Dishes were incubated from 20 mins, Hoechst was removed completely, and cells were washed twice with warm PBS. 300 µl fresh media was then added to each well again. Dishes were protected from light to prevent photo-bleaching during the process. 1.5, 3, 6 and 12 µL of ruthenium cylinder stock (2,500 µM) in 50:50 DMSO-water was used to treat cells. 1.5, 3, 6 and 12 µL iron cylinder stock (2,500 µM) in water was added to wells to treat cells. In every dish of each column, one well was allocated for testing and one well was used as a positive

control. For ruthenium treatments, 1.5, 3, 6 and 12 µL of 50:50 DMSO-water was added to wells as a control, and 1.5, 3, 6 and 12 µL of water was used as an iron cylinder control. After 2 hours of incubating dishes in the incubator, cylinders were completely removed from each well and washed with 300 µl PBS three times.
300 µl formalin was added to each well, and they were incubated at room temperature for 10 mins. Formalin was removed and the wells were washed three times with PBS. Cell plates were removed from wells with extra PBS on the correct side and were washed once again with PBS and once with water. A small oil drop was placed on the microscopy slide and the cell plate was placed from the cell site onto the oil. It was then pressed gently to remove bubbles. Slides were stored in a box and placed in the fridge to set.

2.6 Protocol for uptake studies of the ruthenium cylinder in adherent tumour cells

2.6.1 Cell preparation

Cells were trypsinised for 2 min at 37 °C in an incubator. The suspension of cells and media was then centrifuged at 1,500 rpm for 5 min at room temperature. The pellet was resuspended in 1 ml medium and viable cells were counted, with the 0.4% trypan blue solution in PBS applied (as described in section 2.3.8). In order to have a negative control sample alongside the sample treated with the cylinder, two 10 mm petri dishes were prepared by seeding with 5×10^6 cells in 10 ml complete growth media. The dishes were left in an incubator for 24 hours at 37 $^{\circ}$C under 5% CO2 to ensure that they adhere completely to the dishes' surface.

2.6.2 Compound treatment preparation

An appropriate concentration of drug to treat U2OS cells in this process was found after treating the cells in an MTT assay test with ruthenium cylinder. To obtain the best results of cells' drug uptake levels, the highest toxic concentration of cylinder was considered as an equal concentration in an ICP-MS test to treat cells; in this way, 50 µM was considered to be an optimum concentration of ruthenium cylinder. Considering the fact that using DMSO in biological systems has a limitation range due to DMSO toxicity, 2% of DMSO was found to be a safe minimum toxicity range in U2OS cells.

To make 2,500 µM stock solution of ruthenium cylinder in DMSO, the UV-vis spectrophotometry technique and Beer-Lambert law were employed when measuring the absorbance of the solution.

$$A = \varepsilon . l . c \qquad [1]$$

The Beer-Lambert equation (equation [1]) was used to find the concentration. In equation [1], A is absorbance (since $A = log \frac{P_0}{p}$), ε is the molar absorptivity with units of L mol^{-1} cm^{-1}, l is the path length of the sample in cm (that is, the path length of the cuvette in which the sample is contained) and c is the concentration of the compound in solution, expressed in mol L^{-1}. The epsilon for ruthenium cylinder in acetonitrile is 16,895 L/mol.cm. Subsequently, about 2 mg of ruthenium cylinder was solved in 500 µl of acetonitrile and the absorbance of the solvent was read at λ_{max}: 16,895 cm^{-1}. The concentration was checked and corrected using the Beer-Lambert equation. The acetonitrile in the optimum sample was evaporated completely and an equal amount of DMSO was added to the sample (of pure ruthenium cylinder) and vortexed, to produce a 2,500 µM stock sample of ruthenium cylinder.

2.6.3 Compound treatment

Following 24 hours of incubation, 200 µl of the stock solution was added to 10 ml media in one of the prepared petri dishes that was labelled as a test, or T. The second petri dish was considered as a positive control; 200 µl of DMSO was added and the petri dish was labelled as a control, or C (the same solvent was used at the same time to make it blank). Petri dishes T and C were both incubated for 4 hours until cells had uptaken the drugs.

2.6.7 ICP-MS

After 24 hours, cells were washed several times with warmed PBS to remove complex excess. Cells were trypsinised, then centrifuged at 1,500 rpm for 5 mins at room temperature to make a pellet. The pellet was resuspended in 600 µl of growth medium, then 20 µl of the suspension was counted with the hemocytometer. The cell suspension was divided into two equal amounts of S1 and S2. S1 was kept as a test sample and used for fractionation using a kit. Meanwhile, S2 was kept as a sample of the whole cell and labelled with this name. The same steps were taken for the positive control sample at the same time.

To separate the nucleus from the cytoplasm, the Nuclear/Cytosol Fractionation Kit (BioVision, Catalog#K266-25) was used.

The contents of the kit are presented in Table 2.1. All reagents were stored at -20 °C after opening.

Table 2.1. The table of kit contents.

Component	K266-25 25 assays	K266-100 100 assays	Cap code	Part number
Cytosol extraction buffer A (CEB-A)	5 ml	20 ml	WM	K266xx(x)-1
Cytosol extraction buffer B (CEB-B)	300 µl	1.2 ml	Green	K266xx(x)-2
Nuclear extraction buffer A (NEB)	25 ml	10 ml	NM	K266xx(x)-3
DTT (1M)	100 µl	100 µl	Blue	K266xx(x)-4
Protease inhibitor cocktail	1 vial	1 vial	Red	K266xx(x)-5

2.6.7.1 Reagent preparation

Initially, an ice box was prepared to ensure that all buffers, inhibitors and extractions were kept on ice during the experiment. Then, 250 µl of DMSO was added to 500X protease inhibitor cocktail to solve it before use, and it was placed on ice.

For the experiment, a sufficient amount of cytosol extraction buffer A (CEB-A) and nuclear extraction buffer A (NEB) were prepared before starting the procedure. 2 µl of protease inhibitor cocktail and 1 µl of DTT were added to each 1 ml of CEB-A and each 1 ml of NEB, individually, and they were kept on ice ready for use.

2.6.7.2 The fractionation protocol

After 4 hours of incubation, cells from both petri dishes were trypsinised and then centrifuged at 1,500 rpm for 5 min. The pellets were resuspended with 1 ml growth medium and each was divided into two different vials. The cell numbers were counted with a hemocytometer and recorded. Two samples (S2 and C2) were kept on ice at 4°C as whole cells (sample whole cells and control whole cells).

The kit protocol was followed for both S1 and C1 at the same time. Cells were collected by centrifugation at 600×g for 5 mins at 4 °C. Subsequently, 0.2 ml of CEB-A mix containing

DTT and protease inhibitors was added to the cell pellets. The mixtures were vortexed strenuously for 15 seconds at the highest speed. The cell pellets were incubated on ice for 10 mins before 11 µl of 0–4 °C cytosol extraction buffer-B was added to the tubes. Tubes were vortexed at the highest speed for 5 seconds and then incubated on ice for 1 min. The vials were vortexed on the highest setting for 5 seconds. Tubes were centrifuged with a microcentrifuge at the high speed of 16,000×g for 5 mins at 4 °C.

The supernatant (cytoplasmic extract) fractions were immediately transferred to a clean pre-chilled tube and placed on ice. The pellets (containing nuclei) were resuspended in 100 µl of ice-cold NEB mix. The samples were vortexed on the highest setting for 15 seconds and the samples were then returned to ice. This step was repeated 8 times every 10 mins, for a total of 40 mins. Tubes were centrifuged at 16,000×g for 10 mins at 4 °C. The supernatants (nuclear extract) were immediately transferred to the clean pre-chilled tubes and were placed on ice. The extractions were stored at -80 °C.

2.6.7.3 Sample preparation

To prepare the samples, all cell fractions were transferred to clean vials. To clean the vials, they were washed very carefully (they were initially washed for 30 min in HNO_3 5%, the HNO3 was washed in Distilled Deionized (dd) water for 30 min, vials were cleaned for 15–30 min in methanol and 15–30 min in acetone, then dried completely in a clean oven. Contact with any solvent or dirt was avoided).

After cleaning the vials, the cellular fraction was transferred into vials and 2 ml of HNO3 70% (Traceselect Ultra Aldrich) was added to each one. Vials were kept in a freezer at -80 °C overnight for digestion. Samples were transferred to falcon tubes the next morning. Ultrapure water was added to each vial to dilute the HNO_3 to 5%, and falcon tubes were kept on ice for analysis.

2.7 Alkaline comet assay

Comet assay is a technique used to measure DNA damage from treating cells with a drug, which combines DNA gel electrophoresis with fluorescence microscopy. It aims to visualise the migration of DNA strands from individual agarose-embedded cells.

2.7.1 Cell preparation

2×10^6 cells were cultured in 3 separate 6-well plates and were incubated overnight in an incubator at 37 °C. Each plate had 3 columns and each column had 2 rows (A and B). The cells in plate 1 were treated with 3 different concentrations of ruthenium cylinder (15, 25 and 50 and 100 µM); plate 2 was treated with 3 different concentrations of iron cylinder (15, 25 and 50 and 100 µM); and plate 3 was treated with cisplatin in column 1 as a positive control. Column 2 was used as the negative control.

2.7.2 Preparation of buffers and slides

2.7.2.1 Lysis buffer

To make the lysis buffer, 146.4 g of NaCl, 37.2 g of $Na_2EDTA.2H_{20}$ and 1.21 g of Tris base were dissolved in 800 ml H2O to give 2.5 M NaCl, 0.1 M Na2EDTA.2H20 and 10 mM Tris base. The pH was set at 10 with NaOH pellets and pH was checked continuously with a pH meter, which was calibrated with standard solutions before the test. 33.3 ml sodium lauryl sarcosinate was added to the solution, which was then made up to 1 L with deionised water. The lysis buffer was stored at 4 °C in a cold room.

2.7.2.2 Neutralisation buffer

24.6g Tris base was solved in 500 ml deionised water; the pH was adjusted using HCl to 7–7.5 and the solution was stored at 4 °C in cold room.

2.7.2.3 Electrophoresis buffer

Initially, two stock solutions were made. The 9 M stock solution of sodium hydroxide was prepared with a mixture of 180 g NaOH pellets in 500 ml deionised water (stock A), and the 200 mM stock solution of Na2EDTA.2H2O by solving 37.2 g of its powder in 500 ml deionised water (stock B). 80 ml of stock A and 12 ml of stock B were then mixed together to produce 300 mM NaOH and 1 mM EDTA. The solution was made up with deionised water to 2,400 ml and was stored at 4 °C in a cold room. This buffer was made up one night before the test.

2.7.2.4 Preparation of slides

0.5% w/v normal melting point agarose (NMPA) solution was prepared by dissolving 1 g NMPA powder in 200 ml dd H_2O, which was then warmed in a microwave to dissolve the agarose completely. The evaporated H_2O was compensated and cooled down to around 60 $^{\circ}$C before use. Slides were prepared 1–2 days before the experiment. To make the slides, ¾ of clean frosted slides (unfrosted portion) were dipped in molten NMPA one by one, and the agarose was cleaned from the underside of the slides. Slides were then left horizontally to dry.

2.7.2.5 LMPA preparation

To prepare the 5% (w/v) LMPA solution, 1 g LMPA was dissolved in 200 ml PBS in a microwave for 5 mins and stored at 37 °C.

2.7.2.6 SYBR gold staining solution preparation

1 µl of concentrated SYBR gold staining was dissolved in 1 ml deionised water and used immediately. This amount was enough for 20 slides.

2.7.3 Comet assay procedure

After 4 hours of treating cells, drugs and medium were removed from wells and washed 3 times with 2 ml pre-warmed PBS. 300 µl of PBS was added to each well and scraped carefully to detach cells from the surface without using trypsin. The mix of cells and PBS was transferred into an Eppendorf and then labelled with the correct name. Cells were centrifuged with a micro-centrifuge at 13,000 rpm for 5 mins. The pellet split from PBS and responded it in 150 µl of PBS. An ice-cold silver tray surface was prepared 5 mins before starting the procedure. 15 µl of the cell suspension was mixed with 150 µl of warmed molten LMPA in a new Eppendorf, which was then vortexed for 15 seconds to mix completely. 150 µl of suspension was transferred onto coated slides, which were labelled with their information and a cover slip was placed gently on top. Slides were placed on an ice-cold surface for 20 mins to solidify. After solidification, cover slips were removed from the slides and a mixture of lysis buffer containing 10 ml DMSO, 89 ml lysis buffer and 1 ml Triton X was transferred into a coplin jar. Slides were placed into jars, wrapped with foil and placed in a cold room for 1 hour. Slides were then removed from coplin jars and placed into an electrophoresis tank from left to right. An electrophoresis buffer was added to the tank and slides were left there for 20

mins. The instrument power pack was turned on at 32 V, 300 mA and electrophoresed for 20 mins.

Slides were removed and washed with neutralisation buffer 3 times for 5 mins, before they were washed with dd water once and then again for 5 mins. 50 µl SYBR gold solution was added to each slide and covered with a cover slip. A moist box was made, where slides were placed and carefully covered with foil. The images were taken by microscope via 40x oil objective one by one.

2.8 Western blot technique

The highly important method of western blotting, which uses gel electrophoresis to separate native proteins by 3D structure or denatured proteins by polypeptide length, is a tool for protein identification and relative quantitation in complex samples. This technique combines size-based electrophoretic separation with immunoaffinity to identify specific proteins.

2.8.1 Cell preparation and treatment

Cultured cells were trypsinised and centrifuged to produce a pellet, which was resuspended in 1 ml PBS and counted by a hemocytometer. 1.5×10^6 cells were seeded in 18 different 10 cm dishes and incubated overnight to inherent cells. The next day, cells were treated with different concentrations of iron cylinder (50, 200 and 500 µM), ruthenium cylinder (50, 200 and 500 µM) and cisplatin (5 and 50 µM) for 1 hour and 24 hours. Cisplatin was considered as the positive control and two untreated dishes were considered as negative controls after 1 and 24 hours. In total, two treatment times were used for each compound and concentration. All of the dishes were washed with 2 ml pre-warmed PBS, then trypsinised for 2 mins. Cells were centrifuged at 3,000 rpm for 5 mins to make a pellet. Split pellets were washed once with cold PBS. Cells were pelleted again and all PBS was removed with 200 µl tip carefully. The pellets were then frizzed in liquid nitrogen and stored at -80 $^{\circ}$C.

2.8.2 Cell lysis

For lysis cells, a UTB buffer was made with a mix of 8 M urea, 50 mM Tris base and 150 mM mercaptoethanol. To make 100 ml of UTB buffer, 75 ml dd water was heated in a water bath to 50 °C, and 48 g urea was added to the water and stirred to dissolve. The solution was

cooled to room temperature, and 0.61 g Tris base and 1.172 ml beta-mercabthanol were added to the urea solution. The pH was then adjusted to 7.5.
Next, 100 µl UTB lysis buffer was added into each frizzed cell Eppendorf. Cells were sonicated on ice (2 cycles, max power for 10 mins). Samples were then centrifuged at 13,000 rpm at 4 °C for 20 mins with a benchtop centrifuge.

2.8.3 Bradford protein assay

In the Bradford protein assay, colour changes (from orange-brown to blue) resulting from the binding of protein molecules to Coomassie dye under acidic conditions is investigated (colourimetric assay). This technique helps to measure the concentration of total protein in a sample.
1 mg/ml bovine serum albumin (BSA) in PBS was prepared as stock solution. 0, 1, 2, 3, 4, 5 and 10 µg/µl standards were prepared from stock. Each sample was diluted with dd water to 1/10 by adding 36 µl of dd water to 4 µl samples. 10 µl of the standard samples were added to 18 wells of a 96-well plate (6 columns each of A, B and C rows). 5µl of each sample was transferred into wells. 200 µl of Bradford buffer was added to the wells, and the plate was incubated in a dark room for 5 mins. The plate was read on a plate reader, and the concentrations were calculated for the preparation of lysates to load 20 µg protein/gel.

2.8.4 Gel electrophoresis

2.8.4.1 Gel, buffer and solution preparation
A. 10% SDS
10 g sodium dodecyl sulphate (SDS) crystals were dissolved in 90 ml water. SDS crystals were solved at 68 °C. The pH was checked with a pH meter and then adjusted to pH 7.2 with the addition of HCl. The volume was made up to 100 ml with water and the solution was stored at room temperature.

B. Tris solution (0.5 M, pH 6.8)
60.57 g Tris(hydroxymethyl)aminomethane was solved in 800 ml water. The solution was autoclaved for 24 hours and pH was adjusted to 6.8 with 100 ml HCl 37%. The volume was made up to 1 L with water and the solution was stored at room temperature.

C. Tris solution (1.5 M, pH 8.8)

181.71 g Tris(hydroxymethyl)amoniumethane was dissolved in 800 ml water and was autoclaved for 24 hours. The pH was adjusted to 8.8 with the addition of 40 ml HCl 37%, and the volume was made up to 1 L with water. The solution was kept at room temperature.

D. Make10X Laemmli buffer stock

30.25 g Tris base and 144.20 g glycine were solved in 650 ml water. 100 ml 10% SDS was added to the solution. It was then brined up to 1 L with dd H2O, and diluted to 1X for running gel.

E. Make 6X SDS loading buffer

7 ml 0.5 M Tris and 1 g SDS were dissolved by vortexing for about 5 mins. 3 ml glycerol, 1.2 mg bromophenol blue and 680 µl mercaptoethanol were mixed with the solution.

F. Make staking gel

To make staking gels, 11 ml water, 2.4 ml acrylamide 30%, 5 ml Tris solution (0.5 M, pH 6.8) and 200 µl SDS 10% were mixed together and kept at room temperature.

G. Make running gel

To make two running gels, 15.8 ml water, 13.4 ml acrylamide 30%, 10 ml Tris solution (1.5 M, pH 8.8) and 400 µl SDS solution 10% were mixed and stored at room temperature.

2.8.4.2 Protocol

For gel electrophoresis, the gel apparatus and glass plates were cleaned thoroughly with soap and water and rinsed with ethanol. They were left to air dry and were then assembled. Two gels were made for each cylinder: one for the CK1 protein and one for P-CK1. Gels were made of two different gel phases: running gel at the bottom of plates, and staking gel at the top. Two gels were made up as described in steps F and G in the section above. The running gel was mixed with 400 µl APS 10% and 40 µl TEMED to set, and plates were immediately poured with 7 ml of complete running gel. 1 ml/gel butanol (H20-saturated) was added to the top of each gel to reduce bubbles, and was left to set for 20 min. Gels were checked after 20 mins (the remaining gel in the tube was examined to establish whether the gels had set well) and they were washed appropriately with dd water to completely remove butanol. Staking gel was mixed well with 200 µl APS 10% and 10 µl TEMED to fix, and was immediately poured

on top of the running gels in the plate. Combs were then inserted at an angle (to prevent the formation of bubbles). The spaces on both sides of the combs were checked to ensure that all wells had complete walls before they were left to set. During the setting time, samples were prepared through mixing with a loading buffer (20 µg/gel, 5X; see the data from the Bradford protein quantification in Table 3.2.) and boiling in a heating block for 10 mins at 100 °C, then centrifuged with 1,300 rpm for 20 mins at 4°C. Once the stacking gel was set, the combs were gently pulled out of the gel and the wells were washed out with dd H2O. The tank was filled inside and outside with 1X Laemmli buffer. The samples and marker were loaded in their wells and electrophoresis was performed with 75 V and 0.09 A for 90–120 mins.

2.8.5. Protein transfer

In this step, the protein was transferred from gel to membrane, which is conventionally made of a chemically neutral substance such as nitrocellulose or polyvinylidene difluoride (PVDF).

2.8.5.1 Preparation of buffer and solutions

The following buffer and solutions were used in this step of the process.

A. Transfer buffer

5.8 g glycine and 11.6 g Tris was dissolved in 400 ml methanol, and the solution was made up to 2 L with water.

B. Block

25 g milk powder was dissolved in 500 ml TBS-T and stirred to solve completely, then stored at 4 °C in a fridge.

C. TBS 10X

60.5 g Tris and 87.6 g NaCl were mixed with 800 ml dd water to have a pH of 7.5, then adjusted to 1 L with the addition of dd water.

D. TBS-T 1X

100 ml of 10X was diluted with 900 ml dd water, and 1 ml of Tween-20 was added.

2.8.5.2 Protocol

To transfer the gel to a membrane, a nitrocellulose membrane (one sheet per gel) and Whatman paper (two sheets per gel) were cut and prepared before the procedure. Gels were removed from the tank, and to remove them from between the glass plates, a green wedge was used to gently pry the glasses apart. This was carried out in a tray of transfer buffer. Gels were removed easily from slides into the liquid, but were picked up very gently because of their fragility. They were assembled in cassettes in a particular way, to transfer proteins to the membrane in the correct orientation. Assembly proceeded by this rule; the entire setup was located in a Tupperware container full of transfer buffer. The layers were set from the black side to clear side as follows: black side, pad, paper, gel, membrane, paper, pad, clear side. Layers were rolled with a glass rod to roll out bubbles. Cassettes were then closed tightly and placed in a tank in the correct orientation. The tank was filled with transfer buffer, which was cooled with an ice pack from the 20 °C freezer and stirred with a stir bar. Electrophoresis was performed at 100 V for 1 hour. Membranes were removed carefully and floated in Ponceau solution for 5 mins. They were then washed with TBS to remove the red colour. The excess length of membranes was cut, labelled and placed in block solution for one hour at room temperature with agitation. Membranes were placed in a primary antibody overnight. Two membranes were for ruthenium cylinder and two others for iron cylinder. One membrane of each group was placed into 2 ml of a mixture of 1 µl CK1 (CK1 (G-4)-10t: A17-13, Santa Cruz Biotechnology) antibody in 10 ml block solution. The other two membranes were placed into 2 ml of a mixture of 10 µl CK1-P (Phospho-ChK1 (Ser345) antibody, # 2341L) in 10 ml BSA or TBS-T. They were kept overnight in a cold room with agitation.

2.8.6 Development

Membranes were removed from the bag. The antibodies were recovered and washed in 50 ml TBS-T for 10 mins three times. Secondary antibodies were diluted in block (16 µl of anti-mouse was diluted in 50 ml block, and 50 µl of anti-rabbit was diluted in 50 ml block). Membranes were placed in their antibody for 1 hour at room temperature with agitation, and were then washed three times in 50 ml TBS-T. A chemiluminescent solution was used to develop them (5 ml of HRP swostrate peroxide solution (WBK L0500milipore) was mixed with 5 ml of HRP swostrate luminal reagent (WBK SØ500milipore)), which membranes were placed into for 2–3 mins. Membranes were picked up carefully with forceps and placed

between the plastic sheets in the cassette. The film was placed (cut into ¼ pieces) at the bottom right corner of the other side of the cassette in a dark room, and the cassette was closed tightly for 1 min. Film was then run through the developer. The ladder was traced in each film and lined up exactly. [7]

2.9 References

1. Hotze, A. C., Hodges, N. J., Hayden, R. E., Sanchez-Cano, C., Paines, C., Male, N., Tse, M. K., Bunce, C.M., Chipman, J. K. Hannon, M. J. (2008) Supramolecular iron cylinder with unprecedented DNA binding is a potent cytostatic and apoptotic agent without exhibiting genotoxicity. Chem. Biol. 15 (12): 1258-1267.
2. Pascu, Gabriel I., et al. "Dinuclear Ruthenium (II) Triple- Stranded Helicates: Luminescent Supramolecular Cylinders That Bind and Coil DNA and Exhibit Activity against Cancer Cell Lines." *Angewandte Chemie* 119.23 (2007): 4452-4456.
3. Freshney, R. Ian. *Culture of specific cell types*. John Wiley & Sons, Inc., 2005.
4. Niforou, Katerina N., et al. "The proteome profile of the human osteosarcoma U2OS cell line." *Cancer Genomics-Proteomics* 5.1 (2008): 63-77.
5. https://www.atcc.org/~/media/AnimCellCulture_Guide.ashx
6. https://www.microscopyu.com/applications/live-cell-imaging/live-cell-imaging-culture-chambers
7. BioVision, Nuclear/Cytosol Fractionation Kit datasheet, http://www.biovision.com/documentation/datasheets/K266.pdf

Chapter 3

Results and Discussion

3.1 Introduction

Today, different types of cancer are treated by methods such as surgery, radiotherapy and chemotherapy. Among these treatment strategies, chemotherapy is considered to be an effective way to fight cancers because it uses chemistry to manipulate the biochemistry and way of survival of cells. Various anticancer drugs and medicines have been designed in recent years to treat a variety of cancer types by preventing their ability to grow and divide.

In contrast to surgery and radiotherapy, which specifically target cancerous organs and tissues, chemotherapy can have various effects on all organs of the body. Depending on the types of medicines used in a chemotherapy treatment, an extensive range of side effects can be produced. To avoid the destruction of normal cells by chemotherapy, in recent decades many research activities have focussed on designing targeted (or 'smart') drug delivery as a new pathway for developing less aggressive chemotherapy drugs. Cell cycle drugs are desirable because they have fewer side effects as anticancer drugs, and they can enhance a patient's quality of life during the treatment.

Cancer cells are classified into two groups: proliferating cells and non-proliferating cells. Depending on the class, different approaches must be applied in their treatment. [1]

Small molecules, hormones and other kinds of antineoplastic drugs are used to inhibit or kill the cell growth progress in proliferating cancer cells. For instance, DNA replication is impeded by anticancer drugs; accordingly, topoisomerase enzymes can be inhibited as an impact of this process. Cell biochemistry can be altered by disordering protein synthesis as a result of topoisomerase enzyme inhibition, which can stop cell growth or drive cells to death. [2,3]

While targeting DNA is now known to be an effective approach to address the cancer problem, it is also important to consider the possible disadvantages and complications that may arise from choosing this treatment strategy. The significant side effects of this line of treatment can include an increase in the chance of developing secondary cancers resulting from damaged DNA, which should be taken as a huge drawback. Some small molecules such as cisplatin – a well-known and effective drug classified under the alkylating group of anticancers – can form permanent covalent bonds with DNA. Such a permanent change might improve the risk of secondary cancers developing, resulting in further gene mutation. [4]

In this study, ruthenium and iron cylinders are used to treat osteosarcoma (U2OS) cells, which are classified as high proliferation cancer cells, with DNA-targeted anticancer drugs.

It is expected that both cylinders stop the replication fork and transcription process, by blocking the DNA groove through the formation of noncovalent bonds with DNA, and disorder the cell growth progress, by changing the biochemical processes inside cells, thereby killing cancer cells due to their high toxicity and lack of genotoxicity effect.

3.2 Fluorescenc microscopy

To study the effects of ruthenium and iron cylinders on U2OS cells, Fluorescence microscopy was used to establish how they uptake and localise in cells (i.e. the uptake process). In contrast to the iron cylinder, the ruthenium cylinder has a fluorescent property that provides the possibility to directly study its activity in cells by Fluorescence microscopy, although it does not have an intensive absorption. So, in both cases, a better strategy for imaging is required. Therefore, to demonstrate noncovalent bonding in the cylinders and to determine the location of their attraction to DNA, an auxiliary fluorescent probe was used in this research.

Fluorescence microscopy is frequently used in life sciences to investigate biomolecules and their interactions and connections to each other through labelling of biomolecules and organelles. This technique enables the use of multiple lasers combined with a fluorescent filter to capture sharp and multicoloured images. [5]

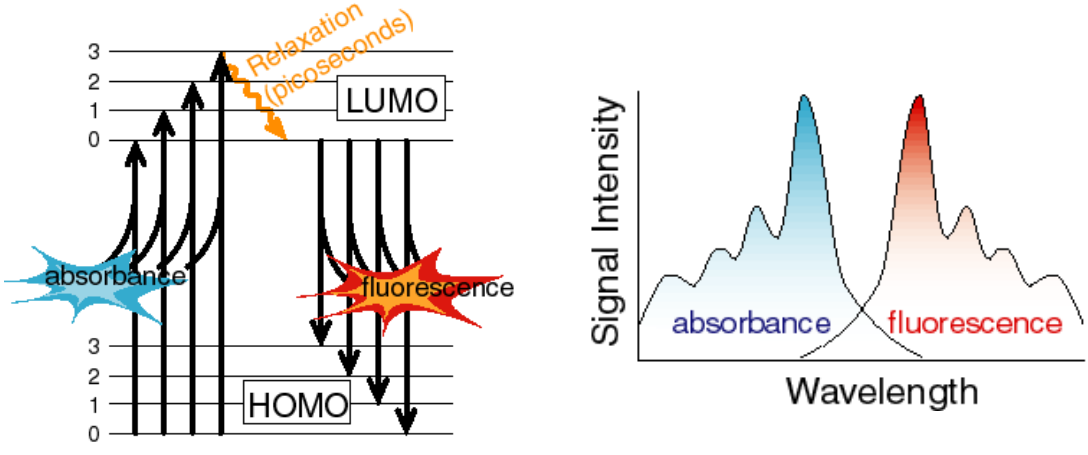

Fig. 3.1. The transition between the zero vibrational levels of the HOMO and LUMO. Taken from ref 7.

Fluorescence is the emission of light accompanying relaxation of a molecule from an excited state to its ground state. In this technique, electrons are excited to unoccupied LUMO state orbitals (with higher energy levels) due to the adsorption of photons; when they relax and return to ground state, the vibrational energy is lost, and thus the emission spectrum is shifted towards longer wavelengths.

Molecules with this property are called fluorophores. These structures frequently contain many aromatic rings, long conjugate bond networks and, frequently, hetero atoms. Three examples are rhodamine, fluorescein and anthracene. [6,8]

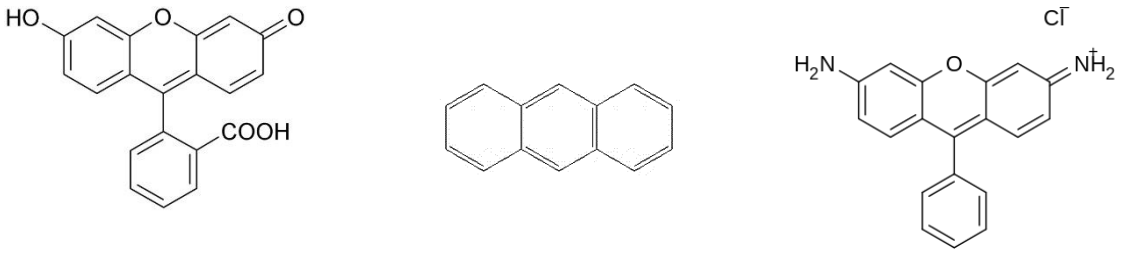

Rhodamine Anthracene Fluorescein

Fig. 3.2. The structures of some fluorescent compounds.

Fluorescent probes are essential factors in nucleic acid imaging, for both live- and fixed-cell imaging. Fluorescent labels are designed depending on the location of their interaction with DNA and RNA. Fluorescent gene probes are classified into three groups: sequence-specific DNA bonding peptides and proteins, triplex-forming oligonucleotides gene targeting and groove binders. In most studies, these repeated DNA sequences, which are localised in the specific loci of chromosomes, such as centromeres or telomeres, have been used as targets. The local concentration of the desired sequence is quite high and it can therefore be detected with the fluorescent probes. [9,10]

Polyamides with conjugate minor groove binders are understood to be better choices because of the fact that fluorophore probes must have high cellular uptake and penetration, stability in various physical conditions (live-cell microscopy) and the ability of easy detection. Fluorophore stain stability is considered to be an important property of DNA probes; fluorescent probes mostly lose their fluorescent ability during the imaging process (during photo-bleaching or dye photolysis). The photo-bleaching phenomenon is a photochemical modification of the dye which results in a permanent loss of the ability to fluoresce. [11]

Hoechst is a blue stain minor groove DNA binder with high specificity and low background, which is used in both live- and fixed-cell microscopy. It is a bis-benzimide derivative that can be classified into three groups: Hoechst 33258, Hoechst 33342 and Hoechst 34580.

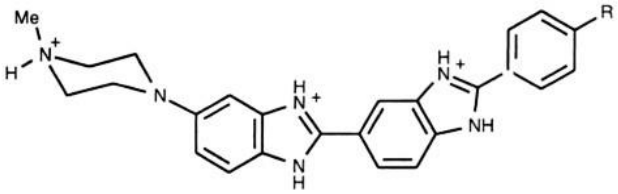

Hoechst 33258 R=OH
Hoechst 33342 R=OEt
Hoechst 34580 R=N(Me)$_2$

Fig. 3.3. The Hoechst structure. Taken from ref 12.

Hoechst is a minor groove binder stain with a tendency to bind to the AT reach sites of double-strand DNA. Its fluorescent intensity is increased when it forms a bond with DNA.

Kinetic studies have demonstrated high rates of association constants Ka of Hoechst 33258 to DNA AT reach sites. The affinity of Hoechst binding to DNA produces AATT as the strongest binding sequence and TATA, like TTAA, as the weakest binding sequence. [13]

To survey the cell uptakes of cylinders and to determine the position of their action on DNA, Fluorescence microscopy imaging was used as an effective technique. The additive factor was used to help with detection of the nonfluorescent iron cylinder as a minor groove DNA binder.

In this method, Hoechst was used as a DNA fluorescent probe to bond with the DNA minor groove; the displacement of Hoechst with iron cylinders was the basis of the investigations presented here. Hoechst 33258 is excited at 350 nm and emits at 461 nm, while Hoechst 33342 is excited at 352 nm but also emits at 461 nm. While Hoechst 34580 used in these experiments is excited at 370 nm and emits at 437nm. In addition, ruthenium cylinder interaction with DNA was studied using this technique. The ruthenium cylinder has fluorescent absorbance and was imaged at 488 nm with an FITC channel separately. [14,15]

3.2.1 Live cell imaging

Iron and ruthenium cylinders are able to interact with the major groove and replication fork junction of DNA. In this way, they can inhibit DNA replication and destroy cell growing paths. Examining cylinders' modes of action and their sites of localisation are the goals of this investigation. Since Hoechst (the blue fluorescent probe) demonstrates interaction with the minor groove of DNA, it can be considered as a suitable indicator to find the location of cylinder action. Previously published research has demonstrated that the Hoechst blue colour was bleached when iron or ruthenium cylinders replace Hoechst on the minor groove of DNA.

To carry out live-cell microscopy, U2OS cells were cultured in MatTeks and incubated with Hoechst 34580 for 20 mins before imaging. Blue dye was washed completely with PBS, and medium was added to each dish again. Cells were imaged with a Nikon microscope with different channels to record all changes in the vast range of absorbance. Images were taken before treatment from the test and negative and positive control MatTeks. In the initial test, the first sample was treated with the minimum effective concentration, 25 µM, of iron cylinder, while the second sample was treated with 15 µM of ruthenium cylinder. A negative control was used to assess the process in samples with compression. Consequently, the negative controls act as evidence to differentiate photo-bleaching from Hoechst displacement. In addition, 1% of DMSO was used as a positive control to expose U2OS cells to ruthenium cylinder solvent and investigate its impact on the cells (i.e. Hoechst replacement or bleaching).

To capture images of the samples, they were observed through a DAPI blue fluorescence filter with 75 nm bandpass within the 420–495 nm range. The blue colour of Hoechst was observed in the nucleolus of cells in all samples before treatment. To confirm the fact that the ruthenium cylinder has absorbance at 488 nm, cells were also checked by an FITC green filter in spectral regions of 450–500 nm. The cells did not show a green shade before treatment. They were also checked with a DAPI-FITC dual band fluorescence filter combination, where all samples showed a blue colour only in images.

Images were captured after 1 and 2 hours of treatment and did not show a marked contrast in the intensity of the blue colour compared with the primary images and negative control sample. The blue shade of Hoechst remained remarkably blue, whereas the green colour was additionally seen in samples treated with ruthenium cylinder after 1 hour (Fig. 3.4c).

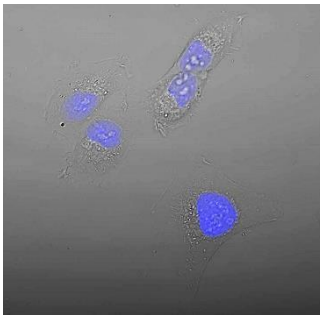

(a)

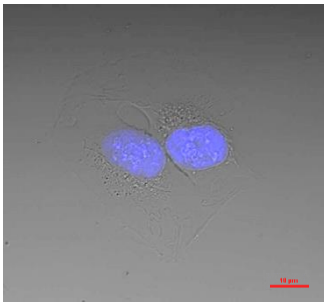

Dual filter DAPI-FITC (420-500 nm)

DAPI filter (420-495 nm)

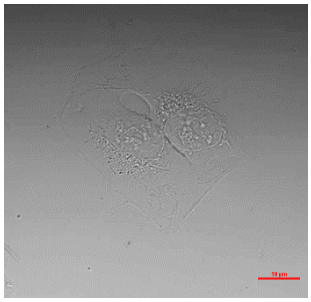

FITC filter (450-500 nm)

(b)

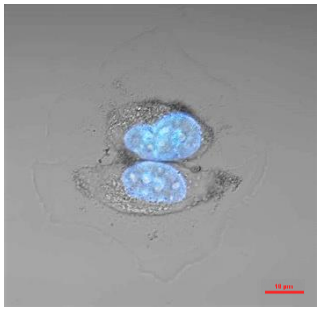

Dual filter DAPI-FITC (420-500 nm)

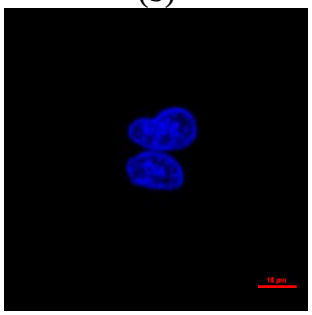

DAPI filter (420-495 nm)

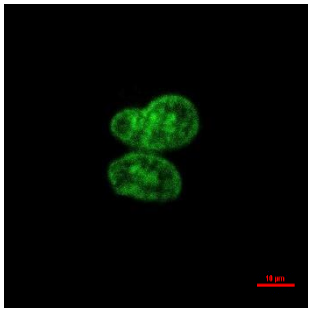

FITC filter (450-500 nm)

(c)

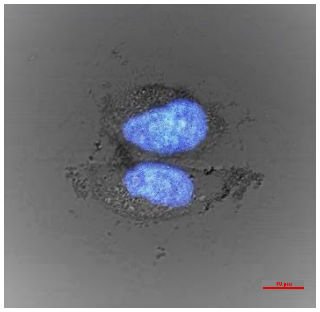

Dual filter DAPI-FITC (420-500 nm)

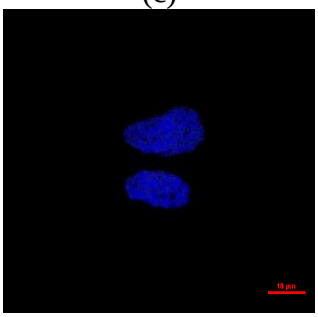

DAPI filter (420-495 nm)

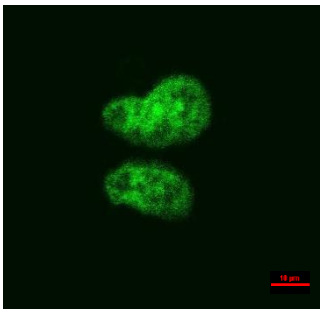

FITC filter (450-500 nm)

(d)

Fig. 3.4. Live imaging in different channels of U2OS cells treated with 15 µM ruthenium cylinder: a) positive control imaging after 2 hours (the image original size was 2048 x 2048 pixels, with 0.16 micron / pixel scale means 328 µm x 328 µm); b) imaging of samples before treatment; c) imaging after 1 hour of treatment; d) imaging after 2 hours of treatment.

In Figure 3.4d, cells appear to be alive with healthy membranes, but some changes can be observed around the nucleus area. After 2 hours, the blue and green shades decrease and the membrane still looks healthy, but the damage around the nucleus area is increased. In the positive sample test there is no significant difference between images before and after treatment, meaning that cells appear to be alive and no damage is observed in the membranes or around the nucleus area. Notably, Hoechst displacement was not observed in any of the samples in this test.

Following the previous test, U2OS cells were treated with 0, 15, 25, 50 and 100 µM of ruthenium and iron cylinders to check the effect of a high cylinder concentration on Hoechst replacement (Fig. 3.5). Even though concentrated cylinder samples were used in this test, the final results were similar to those of the first experiment.

Figure 3.5 shows the U2OS cells treated by 50 µM ruthenium cylinder for 2 hours. Initially, it appears that the ruthenium cylinder was replaced with Hoechst due to the reduction in the intensity of the blue colour over 2 hours. In addition to this observation, the green colour that was absorbed in the FITC filtration channel flourishes and then declines in its intensity during imaging, but the blue colour fades simultaneously. The green colour is a sign of the existing ruthenium cylinder in cells which was not initially observed in the green channel, but was made to fade by Hoechst during the imaging time. Despite the observations of the first test, Hoechst could have been replaced by a highly concentrated solution of ruthenium cylinder over 2 hours.

However, the option of light bleaching following multi-capture imaging is possible; therefore, quantitative imaging was carried out to assess the results. Alternatively, the green colour of the ruthenium cylinder might appear as a result of hydrogen bonds formed with Hoechst and the formation of long conjunction bonds to improve fluorescent adsorption. Subsequently, it faded due to Hoechst at the same time. In other studies, the green shade in the FITC filtration channel has been explained differently, and presented as a Hoechst photoproduct with emission at 458 nm.[8] Fixed-cell microscopy was carried out to eliminate the photo-bleaching element from the process, and to enable cells to be studied by removing environmental effects. The ruthenium cylinder adsorption at 458 nm (the green channel) was checked by fixed-cell microscopy in the absence of Hoechst after treating cells.

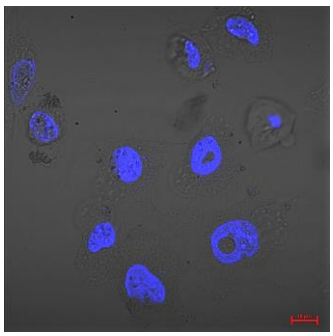

Dual filter DAPI-FITC (420-500 nm)

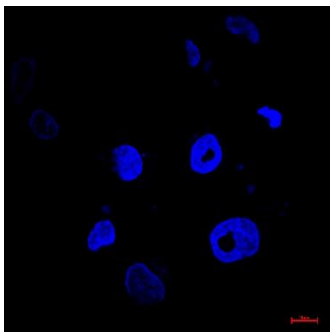

DAPI filter (420-495 nm)

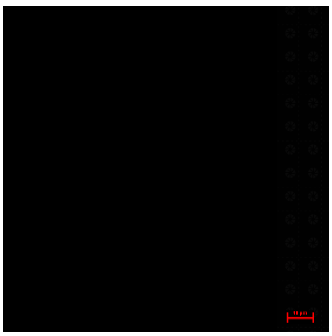

FITC filter (450-500 nm)

(a)

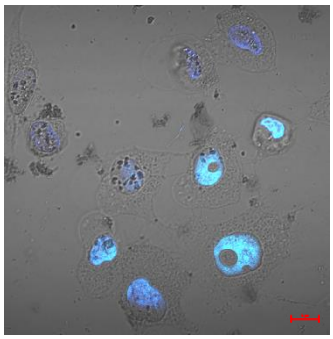

Dual filter DAPI-FITC (420-500 nm)

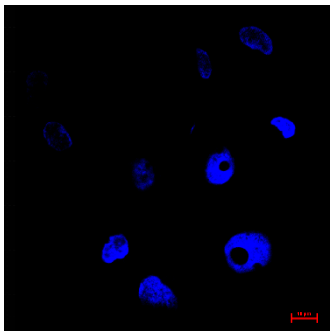

DAPI filter (420-495 nm)

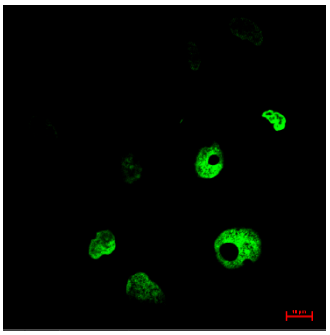

FITC filter (450-500 nm)

(b)

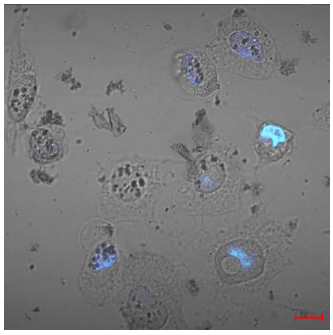

Dual filter DAPI-FITC (420-500 nm)

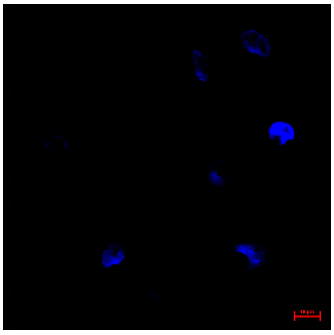

DAPI filter (420-495 nm)

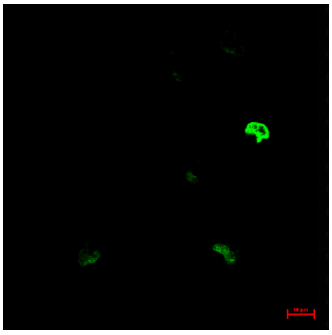

FITC filter (450-500 nm)

(c)

Fig. 3.5. Live imaging in different channels of U2OS cells treated with 50 µM ruthenium cylinder: a) samples before treatment; b) after 1 hour of treatment; and c) after 2 hours of treatment. (the micron bar shows the scale of 10µm)

3.2.2 Fixed cell imaging

Fixed-cell microscopy is a type of Fluorescence microscopy whereby cells are fixed and killed with formaldehyde before imaging. This is known as chemical fixation, which applies special compounds to preserve cell structure, both chemically and structurally, to be as close as possible to a living tissue. Fixation protects cells by the destruction of biochemical processes within them, such as autolysis and putrefaction. This is typically done by disabling intrinsic biomolecules (particularly enzymes) which may otherwise digest or damage the sample. Fixation causes cell death, and the mechanical strength or stability of supermolecules and cells are increased by chemical fixation at the molecular level. [16]

In the first test, U2OS cells were cultured in multi-well dishes and on microscopy circle slides. After one night, the adherent cells were treated by 0, 12, 25 and 50 µM iron and ruthenium cylinders for 2 hours and washed with PBS several times, in order to totally remove the cylinders. Cells were fixed with 10% formalin and then fixed on microscopy slides with oil. Cells were stained by Hoechst (33258) 20 mins before the treatment, in order to observe Hoechst replacement by cylinders. An untreated sample was fixed as a negative control, to observe the fluctuations in Hoechst adsorption intensity for comparison with treated samples. Fixed slides were imaged by a Nikon microscope using the same program as live microscopy, and with the same settings for all slides.

The images represent the same result as in live microscopy, because Hoechst replacement was not observed completely in treated samples when compared to the controls. Figure 3.6 shows that Hoechst is observed in the cell nucleus after 2 hours of treatment with ruthenium cylinder, and the blue colour in the picture was captured by DAPI filtration (Fig. 3.6d) shows that the stain was not replaced by ruthenium cylinder. The green colour in Figure 3.6b does not show the same location as the blue colour in Figure 3.6d; this can be explained by the green colour as a sign of ruthenium cylinder existence in cell parts, particularly the nucleus.

However, since ruthenium cylinder with its special structure is itself fluorescent and highly photo sensitive, the treated cells were imaged without staining by Hoechst. This was done in order to recognise the ruthenium cylinder cell uptake and the location of its effects by applying fixed-cell microscopy to better control the photo-bleaching effect.

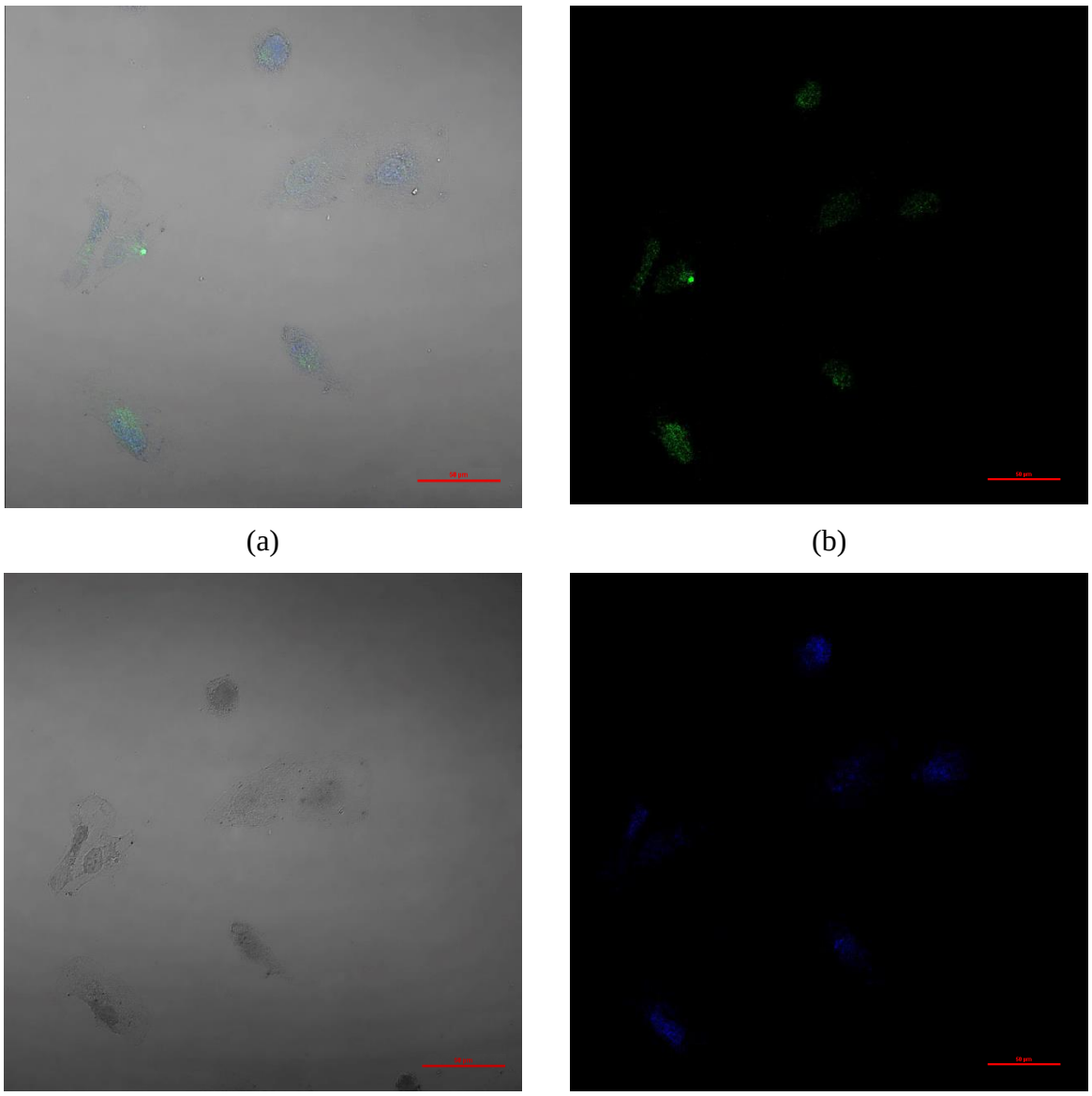

Fig. 3.6. Fixed cell imaging of U2OS cells treated with 25 µM ruthenium cylinder after 4 hours: a) dual filter DAPI-FITC (420-500 nm); b) FITC filter (450-500 nm); c) ND; and d) DAPI filter (420-495 nm). (the micron bar shows the scale of 50µm)

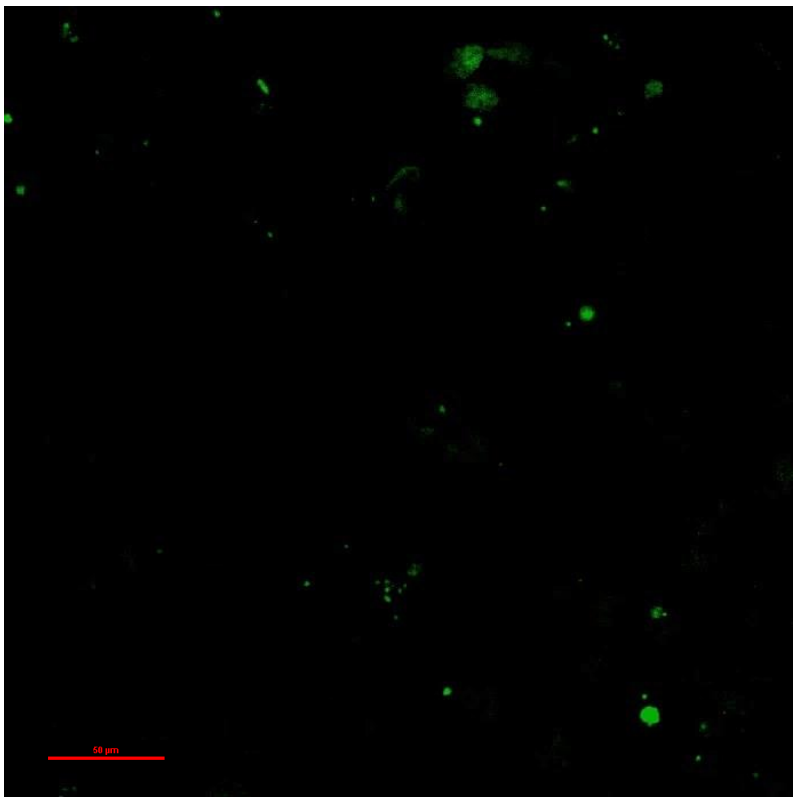

Fig. 3.7. Fixed-cell imaging of U2OS cells treated with 50 µM ruthenium cylinder using FITC filter (458 nm). (the micron bar shows the scale of 50µm)

After several trials of fixed-cell microscopy, the ruthenium cylinder was observed inside the cells (Fig. 3.7).

3.3 MTT assay cytotoxicity

MTT assay is a practical technique to discover the toxicity of cylinders in U2OS cells. This method is part of the class of colourimetry techniques that use MTT to measure cell viability. In this method, MTT (3-(4,5-dimethylthiazol-2-yl)-2,5-diphenyltetrazolium bromide) is used to detect the population of live cells. [17]

A free electron was generated in the process of transferring the NADH to NADP in the metabolic activity of mitochondrial live cells. The reduction of the tetrazole part of the MTT structure opens the tetrazole ring and makes formazan; consequently, the yellow colour changes to purple during the process. [18]

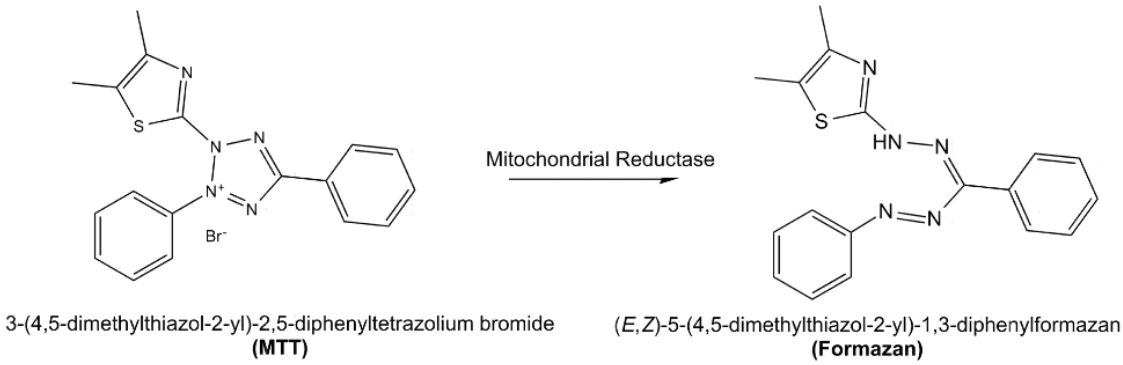

Fig. 3.8. Scheme of the mitochondrial reduction of MTT (yellow solids) to purple formazan in live cells. Taken from ref 19.

DMSO is used to dissolve the insoluble formazan to make a coloured solution, which is necessary for reading with a UV spectrophotometer. The concentration of purple formazan represents the live cell population that can be checked at 510 nm by a UV spectrophotometer plate reader. [20]

During the test, U2OS cells were cultured in 98 multi-well plates and treated with ruthenium cylinder, iron cylinder, cisplatin, DMSO and water to determine their cytotoxicity for osteosarcoma cells. To obtain accurate results, different drug concentrations were used to treat cells.

As an important anticancer drug for various types of cancers, cisplatin was considered as a standard sample for test evaluation. Its use as a positive control makes it possible to compare these results of cisplatin cytotoxicity in U2OS cells with those of other published works. Moreover, to evaluate the results of ruthenium cylinder cytotoxicity in U2OS cells compared to cisplatin, DMSO was used as a solvent of cisplatin as well as water, to provide two different positive controls (i.e. cisplatin in DMSO and cisplatin in water) in this test.

3.3.1 Results and discussion

To determine the minimum concentration of ruthenium and iron cylinders toxicity in U2OS cells, the cells were treated with various concentrations (0, 5, 7.5, 10, 15, 20, 25, 75 and 150 µM) of cylinders for 72 hours. Initially, DMSO as a ruthenium cylinder solvent was used as a positive control in U2OS cells in different percentages (0, 1, 2, 3, 4, 5 and 6). This test demonstrated that a concentration of higher than 1% DMSO is toxic for the cells, and that 50% of cells were killed when 2.5% DMSO was used as a control in treating. Accordingly, the ruthenium cylinder was dissolved in DMSO or a mixture of DMSO and water,

subsequently producing a total concentration of less than 1% DMSO in the samples. As an example, 0.6 µl from the 2,500 µM stock of ruthenium cylinder in DMSO was added to 300 µl media in wells (A_1, A_2, A_3 and A_4) to obtain a 5 µM concentration overall. As a result, 0.2% DMSO was used in these treatments. In contrast, in high concentration treatment (75 and 150 µM), a 5,600 µM stock of ruthenium in DMSO was used for the treatment. For 75 µM treatment, 8 µl of stock was diluted in 8 µl of dd water and 4 µl of the mixed solution was added to 300 µl of medium in the intended wells, to give a total of 0.6% DMSO. There are published works that demonstrate the application of cisplatin to treat U2OS cells. Consequently, cisplatin was used as a positive control in this study. Cells were treated with various concentrations of 0, 5, 10, 15, 25, 75 and 150 µM ruthenium and iron cylinders four times under the same conditions. As well as cisplatin in water and in DMSO, water and DMSO as a positive control was used with the same concentration to treat cells. Plates were read at 570 nm by a plate reader after 72 hours from the start of treatment. The results suggest that ruthenium cylinder with an IC50 value of 18 µM is more toxic in U2OS cells than iron cylinder, with IC50 26 µM. The samples treated with cisplatin in water lost just 20% of their cell viability in total, while using cisplatin in DMSO for treatment resulted in a 40% loss of cell viability with a cisplatin concentration of 59 µM cisplatin concentration.

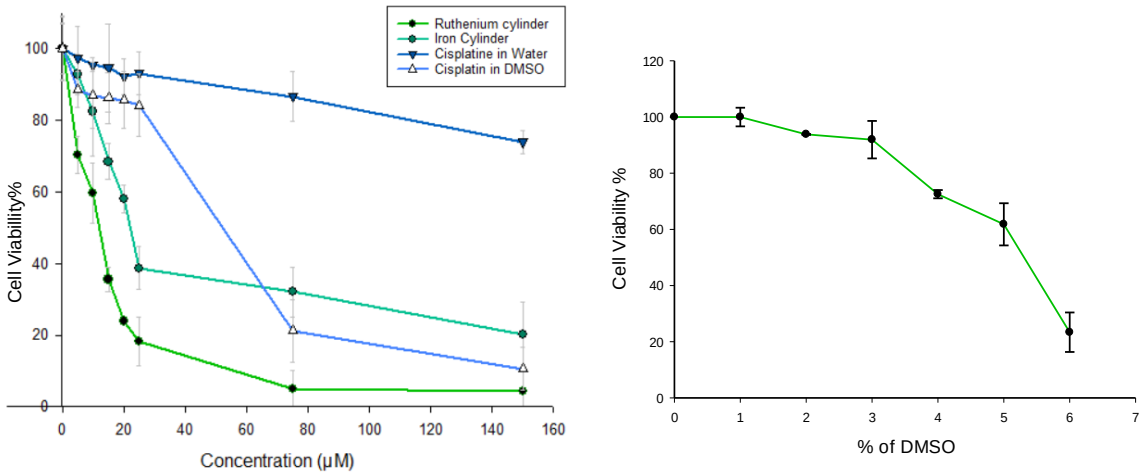

Fig. 3.9. Results of the MTT assay for evaluation of cell viability: a) cells were exposed to the indicated concentration of ruthenium cylinder, iron cylinder, cisplatin in water and cisplatin in DMSO; b) U2OS cells were exposed to various percentages of DMSO to find a safe dosage of DMSO as a ruthenium cylinder solvent.

Nevertheless, this data may indicate that the U2OS cell line is resistant to cisplatin. This reasoning differs from the results mentioned by Lippard et al. [21], which represents dramatic

toxicity of cisplatin (3.9 µM) in U2OS cells. Similarly, 5.6–8.6 µM has also been given as the cisplatin toxicity in this cell line. [21,22] Despite these reports, there are other published works showing that U2OS cells are resistant to cisplatin. [23,24] In contrast to the results of cisplatin solved in DMSO and water, Hall and his co-workers [48] found the negative impact of DMSO on cisplatin and other platinum complexes as an inactivator element. This means that the structure of cisplatin can be changed by replacement of cisplatin ligands with DMSO.

According to the microscopy and MTT assay results presented in sections 3.2 and 3.3, while iron and ruthenium cylinders exhibit their toxicity in U2OS cells, Hoechst replacement was not observed even after 24 hours. Consequently, to find the location where cylinders affect the DNA, their cellular uptake was tested by ICP-MS.

3.4 Cellular uptake

Inductively coupled plasma mass spectrometry (ICP-MS) is a sensitive, accurate and multifunctional type of mass spectrometry which makes it possible to precisely detect low concentrations of elements, such as metal and nonmetal ions at or below a single part per trillion (ppt) level in samples. A vast range of elements can be determined by ICP-MS with the instrumental detection limit shown in Figure 3.10. [25]

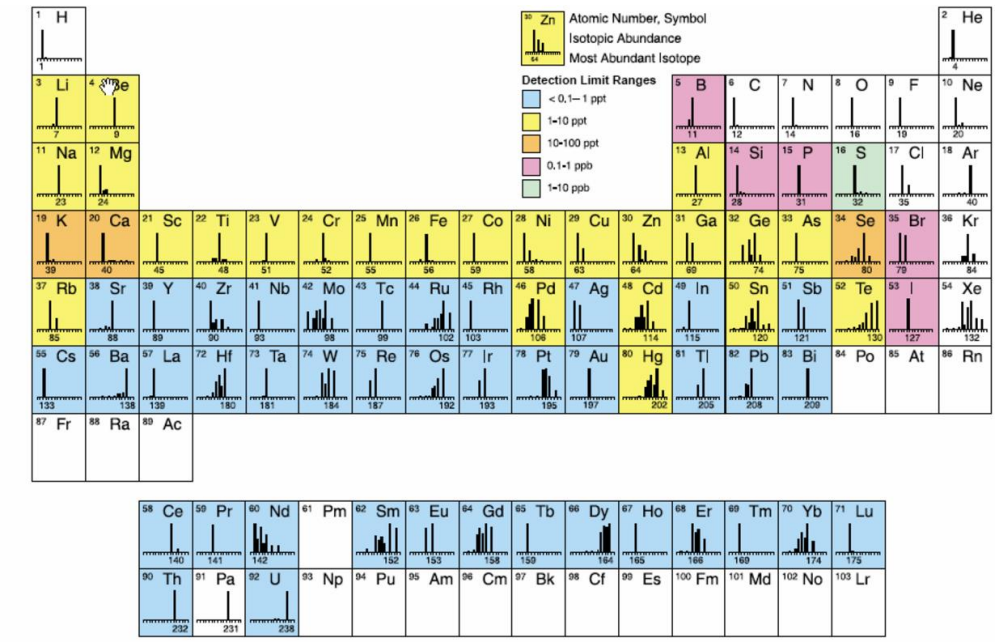

Fig. 3.10. Elements analysed by ICP-MS (in colour). Taken from ref 26.

This technique is widely used in a range of fields such as toxicology, medicine and forensics. [27] As an example, it is used to trace the amounts of metal elements in drugs uptaken by cells for various purposes. Nevertheless, ICP-MS can be used to quantify the amount of iron and ruthenium uptaken by cells after treatment.

To investigate the amount of iron and ruthenium uptaken by U2OS cells, and to detect their separate amounts in cell parts, cells were treated with a single 50 µM concentration of ruthenium cylinder and iron cylinder in two separate flasks for 4 hours. DMSO was used as a positive control. Different parts of cells were separated, so that supernatant and nucleus fractions resulted from the fractionation process. Supernatant is a cytoplasmic extract that includes the cytoplasm organelles. To normalise all parameters, all samples were produced under the same conditions. The dark orange colour of ruthenium cylinder was observed in all cell fractions, indicating that cell uptake was confirmed visually. The purple colour of iron cylinder was observed in every cell fraction with the exception of the membrane, which remained as a solid part from the end of the fractionation process.

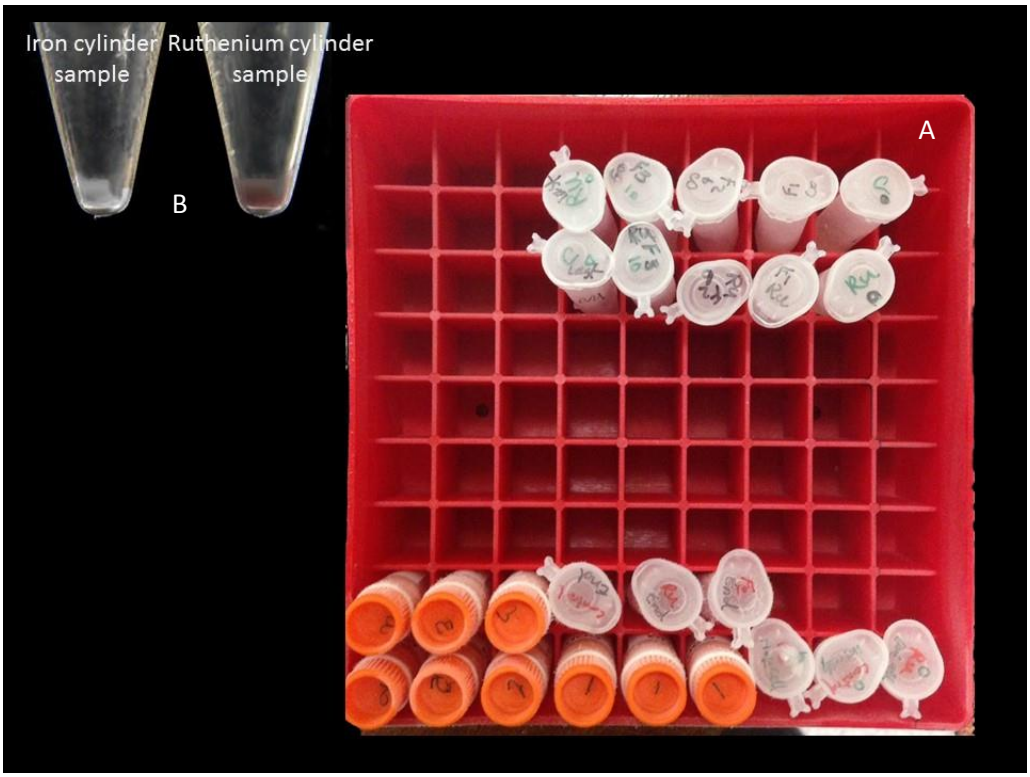

Fig. 3.11. a) Fractionation samples of U2OS cells from both treatments (iron cylinder and ruthenium cylinder), parts 1 and 2; b) scheme of the last part of cells following the fractionation process, including the cell membrane; this shows that the main portion of ruthenium cylinder was trapped in the cell membrane (the dark orange colour remained in the Eppendorf). This is in contrast to iron cylinder; in this figure, the last fraction of this sample does not show a purple colour trapped in the cell membrane.

The average cellular amount (C_c) of the respective metal (fg cell^{-1}), as well as the related standard deviation (scc), can be calculated using Equation 3.1:

$$c_c = \frac{(c_t - c_b) \times 10}{N} \times 10^6 \qquad [3.1]$$

where C_c is the average cellular amount (fg cell^{-1}), C_t the average measured metal concentration in the uptake samples ('total concentration', ng ml^{-1}), cb is the average measured metal concentration of the adsorption samples ('blank concentration', ng ml^{-1}) and N is the average cell number (cells well $^{-1}$). [32]

The results showed that 26% of ruthenium cylinder was uptaken into U2OS cells, 74% of which was trapped inside the cell membrane (as shown in Figure 3.12). From this calculation, 16% of ruthenium was detected in the nucleus and 10% was detected in the cytoplasm.

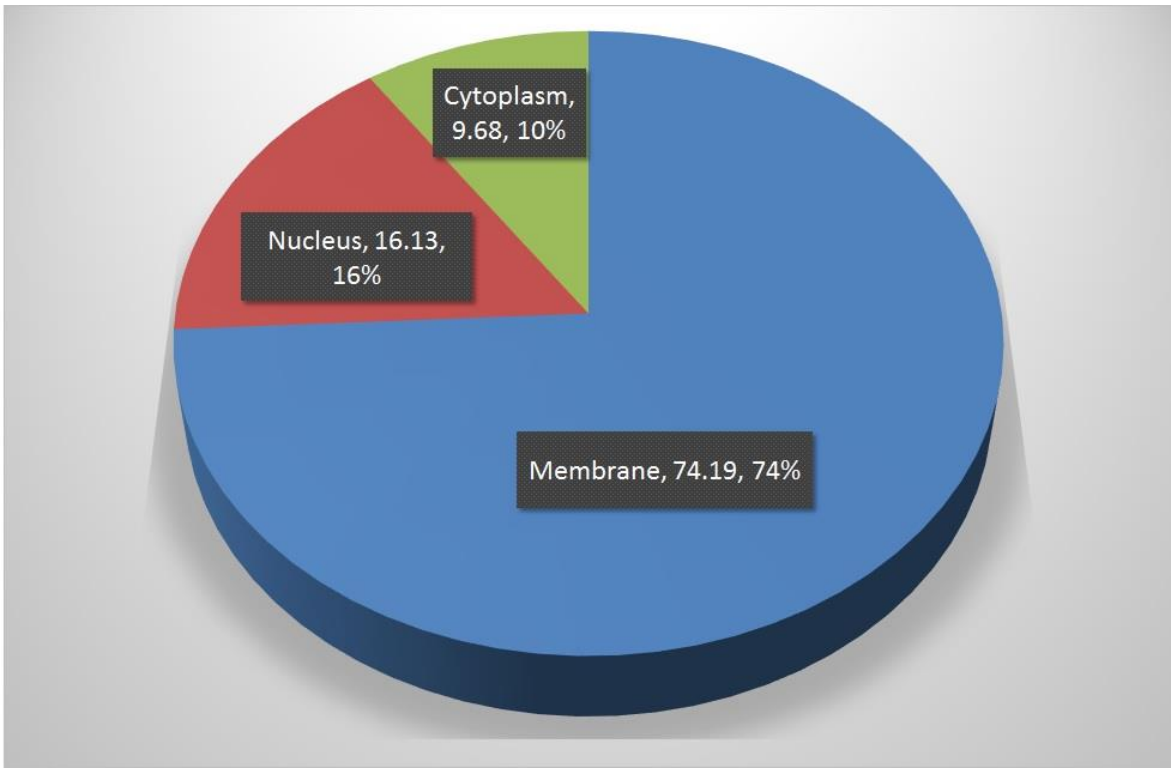

Fig. 3.12. Representation of the portion of ruthenium cylinder uptaken in different parts of U2OS cells.

This process was simultaneously performed for iron cylinder, but Fe is hard to assess accurately by ICP-MS because of the levels of Fe found in the environment, glassware and solvents including nitric acid.

3.5 DNA damage detection

Despite the fact that antineoplastic drugs are designed to treat growing cancer cells, they can also be the cause of triggering secondary cancers in patients due to their gene mutation ability or their genotoxicity. Some anticancer drugs, such as cisplatin, have shown genotoxicity to be their disadvantage. Accordingly, research on the effects of anticancers on genes, particularly on DNA, is highly desirable. To measure DNA strand breakage in eukaryotes, single cell gel electrophoresis assay (SCE), or comet assay, can be used as an accurate method. In this technique, treated cells are suspended in agarose gel, lysed with detergent to remove cells and nuclear membrane, and electrophoresed to draw out the charged fragments of DNA towards the anode. This is then stained with fluorescent DNA dye to enable image capture by Fluorescence microscopy. [28,29] The comet-like images display a spherical head and DNA breaking within their tail (Fig. 3.13). The amount of DNA damage is proportional to the comet's tail length, meaning that greater DNA breakage results in more DNA in the comet's tail. [31]

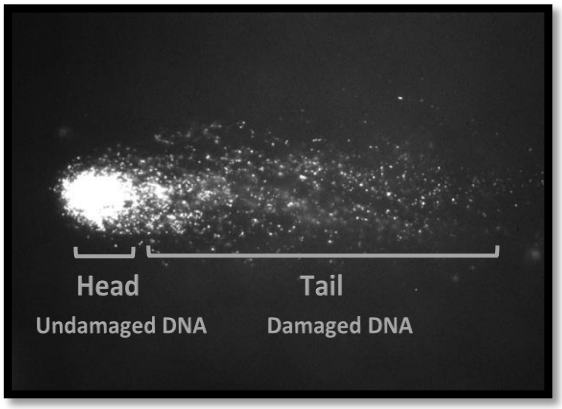

Fig. 3.13. Different parts of the cell 'comet': the head (undamaged DNA) and tail (damaged DNA). Taken from ref 30.

There are two different comet assay methods, depending on the lysis pH: neutral comet assay uses pH ≈ 9.5–10, and alkali comet assay uses pH ≥13. There is a widespread belief held by

published studies [29] that only double-strand breaks are detected with neutral pH, even though both single- and double-strand breaks can be detected by applying an alkaline pH. It is worth noting that single-strand breaks are not considered to be a significant lethal or mutagenic lesion on DNA due to their fast repair ability. A pH of above 13 can break the alkali-labile AP (apurinic/apyrimidinic) sites of DNA made by genotoxic agents. Alkali comet assay is therefore a popular technique for DNA damage detection. [29]

In the literature, iron and ruthenium cylinders have exhibited nongenotoxic effects in various types of cancer cell lines. To investigate their effects on the genome of U2OS cells, the cells were treated with 15, 25, 50 and 100 µM of ruthenium and iron cylinders in multi-chamber plates for 4 and 24 hours, with two wells being allocated for each concentration to increase accuracy. To calibrate the test, untreated cells were used as a negative control to exemplify minimum DNA damage, and hydrogen peroxide (H2O2) was used as a positive control to treat cells and cause maximum DNA damage. Although U2OS cells show cisplatin resistance in the results of this study, cells were treated by 50 µM of cisplatin (meaning minimum DNA damage) for comparison with ruthenium and iron cylinders. In addition, 1% DMSO was used to treat cells to evaluate its impact on DNA and to compare the results with the negative controls.

Importantly, many different parameters can affect the comet tail, such as the lysis conditions, electrophoresis time and agarose gel loading quality. Thus, negative controls play a significant role in producing reliable results for comparison. Moreover, to assess the results statistically, it is essential to sum the value of 100 randomly selected comets to provide a total damage level of the cell population, and it is also necessary to repeat the entire process at least three times for the sake of accuracy.

Depending on the level of DNA damage, comets can be found in different shapes: a higher chromatin mass together with a lower comet tail concentration are indications of a lower level of damage, while more damaged DNA results in lowering the chromatin mass, followed by an increase in comet tail concentration. [30]

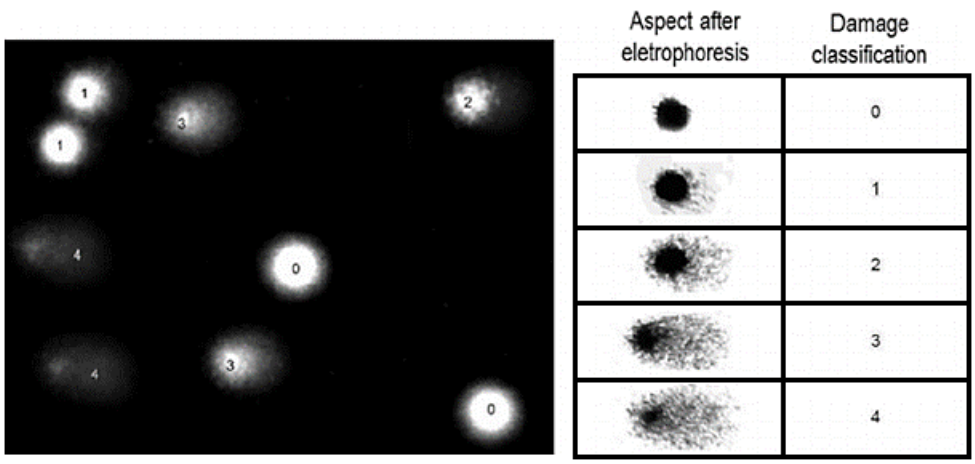

Fig. 3.14. Classification of comets on the basis of DNA damage level. Taken from ref 31.

3.5.1 Results and discussion

The results show that iron and ruthenium cylinders are not genotoxic in U2OS cells, suggesting that the imaged comets did not represent a high concentration of DNA breakage in their tail lengths (see Fig. 3.15 and Table 3.1). Moreover, to compare the iron and ruthenium cylinder comets following treatment with 50 µM (a high concentration of cylinders for treatment) after 4 hours (the minimum time of treatment) and 24 hours (the maximum time of treatment), as shown in Figure 3.15, the comets can be classified on a scale of damage from 0 to 1.

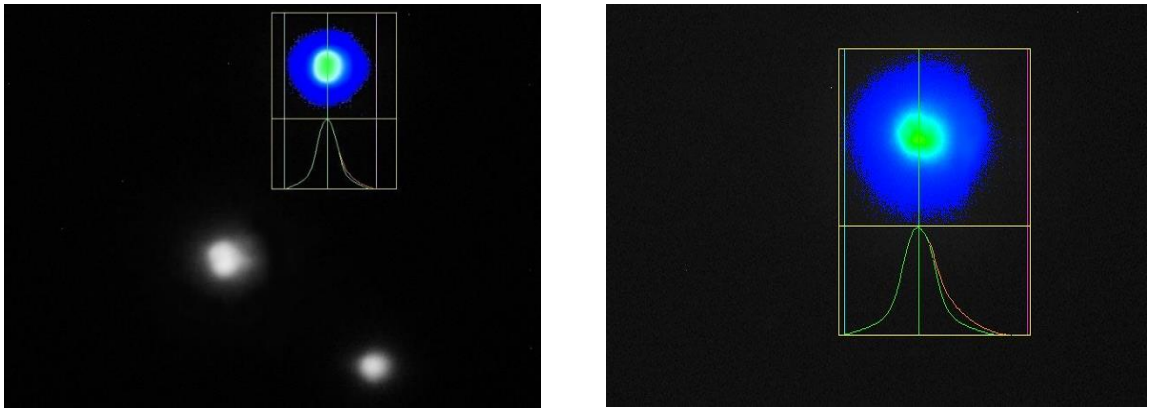

(a) (b)

Fig. 3.15. Demonstration of cell comets after 24 hours of treatment by 50 µM of cylinders; a) iron cylinder, and b) ruthenium cylinder.

The results of U2OS cell treatment with cisplatin produced the observation of DNA damage in comet tails after 4 and 24 hours of treatment. These comets can mostly be classified in the damage level class of 2, and less so in the damage class of 3. Considering the MTT assay results, which showed that U2OS cells are slightly resistant to cisplatin, it is unsurprising the dramatic DNA damage was not observed in U2OS cells after this treatment.

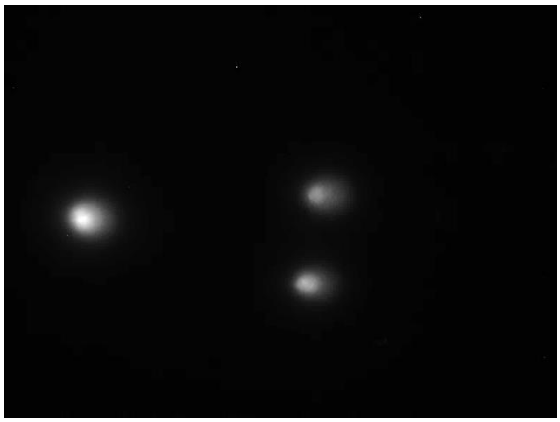

Fig. 3.16. The state of cell comets after treatment with 50 µM cisplatin for 24 hours.

According to Figure 3.15, 1% DMSO is not toxic in U2OS cells in the captured images. The comets had a class 0 DNA damage level, as observed in Figure 3.17.

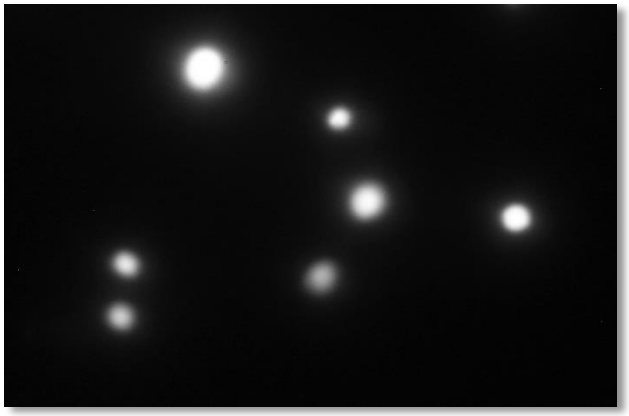

Fig. 3.17. The state of U2OS cell comets treated with 1% DMSO after 24 hours.

The maximum damage results from the 1% H_2O_2 used as a positive control. A dramatic reduction in chromatin mass and the tail length of comets compared to the positive controls are clear representatives of the high level of DNA damage (Fig. 3.18).

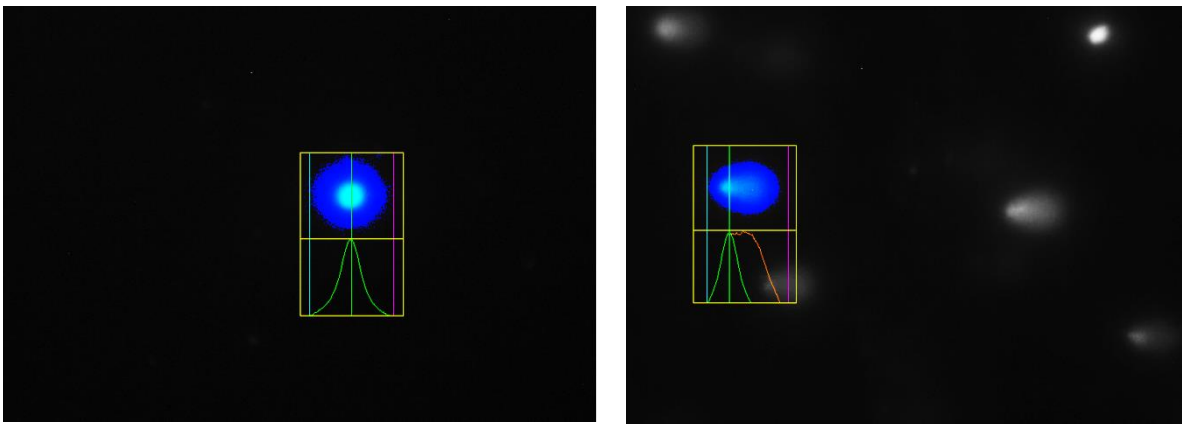

(a) (b)

Fig. 3.18. U2OS comets; a) the negative control after 24 hours; b) the positive control of 1% H_2O_2.

The comet assay results of U2OS cells treated with ruthenium cylinder (15, 25, 50 and 100 µM), iron cylinder (15, 25, 50 and 100 µM) and 50 µM of cisplatin solution in water after 24 hours are presented in Table 3.1.

Table 3.1. The average DNA tail migration in U2OS cells treated by various concentrations of ruthenium cylinder, iron cylinder and cisplatin as a negative control.

DNA tail migration % ± SD (n=4)			
Concentration (µM)	Ruthenium cylinder	Iron cylinder	Cisplatin
0	0.1±0.08	0.1±0.08	0.1±0.08
15	1.12±0.04	1.02±0.03	
25	1.6±0.38	1.34±0.15	
50	3.08±0. 3	2.93±0.25	16.03292
100	8.2±0.2	6.6±0.32	
PC	100±0.05	100±0.05	100±0.05

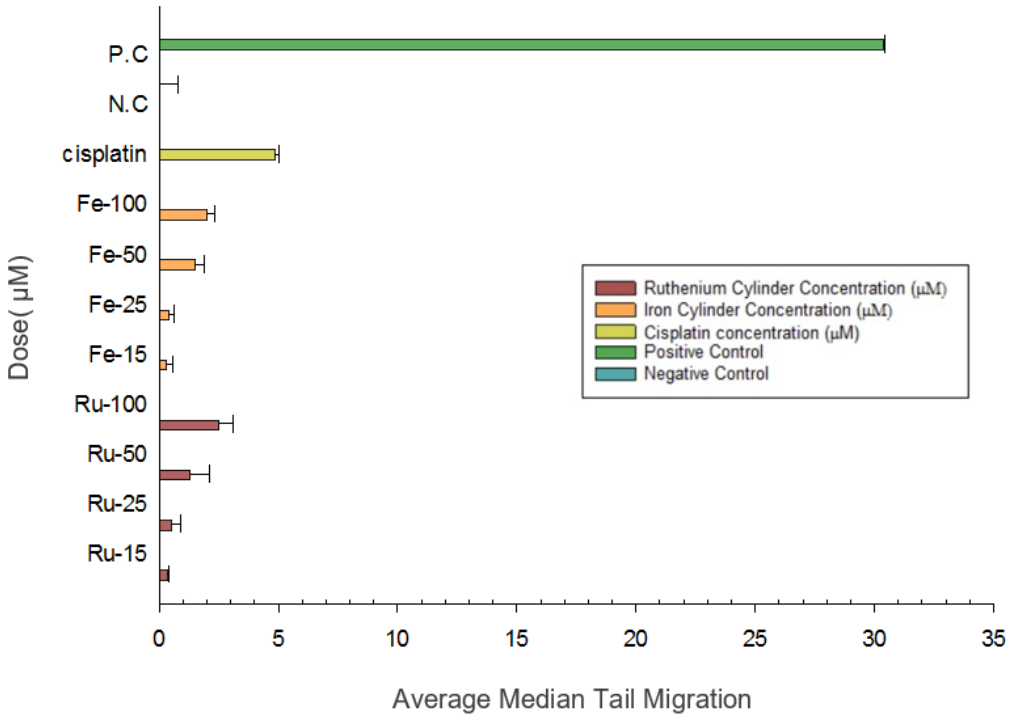

Fig. 3.19. The median DNA tail migration of U2OS cells exposed to different drugs and conditions.

According to Figure 3.19, cylinders did not demonstrate total genotoxicity in U2OS cells. However, when 100 µM of ruthenium cylinder was used to treat cells, it showed a maximum strand breaks (8.2%) which was almost similar to the DNA tail migration of the iron cylinder (6.6%). This dose (100 µM) is far higher in concentration than the effective dose of ruthenium cylinder (15 µM) and iron cylinder (25 µM). Accordingly, DNA could be damaged in a high-stress situation, particularly by a high dose of ruthenium cylinder in DMSO and cisplatin does not exhibit dramatic DNA damage in U2OS cells (16%).

3.6 Protein immunoblotting

Protein immunoblot, which is a crucial technique in cellular and molecular biology, is referred to by different names in the literature, including protein blotting or western blotting. Essentially, this technique is applied to identify the existence of an individual protein within a complex mixture extracted from cells. Western blotting is used to separate proteins from cell lysate by applying gel electrophoresis to sort them by their size, charge or another characteristic, to form separate protein bands. Many polyacrylamide gels are used in

protein electrophoresis which, depending on their function, can provide specific information about proteins. As an example, nondenaturing poly-acrylamide gel electrophoresis (PAGE) separates proteins based on their mass-to-charge ratio; two-dimensional (2D) PAGE separates proteins by native isoelectric point in the first dimension, and by mass in the second dimension. [33]

Blotting is the process of transferring the segregated protein bands to the safe career called membrane, which could be made of nitrocellulose, nylon or PVDF. [33,35]

There are some significant aspects which are worth mentioning, as the western blot results make this technique routine for visualising protein bands; the size-based separation of protein mixtures using gel electrophoresis is a practical way to transfer the separated proteins to a solid support. In addition, it offers the possibility of a rapid and inexpensive method for detecting a target protein by appropriately matched antibodies. [34,35] Protein immunoblotting is an effective method for recognising and targeting specific proteins from various complex sources, to investigate the contribution or effects of disease in normal cells and to understand how the targeted protein responds to treatment drugs.

3.6.1 Bradford protein assay

The process is initiated by Bradford protein assay as a spectroscopic analytical technique to measure the total concentration of protein in each prepared lysate sample. [33,35]

Coomassie Brilliant Blue G-250 dye is used in this colourimetric protein assay to measure the converting absorbance of dye before and after application. The fundamental part of this procedure is that the colour of the Coomassie Brilliant Blue G-250 dye changes from orange-brown to blue when bonds are formed between the dye and proteins. Unbound dye has a maximum absorbance of 465 nm, and the negative charge produced by binding to proteins increases the maximum absorbance to 595 nm. [36,37] Crucially, binding occurs between some simple amino acids such as histidine, arginine and tyrosine with dye in acidic conditions. The intensity of the blue colour represents the protein concentration in each sample. [36,37]

To perform Bradford assay, cells were lysed using a UTB buffer. Cell disintegration was then sonicated on ice to break and to disrupt cell membranes and to homogenise the lysate, to ensure a better calculation of protein concentration. Since the amount of protein in unknown

samples is difficult to measure, using a standard curve produced from standard proteins was used as a common method to eliminate computational errors and to provide accurate protein determination. Reference proteins should be chosen based on their properties, which should be similar to the proteins of analysed samples, such as BSA or bovine γ-globulin (IgG). BSA was used as a standard protein at various concentrations of 0, 1, 2, 3, 4, 5 and 10 µg/µl. At least six standard samples should be prepared to create a standard curve. Protein calculation was performed to prepare 20 µg of protein per gel for the following samples: a) samples treating cells with 50, 200 and 500 µM iron cylinder for two different treatment times of 1 and 24 hours; b) samples treating cells with 50, 200 and 500 µM ruthenium cylinder for two different treatment times of 1 and 24 hours; c) a positive control treating cells with 5 and 50µM cisplatin; and d) negative controls for 1 and 24 hours. Following dye addition, the plate was read by plate readers.

According to the presence of ChK1 phosphorylation in protein immunoblotting test demonstrates the DNA damaging or the stress on DNA strands, detection of the ChK1 phosphorylation is the aim of this technique. It is worth noting that, the much higher concentration of cylinders than cisplatin were considered to have adequate ChK1 phosphorylation levels following genotoxic stress in all samples to detect that well via sensitive films.

To measure the protein concentration in samples, a protein standard curve was generated considering the use of 10 µl standard protein, according to equation [3.2]:

Starting protein concentration (µM) x volume of protein standard (µl) = amount of protein (µg) [3.2]

After calculating the dilution factor, unknown samples were diluted twofold.

The protein estimation is represented in Table 3.2.

Table 3.2. Protein estimation in lysates of iron cylinder samples, measuring loading samples per gel.

Iron cylinder	50 µM 24 hrs	50 µM 1 hr	200 µM 24 hrs	200 µM 1 hr	500 µM 24 hrs	500 µM 1 hr
Average	0.865	0.256	0.406	0.32745	0.415	0.25
5X µg protein/µl	3.7	0.5	1.3	0.9	1.4	0.5
For 20 µg/gel	5.4	38.8	22.4	15.3	14.7	41.3
2X LB	5.4	38.8	22.4	15.3	14.7	41.3

Table 3.3. Protein estimation in lysates of ruthenium cylinder samples, measuring loading samples per gel.

Ruthenium cylinder	50 µM 24 hrs	50 µM 1 hr	200 µM 24 hrs	200 µM 1 hr	500 µM 24 hrs	500 µM 1 hr
Average	0.49	0.28	0.38	0.23	0.25	0.22
5X µg protein/µl	0.3	0.5	0.4	1.2	0.6	1.8
For 20 µg/gel	57.3	39.5	50.1	16.7	31.6	10.9
2X LB	57.3	39.5	50.1	16.7	31.6	10.9

Table 3.4. Protein estimation in lysates of negative and positive control samples, measuring loading samples per gel

Controls	(-) Control 24 hrs	(-) Control 1 hr	Cisplatin 5 µM -24 hrs	Cisplatin 5 µM -1 hr	Cisplatin 50 µM -24 hrs	Cisplatin 50 µM -1 hr
Average	0.3645	0.545	0.565	0.7855	0.265	0.6825
5X µg protein/µl	2.8	0.6	3.3	2.2	2	1.1
For 20 µg/gel	7.2	33.5	6	9.3	18.2	9.8
2X LB	7.2	33.5	6	9.3	18.2	9.8

The above data was analysed to load 20 µg of unknown protein in each gel, and the samples were diluted by loading the buffer into prepared samples for gel electrophoresis.

3.6.2 Protein gel electrophoresis

Two different gels were made for each ruthenium cylinder and iron cylinder to assess the results. The goal was to separate proteins according to their size. [38]

SDS, a kind of polyacrylamide gel, was used in this process to separate the proteins homogenised in lysate. Acrylamide was chosen to separate proteins depending on their size. The polymerisation process to make acrylamide gel was carried out when ammonium persulphate (APS), a polymerising agent, and N,N,N,N'-tetramethylenediamine (TEMED), a polymerisation catalyser, were mixed by a primary gel mixture. [39]

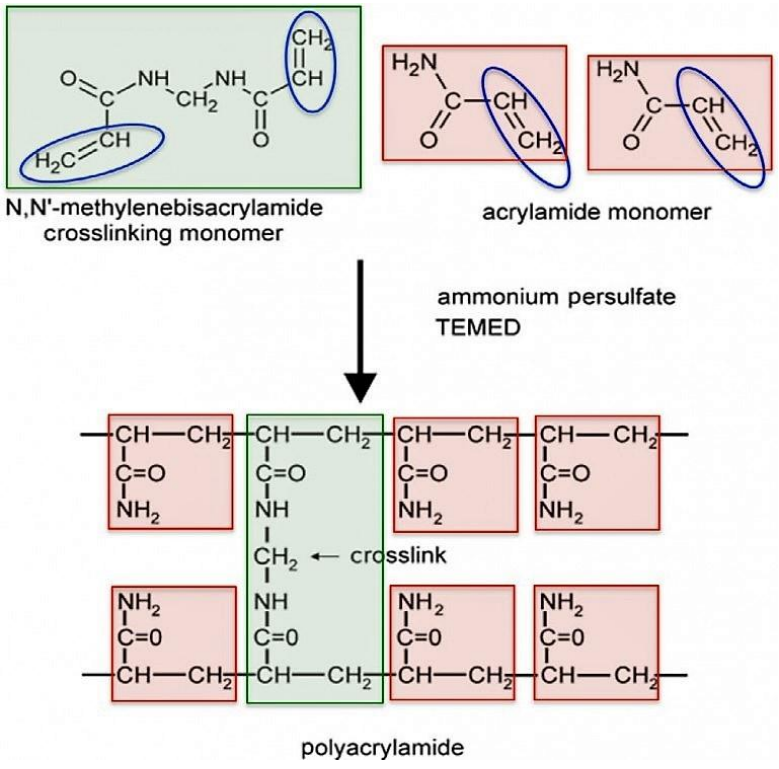

Fig. 3.20. Polyacrylamide protein polymerisation using bis-acrylamide for PAGE ammonium persulphate. Taken from ref 40.

Notably, nonpolar protein chains were transformed into linear polar chains with SDS gel. To this end, ionic SDS forms a bond with proteins to produce a homogeneously negative charge on the protein chain. All proteins bonded to SDS move through gel from a negatively charged cathode electrode to a positively charged anode electrode when a current is applied. Evidently, the sieving effect of the gel matrix impacts on protein migration through gel; lighter proteins move faster than massive ones through gel tunnels with different diameters. Therefore, smaller molecules are found at the bottom of the gel, and larger molecules are found at the top of the gel. [38,39]

On the other hand, protein transformation to a linear shape is an influence of SDS which can move easier and better through the gel matrix. [39]

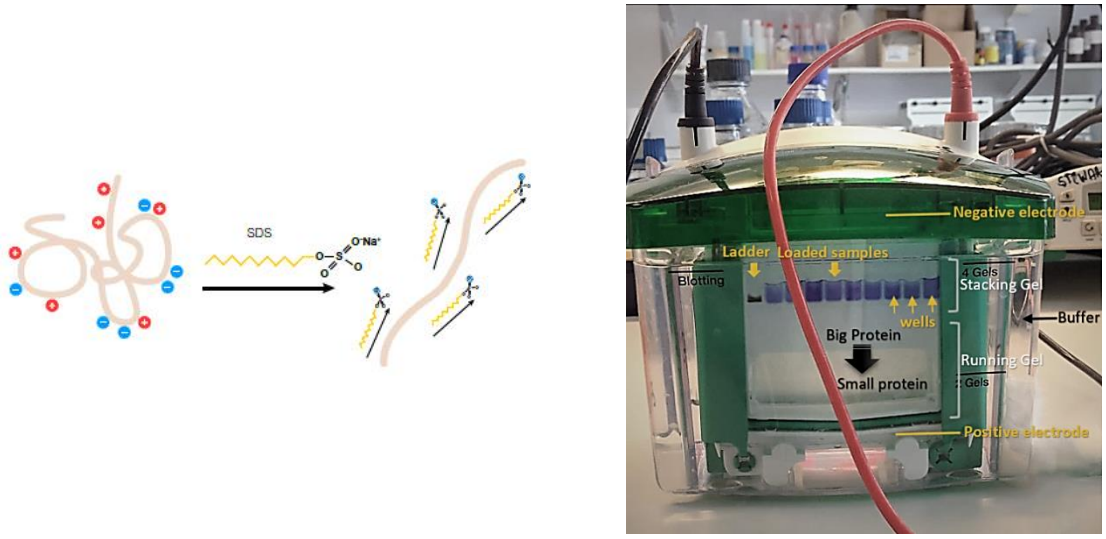

(a) (b)

Fig. 3.21. a) The effect of SDS on the conformation and charge of a protein. Taken from ref 41.; b) electrophoretic protein separation in polyacrylamide gel and protein migration.

In this experiment, two different solutions were prepared to make the electrophoresis gel: running and stacking gel solutions. The difference in their pH, and the concentration of acrylamide, explain the tight bands formed during electrophoresis. The pH of 6.8 and lower concentration of acrylamide in staking gel allows proteins to be concentrated and some constricted bands to be formed at the beginning of electrophoresis, before entering the running gel. [42]

To assess the test, the standard protein ladder was loaded into each gel as a reference of the molecular masses or sizes of proteins in a gel. Several proteins with known molecular masses were placed into a mixture, which was run alongside the testing piece. This can be done in

one or more lanes of the gel. This type of prepared mixture of known proteins is called a ladder. There are different types of protein molecular weight (MW) markers used for different detection modes, which are categorised as unlabelled or pertained. [42]

The ladder is a prepared mixture containing several proteins of known molecular masses is run alongside the test sample in one or more lanes of the gel. Several kinds of ready-to-use protein MW markers are available that are either unlabelled or prestained for different modes of detection.

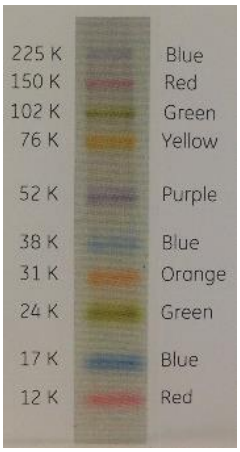

Fig. 3.22. The ladder used as a standard for protein separation.

Ruthenium and iron cylinders in different concentrations (50, 200 and 500 µM) and times of treatment (1 and 24 hours) were loaded into different gels. Four separate gels were prepared for this test; two were loaded by ruthenium cylinder samples, and the other two by iron cylinder samples. Cisplatin in concentrations of 5 and 50 µM, and after 1 and 24 hours of treatments, were loaded as positive controls into gels. The gels were electrophoresed for 1.5 hours and were checked during electrophoresis until completion.

As mentioned above, proteins were moved into gels according to the difference in their size and their charge density. Therefore, the velocity of their movement can be calculated by the equation given in Figure 3.23:

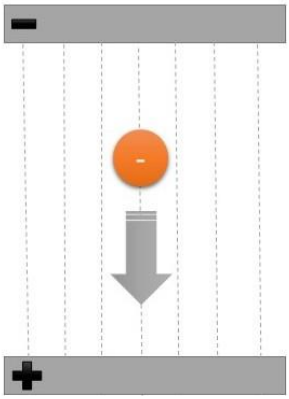

$v = EZ/\mathrm{f}$

v: $velocity\ of\ the\ protein\ or\ DNA\ in\ an\ electric\ field$ $(cm.se$

E: electric field strength (volt.cm^{-1})

Z: net charge on the protein

f: frictional coefficient (depending on the mass and viscosity of the medium)

Fig. 3.23. Protein migration and equation to measure its velocity in protein electrophoresis. Taken from ref 43.

To detect and identify the proteins separated by gel electrophoresis, they were transferred to a membrane. This technique is called blotting. Notably, proteins can be re-natured by swoping the SDS by this wet transferring process, which is suitable for proteins of more than 100 KD. [35]

3.6.3 Blotting

The separated proteins were transferred to a membrane carrier to be specified and identified using the electrophoresis process. Gels were detached from the glasses and washed with transfer buffer in a small tank; they were then sandwiched with membranes in a special cassette in order to transfer the proteins from gel to membrane by electrophoresis. If the sequence of the gel and membrane arrangement in the cassette is not correctly placed, the transfer is not observed on the membrane. [35]

The membrane is a solid support with high affinity to proteins chosen from the nitrocellulose membrane. This kind of membrane has a very good protein binding and maintains it for a long time. [35]

Blotting was run for 1 hour at 100 V. Small proteins have a higher chance of passing through the membrane if the electrophoresis process is run for a longer time. Therefore, 1 hour is the optimum time for all proteins to be on the membrane.

The blotting visualisation of proteins in membranes was carried out using Ponceau Red, which is a kind of stain with low sensitivity. This reversible dye is a suitable choice to visualise whether or not the protein transfer on the membrane has occurred. The high solubility of Ponceau Red is the reason for its use at this step. It was then removed with water before the next step.

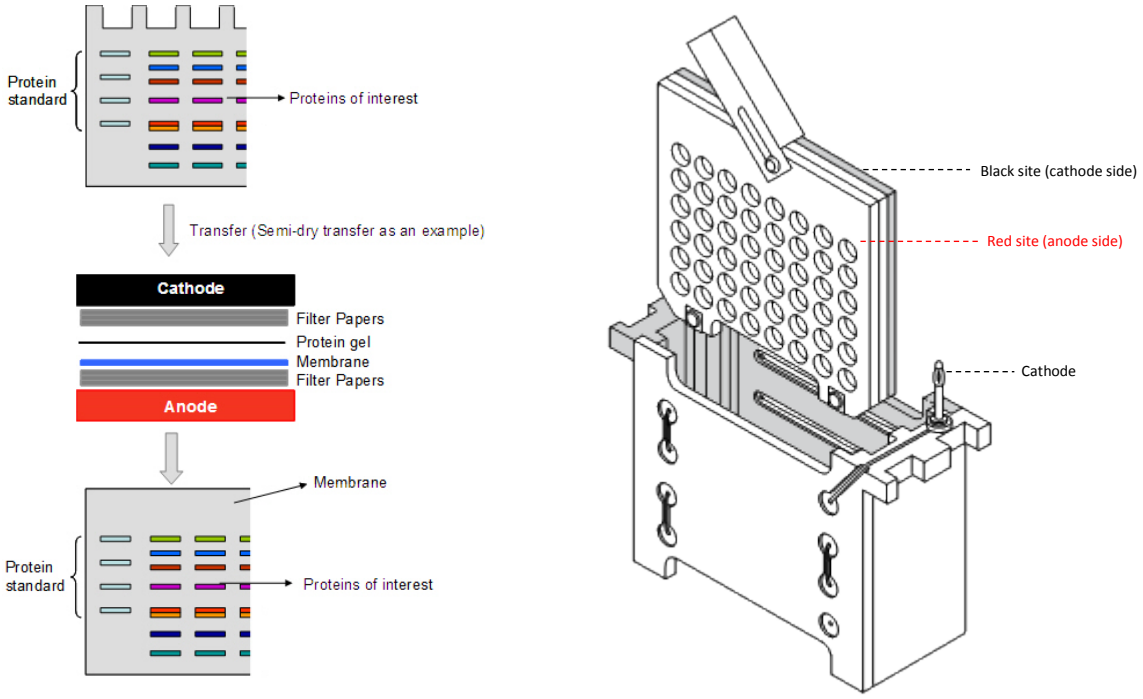

(a) (b)

Fig. 3.24. a) The western blot cassette setup method. Taken from ref 44; b) correct orientation of cassette in the tank. Taken from ref 45.

Protein imaging is the purpose of the western blotting test, which is done to detect specific proteins. High-quality images are necessary to analyse the proteins; therefore, to eliminate or reduce background noise in imaging, the unbound membrane sites should be blocked by washing in milk for 1 hour. Milk covers a thick layer at unbound membrane sites, and leaves tough sites of the membrane containing proteins. Ultimately, blocking the active sites of the membrane is necessary to take high quality images. In addition, this optimises antibody consumption through limiting the membrane sites. [35]

The process of identifying proteins by their specific antibodies is called immunodetection. In this method, antibodies are used to recognise unblocked specific proteins on the membrane by

making bands with their proteins. The antibodies are chosen depending on the proteins targeted for investigation. [35]

Depending on the antigen intended for detection and the related antibodies available, the primary antibody of a western blot is selected. Attention must be paid to choosing the appropriate primary antibody for western blotting, because not all primary antibodies can be used for this purpose. Primary antibodies are frequently applied first and then recognised by a secondary antibody which is conjugated with colour, radioactivity or an enzyme, as well as biotin-conjugated antibodies. [46]

There are two different methods of protein identification: direct and indirect immunodetection methods. They have their own advantages and disadvantages for detection of the target proteins. The labelled primary antibody is used as a direct method, while the unlabelled primary antibody flowed by a labelled secondary antibody is used as an indirect detection method for proteins. [46]

Anticancer agents target DNA as the most effective part of a cell to treat cancers. However, they can also affect the nature of DNA in different ways. For example, cisplatin induces DNA damage and causes cell death, and gemcitabine and etoposide inhibit DNA duplication. Because iron and ruthenium cylinders are categorised as DNA replication fork inhibitors, the antibodies activated during this process should be considered as a checkpoint for evidence of their lack of genotoxicity anticancer activity.
Apical protein kinase (ATR) and its downstream target kinase (ChK1) have a significant effect on DNA, damaging checkpoint control, and on tumour abolition. Any stress on the DNA replication process, such as interrupting DNA duplication, activates the ATR-ChK1 pathway to delay cell cycle progression, and keeps the replication fork feasible. DNA duplication can continue after correction of the primary damage. Moreover, phosphorylation of ChK1 by ATR, which results from DNA damage, triggers its release from the chromatin-enriched fraction into soluble nuclear, cytoplasmic and centrosome compartments, where it coordinates the activation of the cell cycle arrest or repair function, as well as being degraded to terminate the activated checkpoint. [47] ChK1 phosphorylation represents different functions that work continuously together. Interceding the DNA replication checkpoint is known as ChK1 phosphorylation, which is a crucial duty to keep the cell alive and can occur during phosphorylation at Ser-317. This is essential to activate the process of phosphorylation at Ser-345 as a key compound of cell viability. Consequently, the existence of Ser-345

phosphorylation in whole cell lysate is the sign of cylinder activity as an anticancer which drives cells to death by blocking DNA synthesis in U2OS cells. Therefore, ChK1 and ChK1 phosphorylation antibodies were used to represent the disruption of DNA replication in cancerous cells.

The next step is to apply primary antibodies to bind with targeted proteins. To this end, one of the membranes of ruthenium and iron cylinders were placed in ChK1 (mouse, G-4, lot: A1713, from Santacruz Biotechnology) antibody, which was diluted as 1 µl in 10 ml of milk (labelled as ChK1). Two other membranes were placed in phospho-ChK1 (rabbit, Ser-345, CAS: 234 1 L, from cell signalling), diluted as 10 µl in 10 ml of BSA (labelled as ChK1-P). All of the solutions were stored in a cold room and agitated overnight. These two antibodies marked the targeted IgG_{2a} protein and ser-345 phosphorylation in lysate cells. After 24 hours, membranes were washed with TBS several times to completely remove the primary antibodies.

The secondary antibodies were added to provide double coded proteins, in order to produce better images. The membrane labelled ChK1 was placed in the solution of anti-mouse diluted in block (16 µl in 50 ml of block), and the membrane labelled P-ChK1 was placed in an anti-rabbit solution (50 µl in 50 ml block) and kept at room temperature with agitation. Membranes were washed with TBS several times and were then detected by ECL detection reagents. Chemiluminescence was chosen as an adequate detection technique to mark the targeted proteins in the laboratory. Two-component chemiluminescent substrates for horseradish peroxidase (HRP) include a stable peroxide solution and a modified luminal solution. The same amounts of each HRP substrate peroxide solution (WBK LO500 Millipore) and HRP substrate luminal reagent (WBK SØ500 Millipore) were added to each of the mouse and rabbit trays as a working solution, and stored for 3–5 mins. HRP was conjugated to antibodies and light was generated by the chemical reaction, and subsequently detected with sensitive film. Films were prepared in a dark room and analysed in comparison with the membrane ladder.

The process was repeated on the same lysate samples three times to obtain the best repeatable and reliable results for analysis. The results were also compared to each other.

Because the western blotting technique is a highly sensitive process in response to the types of primary and secondary antibodies used, as well as its robust validation and sensitivity to

produce a strong signal from the targeted proteins, the repeated tests did not show the same results.

Since the inhibition of the DNA replication fork with ruthenium and iron cylinders was one of the goals of this experiment, the cell cycle checkpoint kinase ChK1 is important for consideration. The DDR or DNA damage response was activated when any replication stress or DNA damage happened in cells. A direct response to stalled replication fork signals is ChK1 as a kinase checkpoint, which is phosphorylated on ser345 by ATR (ataxia telangiectasia and Rad3-related protein). Consequently, the separated proteins extracted from lysate were exposed to ChK1 of mouse and phosphorylation ChK1 (ser345) of rabbit. In this test, lysates from cells of treated samples of 50, 200 and 500 µM of ruthenium and iron cylinders and 50 µM cisplatin as a positive control for 1 and 24 hours were verified. It is collaboration with Martin Higgs and Lucia Cardo.

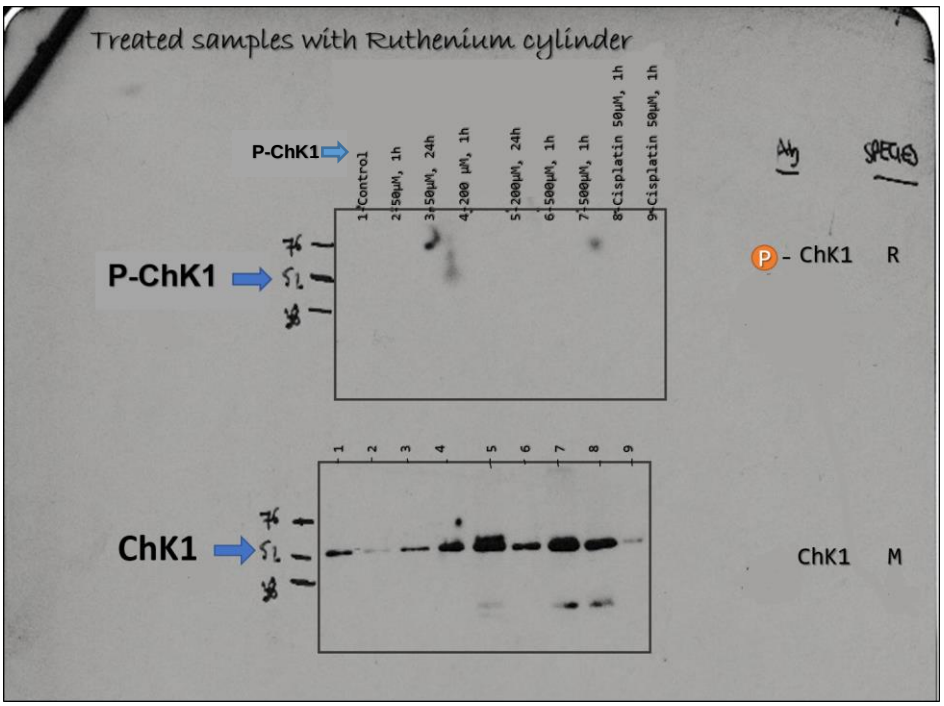

Ruthenium cylinder

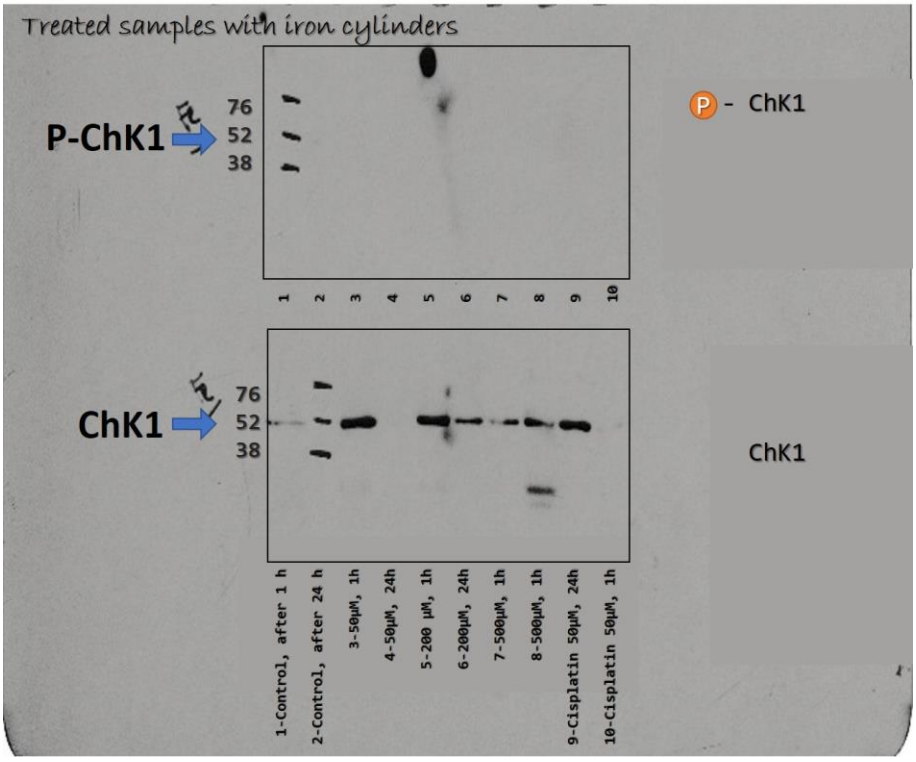

Iron cylinder

Fig. 3.25. Detection of HRP conjugated secondary antibodies (ChK1 mouse & P-ChK1 rabbit) for both ruthenium and iron cylinder-treated samples (Test 1).

As shown in Figure 3.25, the levels of ChK1 and phosphorylation ChK1 is considered to be a sign of DNA replication fork inhibition. The result shows that ChK1 was detected in lysates

of both cylinders (iron and ruthenium) in all concentrations and exposure times, in addition to both positive (cisplatin 50 µM for 1 and 24 hours) control. Samples exposed to the ruthenium cylinder for a longer time (24 hours) showed higher levels of ChK1 in their lysates. Moreover, ChK1 in iron cylinder samples showed the same result except for the samples treated with cisplatin after 24 hours and 50 µM iron cylinder after 1 hour, which did not show ChK1 in their lysates. This could be related to the initial level of protein concentration in their lysates. In contrast, ChK1 phosphorylation on serine 345 as a sign of stalling the replication fork was not observed in any ruthenium and iron cylinder samples. This could have happened due to the expiration of one of the antibodies used in this process. Alternatively, it may suggest that neither cylinder inhibited the DNA replication fork.

The test was repeated on the same samples by applying a new secondary P-ChK1 antibody (anti-rabbit) to reassess the process and results. This repeat produced showed contradictory results compared to test 1. The ChK1 protein was not detected in lysates, but ChK1 phosphorylation was detected only in samples treated with cisplatin 50 and 5 µM and iron cylinder 200 and 500 µM after 24 hours. One explanation for the lack of ChK1 protein in film after detection could be the problem of the primary antibody (Fig. 3.26). Since the ChK1 checkpoint kinase is activated by any minor damage or stress to DNA replication (known as DNA damage response or DDA), it should be identified in all lysates or at least in the cisplatin samples. Nonetheless, none of the samples responded to ChK1 antibody, which could be interpreted as the consequence of the antibody defect. The detection of ChK1 phosphorylation in some samples revealed damage on the replication fork in cisplatin samples, and stress on the replication fork in iron cylinder samples both in the highly-concentrated treatments and after longer times of exposure (Fig. 3.26).

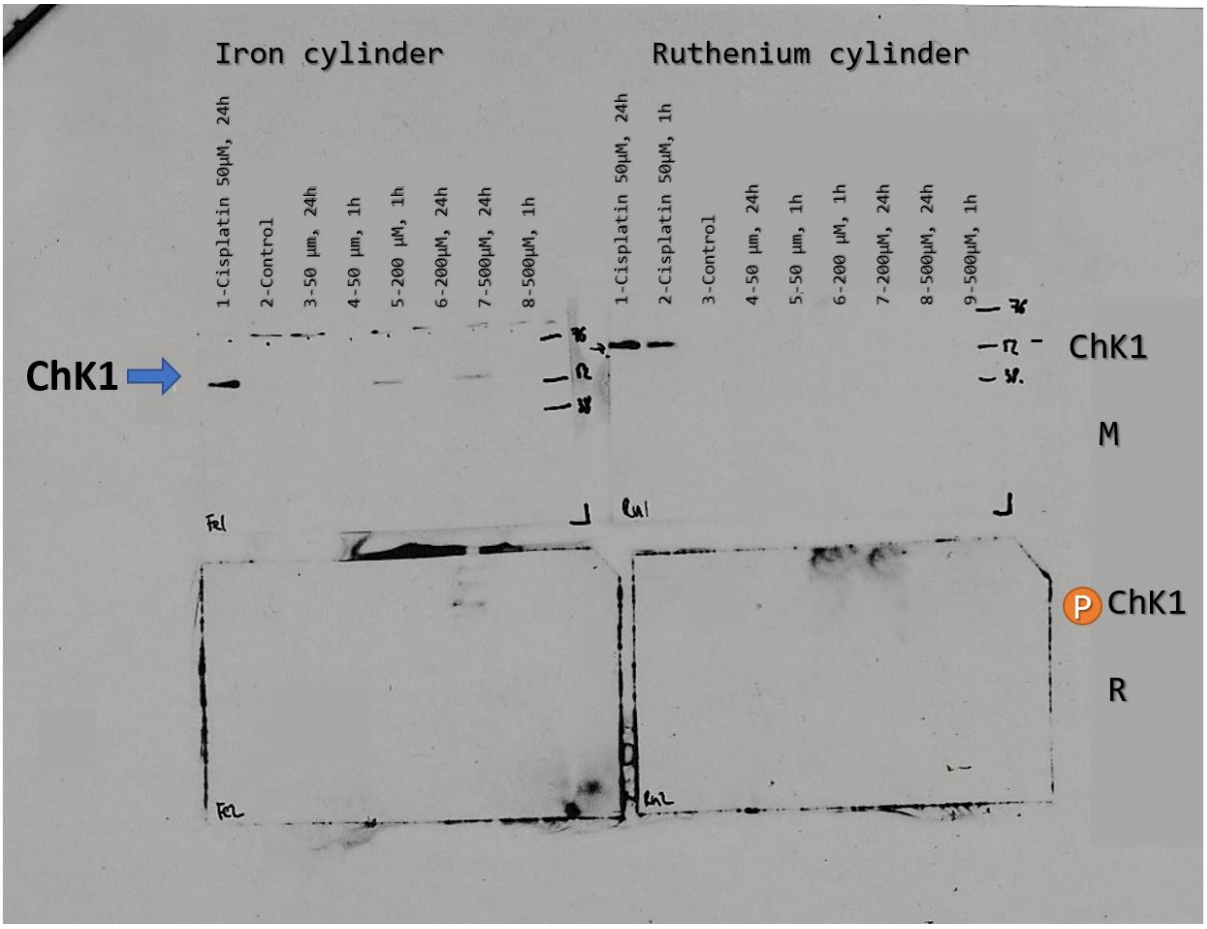

Fig. 3.26. Detection of HRP conjugated secondary antibodies (ChK1 mouse & P-ChK1 rabbit) for both ruthenium and iron cylinder treated samples (test 2).

The process was repeated again using a fresh primary ChK1 antibody on the same lysates (that were kept frozen at -80℃) to evaluate the result of the iron cylinder effect on the replication fork, by the detection of ChK1 phosphorylation protein. Undesirably, the results were similar to those of test 1, and P-ChK1 was not detected in either iron or ruthenium cylinder samples. The level of ChK1 protein in samples as a parameter of DNA stress was high in all samples of iron cylinder. Ruthenium cylinder activated the DDH network in 50, 200 and 500 µM treatments after 24 hours, with a marked difference in the level of ChK1 protein in samples treated with cisplatin.

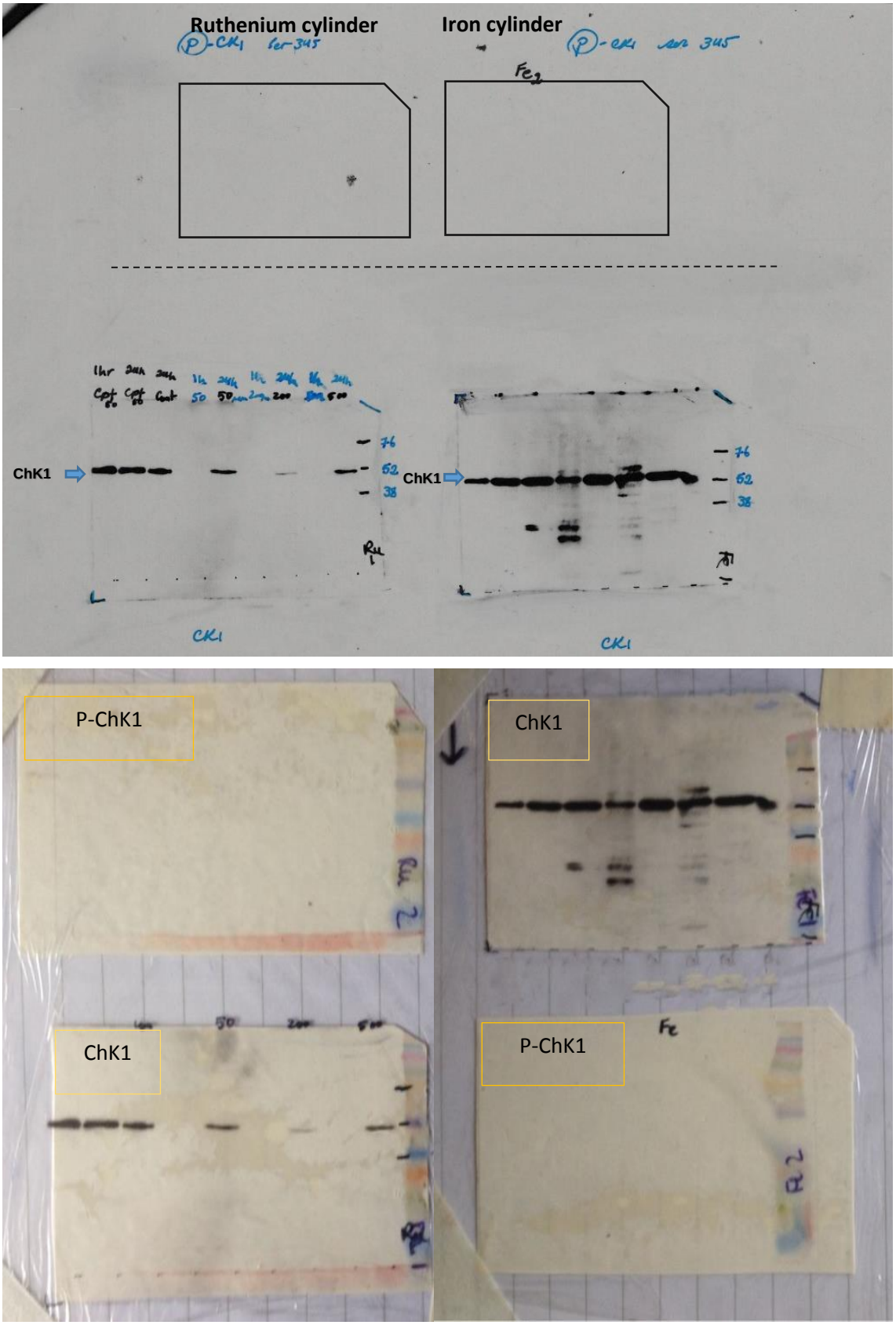

Fig. 3.27. Detection of HRP conjugated secondary antibodies (ChK1 mouse & P-ChK1 rabbit) for both ruthenium and iron cylinder treated samples (test 3).

3.7 References

1. Gerber, David E. "Targeted therapies: a new generation of cancer treatments." *Am Fam Physician* 77.3 (2008): 311-319.
2. Jump up ^ Allen TM (Oct 2002). "Ligand-targeted therapeutics in anticancer therapy". Nature Reviews. Cancer. 2 (10): 750–63. doi:10.1038/nrc903. PMID 12360278.
3. Chen, Helen X., and Jessica N. Cleck. "Adverse effects of anticancer agents that target the VEGF pathway." *Nature reviews Clinical oncology* 6.8 (2009): 465-477.
4. Gurova, Katerina. "New hopes from old drugs: revisiting DNA-binding small molecules as anticancer agents." *Future oncology* 5.10 (2009): 1685-1704.
5. Anna Scordato and Stanley Schwartz - Bioscience Department, Nikon Instruments, Inc., 1300 Walt Whitman Road, Melville, New York, 11747.
6. Kim, T. G., et al. "Correlations of structure and rates of energy transfer for through-bond energy-transfer cassettes." *The Journal of Physical Chemistry A* 110.1 (2006): 20-27.
7. http://www.public.asu.edu/~laserweb/woodbury/classes/chm467/bioanalytical/spectroscopy/absflr.html
8. Mottram, Laurie F., et al. "Hydrophobic analogues of rhodamine B and rhodamine 101: potent fluorescent probes of mitochondria in living C. elegans." *Beilstein journal of organic chemistry* 8.1 (2012): 2156-2165.
9. Ueno, Tasuku, and Tetsuo Nagano. "Fluorescent probes for sensing and imaging." *Nature methods* 8.8 (2011): 642.
10. Valeur, B. "Molecular Fluorescence Wiley." (2002): 161.
11. Agard, D.A., Hiraoka, Y., Shaw, P.J., and Sedat, J.W., 1989, Fluorescence microscopy in three-dimensions, Methods Cell Biol. 30:353–378
12. Fyodorova, I. Yu, et al. "DNA binding properties of dye Hoechst 33258 derivatives containing bulky substituents in the phenyl ring." *JOURNAL OF BIOMOLECULAR STRUCTURE & DYNAMICS*. Vol. 24. No. 6. 2066 CENTRAL AVE, SCHENECTADY, NY 12304 USA: ADENINE PRESS, 2007.
13. EMBREY, Kevin J., Mark S. SEARLE, and David J. CRAIK. "Interaction of Hoechst 33258 with the minor groove of the A+ T- rich DNA duplex d (GGTAATTACC) 2 studied in solution by NMR spectroscopy." *European Journal of Biochemistry* 211.3 (1993): 437-447.

14. https://commons.wikimedia.org/wiki/File:Spectra_of_Hoechst_dyes.svg
15. Fornander, Louise H., et al. "Minor-groove binding drugs: where is the second Hoechst 33258 molecule?." *The Journal of Physical Chemistry B* 117.19 (2013): 5820-5830.
16. http://www.biotek.com/resources/articles/sample-preperation-for-fluorescence-microscopy.html
17. Riss, T. L., et al. "Assay Guidance Manual." *Eli Lilly & Company and the National Center for Advancing Translational Sciences* (2004).
18. Berridge, Michael V., and An S. Tan. "Characterization of the cellular reduction of 3-(4, 5-dimethylthiazol-2-yl)-2, 5-diphenyltetrazolium bromide (MTT): subcellular localization, substrate dependence, and involvement of mitochondrial electron transport in MTT reduction." *Archives of biochemistry and biophysics* 303.2 (1993): 474-482.
19. https://en.wikipedia.org/wiki/MTT_assay#/media/File:MTT_reaction.png
20. Freshney, R. Ian. *Culture of specific cell types*. John Wiley & Sons, Inc., 2005.
21. Graat, H. C. A., et al. "Different susceptibility of osteosarcoma cell lines and primary cells to treatment with oncolytic adenovirus and doxorubicin or cisplatin." *British journal of cancer* 94.12 (2006): 1837-1844.
22. Dhar, Shanta, and Stephen J. Lippard. "Mitaplatin, a potent fusion of cisplatin and the orphan drug dichloroacetate." *Proceedings of the National Academy of Sciences* 106.52 (2009): 22199-22204.
23. Robson, Helen, et al. "Platinum agents in the treatment of osteosarcoma: efficacy of cisplatin vs. carboplatin in human osteosarcoma cell lines." *Pediatric Blood & Cancer* 39.6 (2002): 573-580.
24. Takata, Kei-ichi, et al. "Human DNA helicase HELQ participates in DNA interstrand crosslink tolerance with ATR and RAD51 paralogs." *Nature communications* 4 (2013).
25. Thomas, Robert. *Practical guide to ICP-MS: a tutorial for beginners*. CRC press, 2013.
26. https://icp-ms.wikispaces.com/
27. https://en.wikipedia.org/wiki/Inductively_coupled_plasma_mass_spectrometry

28. Nandhakumar, S., et al. "Evaluation of DNA damage using single-cell gel electrophoresis (Comet Assay)." *Journal of Pharmacology and Pharmacotherapeutics* 2.2 (2011): 107.
29. Møller, Peter. "The alkaline comet assay: towards validation in biomonitoring of DNA damaging exposures." *Basic & clinical pharmacology & toxicology* 98.4 (2006): 336-345.
30. http://www.exploranova.com/products/other/#PhotoSwipe1489529373957
31. Cortés-Gutiérrez, Elva I., et al. "New application of the comet assay: chromosome–comet assay." *Journal of histochemistry & cytochemistry* 59.7 (2011): 655-660.
32. Egger, Alexander E., et al. "Development of an experimental protocol for uptake studies of metal compounds in adherent tumor cells." *Journal of analytical atomic spectrometry* 24.1 (2009): 51-61.
33. He, Mei, and Amy E. Herr. "Automated microfluidic protein immunoblotting." Nature protocols 5.11 (2010): 1844-1856.
34. Ausubel, F. M., et al. "Current protocols in molecular biology New York." NY: Wiley (1987).
35. http://www.antibodies-online.com/resources/17/1224/western-blotting-immunoblot-gel-electrophoresis-for-proteins/
36. Bradford, Marion M. "A rapid and sensitive method for the quantitation of microgram quantities of protein utilizing the principle of protein-dye binding." *Analytical biochemistry* 72.1-2 (1976): 248-254.
37. Zor, Tsaffrir, and Zvi Selinger. "Linearization of the Bradford protein assay increases its sensitivity: theoretical and experimental studies." *Analytical biochemistry* 236.2 (1996): 302-308.
38. Hames, B. David, ed. *Gel electrophoresis of proteins: a practical approach*. Vol. 197. OUP Oxford, 1998.
39. Schägger, Hermann, and Gebhard Von Jagow. "Tricine-sodium dodecyl sulfate-polyacrylamide gel electrophoresis for the separation of proteins in the range from 1 to 100 kDa." *Analytical biochemistry* 166.2 (1987): 368-379.
40. http://capricorn.bc.edu/wp/pathways/protein-expression/sds-page/
41. http://www.gibthai.com/userfiles/image/technote/Western%20Blot/Western-Blot-2.jpg
42. Dunn, Michael J., ed. *Gel electrophoresis of proteins*. Elsevier, 2014.
43. https://en.wikibooks.org/wiki/Structural_Biochemistry/Proteins/Gel_Electrophoresis

44. http://blog.ptglab.com/index.php/western-blotting/
45. http://www.radio.cuci.udg.mx/bch/EN/Western.html
46. Mahmood, Tahrin, and Ping-Chang Yang. "Western blot: technique, theory, and trouble shooting." *North American journal of medical sciences* 4.9 (2012): 429.
47. Nowsheen, S., and E. S. Yang. "The intersection between DNA damage response and cell death pathways." Experimental oncology 34.3 (2012): 243.
48. Hall, M.D., Telma, K.A., Chang, K.E., Lee, T.D., Madigan, J.P., Lloyd, J.R., Goldlust, I.S., Hoeschele, J.D. and Gottesman, M.M., 2014. Say no to DMSO: dimethylsulfoxide inactivates cisplatin, carboplatin, and other platinum complexes. Cancer research, 74(14), pp.3913-3922.

CHAPTER 4

CONCLUSIONS AND OUTLOOK

This thesis investigated the properties of triple-stranded iron(II) and ruthenium(II) helical cylinders and their effects on the osteosarcoma U2OS cell line as anticancer agents. It attempted to answer the following fundamental questions:

i. How do the cylinders enter the cell, and where do they localise in the cell?
ii. How do they interact with key biomolecules in the cell, such as genomic DNA, and what are the downstream cellular effects of these interactions?
iii. What are their effects on the cell in vitro?

The ICP-MS results demonstrate the cellular uptake of the triple helix ruthenium(II) cylinder as a noncovalent DNA binder anticancer drug in different parts of U2OS cells. These results indicate that only 26% of the ruthenium cylinder is absorbed intracellularly over the course of four hours. Consequently, a large amount of the ruthenium cylinder is trapped in the membrane and is not uptaken by U2OS cells. The percentage of ruthenium cylinder cellular uptake in the nucleus (16%) is approximately twice that uptaken in the cytoplasm (9.68%), thus illustrating the greater preference for binding to genomic DNA of the cylinder on cells by gene interactions. Future work should investigate iron cylinder cellular uptake with and localisation in U2OS cells. A subsequent comparison of the iron and ruthenium cylinder results, and examination of the percentage of iron cylinder intake in the nucleus.

Studying the effects of both cylinders on U2OS cells in vitro revealed that the toxicity of the ruthenium cylinder is greater than that of the iron cylinder against U2OS cells; their IC_{50} values are 18 µM and 26 µM, respectively. Although both cylinders demonstrated strong toxicity in the treatments, the water solution of cisplatin did not show a high toxicity against the studied cancer cells. Furthermore, the genotoxicity studies of cylinders on DNA as an important genomic biomolecule demonstrate a low level of DNA damage in U2OS cells after 4 and 24 hours of treating. It is important to note that these results are valuable for smart cancer therapy. In future, iron and ruthenium cylinder cytotoxicity against U2OS cells should be investigated on two different timescales: 1) after 1, 2, 4, 8 and 12 hours; and 2) after 1, 2 and 3 days. These results could help in understanding the toxicity effects of these complexes over time in the studied cells. In addition, this information could help to find the minimum time required for the high toxicity impact of complexes in the studied cells.

Furthermore, this research needs to be extended by examining the reduction in cell growth rates following treatment with iron and ruthenium cylinders after 0, 1, 2, 3, 4 and 5 days,

using the crystal violet assay technique. Comparing the growth curves of U2OS cells unexposed and exposed to cylinders after five days would provide an invaluable set of information about the effects of the complexes on cells. Moreover, CellTrace Violet could be used to track cell proliferation over time by fluorescent dye dilution or flow cytometry.

Microscopy imaging and western blot techniques were used in this study to investigate the modes of interaction of ruthenium and iron cylinders with the DNA of U2OS cells. Previous studies have demonstrated that iron and ruthenium cylinders are active against many cancer cells because they form a noncovalent bond with the major groove of DNA. In this way, cell apoptosis occurs as a result of blocking the major groove, and subsequently the replication process. Similarities in the particular size and structural shape of cylinders are reasons to expect the same activity under the same conditions.

In previous studies, microscopy imaging using the Hoechst stain as a DNA groove binder has demonstrated Hoechst bleaching with cylinders as a sign of Hoechst replacement on the groove of DNA. Despite these outcomes, the replacement of Hoechst is not seen in the iron or ruthenium treatment samples of U2OS cells in this study. In addition, the fluorescent ability of the ruthenium cylinder helped to detect this complex inside cells, particularly in the nucleus, by fixed-cell microscopy. These results indicate that the cylinders cross the cell membrane, and the ruthenium cylinder is then detected inside the nucleus. In this way, the cellular uptake of the cylinders in U2OS cells is demonstrated here. However, there is no evidence for interaction between the cylinders and DNA major grooves.

Inhibition of the DNA replication fork with both iron and ruthenium cylinders was a principal goal of this work on U2OS cells. Since any stress on the DNA replication process, such as the interruption of DNA duplication, activates the ATR-ChK1 pathway to keep the replication fork feasible, the existence of checkpoint kinase in cell lysates signals the effects of the drug on the DNA replication fork. The western blot represents various uncertain results in samples with both iron and ruthenium cylinders in samples after several attempts. The ChK1 protein was detected in all samples treated with the iron cylinder and cisplatin after 1 and 24 hours. Meanwhile, this protein could only be detected in some samples treated by ruthenium cylinders after 24 hours. The detection of P-ChK1 as a sign of DNA replication fork inhibition by cylinders was not proved, although it was observed once in samples treated with iron cylinders. In contrast to samples treated with ruthenium cylinders, these results prove the interaction of the iron cylinder with the DNA replication fork after 24 hours in samples

treated with 200 µM and 500 µM of the cylinder, also it should be noted that those concentrations of cylinders are very high. Accordingly, concerning the similarity in the sizes and shapes of iron and ruthenium cylinders, the results of the western blot do not prove the same activity between iron and ruthenium cylinders in their interaction with the DNA replication fork in U2OS cells. These results did not enable the process to be followed by examination of the possibility of cylinder interaction with the DNA replication fork by DNA fibre analysis. This work clearly needs to be repeated with fresh primary and secondary antibodies in new cell lysates treated with iron and ruthenium cylinders. Positive results in order to detect the P-ChK1 protein in cell lysates are required to further investigate the interaction between cylinders and the DNA replication fork, by fibre analysis.

In conclusion, the thesis work represents the high cytotoxicity and non-genotoxicity effect of ruthenium cylinder and iron cylinder in U2OS cells. Whereas the mechanism of action of both cylinders in U2OS cells especially their interaction with DNA duplex were not clarified.